The Melonic Large-N Limit in Quantum Field Theory

Dario Benedetti

Institut Polytechnique de Paris
Centre de Physique Théorique - CNRS UMR 7644

Mémoire d'Habilitation à Diriger des Recherches

The Melonic Large-N Limit in Quantum Field Theory

Dario Benedetti

Rapporteurs:
Frank Ferrari (PTM, Université Libre de Bruxelles, Belgium)
Igor Klebanov (Princeton University, USA)
Vincent Rivasseau (IJCLab, Univ. Paris-Saclay, France)

Publicly defended on 14 February 2023 at Ecole Polytechnique, Palaiseau,
in front of the following jury members:

Robert de Mello Koch (MITP, University of Witwatersrand, South Africa)
Frank Ferrari (PTM, Université Libre de Bruxelles, Belgium)
Christoph Kopper (CPHT, Ecole Polytechnique, France)
Vincent Rivasseau (IJCLab, Univ. Paris-Saclay, France)
Adrian Tanasa (LaBRI, Univ. Bordeaux, France)

Contents

Preface

The present manuscript is prepared for my *Habilitation à diriger des recherches* (HDR). Its purpose is to provide a concise summary of research, with the stated scope of proving the candidate's ability to master a research strategy in a sufficiently broad scientific field, and their ability to supervise PhD students.

The topic and results presented here are based on my research in the years 2017-2021, during which I have investigated the application of the melonic large-N limit of tensor models in quantum field theory. This work has been done in large part with various collaborators, among which the following students, whom I have co-supervised:

- PhD students: Nicolas Delporte, Sabine Harribey, Davide Lettera. The first two currently have a postdoc position, in OIST (Okinawa) and Nordita (Stockholm), respectively, while the last is still in his PhD (in Heidelberg).
- Master students: Maciej Kolanowski, Ilaria Costa. Both have continued with PhD studies in Poland and Germany, respectively.

I have decided not to cover my previous research work on quantum gravity, as it is older and rather distinct from this more recent work. However, some background will be briefly mentioned on the quantum gravity origins of the melonic limit, thus providing a conceptual link to my previous endeavours. I have also decided not to include my most recent work, as it was only completed while this manuscript was already in progress, and because it opens a new direction (on resurgence and constructive field theory methods).

I will briefly describe in the concluding section a number of open questions that could provide the basis of future work, in particular with PhD students. It goes without saying that unexpected new ideas might take over and lead me to concentrate my efforts on yet newer directions.

Acknowledgements

First of all, I want to express my gratitude to Frank Ferrari, Igor Klebanov, and Vincent Rivasseau for accepting the task of reviewing the manuscript, and to Robert de Mello Koch, Frank Ferrari, Christoph Kopper, Vincent Rivasseau and Adrian Tanasa for accepting to be part of the jury. I would also like to thank all my collaborators, especially those involved in the work directly relevant to this manuscript: Sylvain Carrozza, Ilaria Costa, Nicolas Delporte, Razvan Gurau, Sabine Harribey, Maciej Kolanowski, Davide Lettera, Alessandro Sfondrini, Ritam Sinha, Kenta Suzuki, Reiko Toriumi, and Guillaume Valette. In particular, special thanks to Razvan for the lasting friendship and prolific collaboration, which has played an essential part in my recent research. A big thanks goes also to all the friends and colleagues from the French "tensor models community", in particular Joseph Ben Geloun and Fabien Vignes-Tourneret for setting up the virtual tensor journal club, which helped a lot in keeping us in contact even during the pandemic. I would also like to thank my colleagues at CPHT, and the administration staff, Florence Auger, Fadila Debbou and Malika Lang, for their patient help anytime I have needed it. Last but not least, a special thanks goes to my wife Yuan-Ju, and our kids Alice and Elio, for their support and their patience while I was writing this manuscript.

Relevant publications

The topic covered in this research overview is based on my publications from the years 2017-2021. In order to provide a brief guide to their logical relations, I list them here, arranged by subject, and with some brief commentary, for orientation. Links pointing both to the published versions and to the equivalent arXiv preprints are provided. A full list of publications (without commentary) is provided separately as part of the HDR dossier.

Combinatorial aspects

In these two papers, we studied purely combinatorial models (statistical field theories on zero dimensional spacetime). Their Feynman diagrams can be interpreted as simplicial (pseudo-)manifolds, thus generalizing to higher dimensional manifolds the relations between matrix models and random triangulations. Aside from such interpretation and its geometric construction, the classification of diagrams in the $1/N$ expansion that one finds in these models is relevant also for higher-dimensional versions (proper quantum field theories), as the power of N associated to a diagram only depends on the combinatorial tensor structure.

- D. Benedetti, S. Carrozza, R. Gurau and M. Kolanowski, *The $1/N$ expansion of the symmetric traceless and the antisymmetric tensor models in rank three*, *Commun. Math. Phys.* **371** (2019) 55 [arXiv:1712.00249].

  We have proved that the large-N limit, in the case of tensors with three indices, is dominated by melonic diagrams, not only for the $O(N)^3$-symmetric models, but also for models whose variables transform in two irreducible representations appearing in the product of three fundamentals of the $O(N)$ group, i.e. the symmetric traceless and antisymmetric tensor representations.

- D. Benedetti, S. Carrozza, R. Toriumi and G. Valette, *Multiple scaling limits of* $\mathrm{U}(N)^2 \times \mathrm{O}(D)$ *multi-matrix models*, *Ann.Inst.H.Poincare D Comb.Phys.Interact.* **9** (2022) 2, 367-433 [arXiv:2003.02100].

  We have studied multiple scaling limits of tensor models with different index sizes, interpretable also as multi-matrix models with $\mathrm{U}(N)^2$ "color symmetry" and $\mathrm{O}(D)$ "flavor symmetry". In particular, we classified and resummed (in a triple-scaling limit involving N, D and the coupling constant) the leading large-D diagrams, to all orders in $1/N$.

General quantum field theoretic aspects

In these papers, we explored various aspects relevant to the quantum field theories admitting a melonic limit, but which are also of more general interest.

- D. Benedetti and R. Gurau, *2PI effective action for the SYK model and tensor field theories*, *JHEP* **05** (2018) 156 [arXiv:1802.05500].

  We brushed up the two-particle irreducible (2PI) formalism as a particularly apt approach to the melonic large-N limit. In particular we showed that it provides a valid alternative to the bilocal effective action commonly used for the Sachdev-Ye-Kitaev model, which cannot be obtained in a similar fashion for tensor models.

- D. Benedetti, R. Gurau, S. Harribey and K. Suzuki, *Long-range multi-scalar models at three loops*, *J. Phys. A* **53** (2020) no.44, 445008 [arXiv:2007.04603].

  We pushed the computation of loop integrals for generic long-range multi-scalar models with quartic interactions up to three loops, as these type of computations are relevant to some tensor models we have developed (see below). However, in this paper, we have considered in detail more common models, such as the $O(N)$ vector model, the cubic model, and the $O(N) \times O(N)$ bifundamental model. For such models, two-loop computations had been done in the 1970's, but had never been improved until our work.

- D. Benedetti, *Instability of complex CFTs with operators in the principal series*, *JHEP* **05** (2021) 004 [arXiv:2103.01813].

  We have proved that the appearance of a special type of complex scaling dimension Δ, of the type $\Delta = d/2 + \mathrm{i}\, r$ with d being the spacetime dimension and r an arbitrary real number, found in various large-N models, including some tensor models and fishnet models, implies an instability of the conformal vacuum solution.

Case study of a melonic CFT: the long-range $O(N)^3$ model

In this series of papers, we have carried out an in-depth exploration of one particular model, namely a long-range multi-scalar model with $O(N)^3$ symmetry and quartic interactions. The striking feature of the model is that in the melonic limit the two-point function can be solved exactly, and the presence of interacting fixed-points of the renormalization group can be proved to all orders of perturbation theory. Interestingly, such *melonic fixed points* define conformal field theories which have passed many unitarity tests, despite the fact that at subleading orders in $1/N$ some scaling dimensions become complex.

- D. Benedetti, R. Gurau and S. Harribey, *Line of fixed points in a bosonic tensor model*, *JHEP* **06** (2019) 053 [1903.03578].

  We introduced the model, solved the large-N Schwinger-Dyson equation for the two-point function, proved the existence of fixed points, and computed a first set of scaling dimensions at such fixed points.

- D. Benedetti, R. Gurau, S. Harribey and K. Suzuki, *Hints of unitarity at large N in the $O(N)^3$ tensor field theory*, *JHEP* **02** (2020) 072 [1909.07767].

  We computed other scaling dimensions, as well as operator-product-expansion coefficients, finding that they are all compatible with unitarity constraints.

- D. Benedetti and I. Costa, *$SO(3)$-invariant phase of the $O(N)^3$ tensor model*, *Phys. Rev. D* **101** (2020) 086021 [1912.07311].

  We explored some possible patterns of spontaneous symmetry breaking in this type of model, in particular uncovering an interesting $SO(3)$-invariant solution of the field equations.

- D. Benedetti, R. Gurau and K. Suzuki, *Conformal symmetry and composite operators in the $O(N)^3$ tensor field theory*, *JHEP* **06** (2020) 113 [2002.07652].

  We gave a perturbative proof of conformal invariance of the model at its fixed points. Moreover, we identified various composite scaling operators at the fixed point and computed their two- and three-point functions, finding the expected behavior of a unitary CFT.

- D. Benedetti, R. Gurau and S. Harribey, *The tri-fundamental quartic model*, *Phys. Rev. D* **103** (2021) 046018 [2011.11276].

  We explored some variations of the model, as well as the subleading corrections in $1/N$. The latter show explicitly how the unitarity-violating parts of the CFT data are suppressed in the large-N limit.

- D. Benedetti, R. Gurau, S. Harribey and D. Lettera, *The F-theorem in the melonic limit*, *JHEP* **02** (2022) 147 [2111.11792].

  We tested the F-theorem by computing the sphere free energy at the fixed point of our model at next-to-next-to-leading order in $1/N$, and checking that indeed it is smaller at the IR fixed point than at the UV one. In the process, we showed the power of conformal partial wave methods by resumming an infinite class of vacuum Feynman diagrams.

Other models

In this last set of papers, we have studied other models that admit a melonic limit, namely fermionic tensor models with quartic interactions, bosonic tensor models with sextic interactions, and different type of multiscalar model with cubic interactions.

- D. Benedetti, S. Carrozza, R. Gurau and A. Sfondrini, *Tensorial Gross-Neveu models*, *JHEP* **01** (2018) 003 [1710.10253].

  We studied $U(N)^3$ and $O(N)^3$ fermionic models with quartic interactions. For the $U(N)^3$ model we computed the large-N effective potential in the intermediate field formalism. Melonic fixed points are found for the $O(N)^3$ models in $2-\epsilon$ dimensions.

- D. Benedetti and N. Delporte, *Phase diagram and fixed points of tensorial Gross-Neveu models in three dimensions*, *JHEP* **01** (2019) 218 [1810.04583].

  We studied spontaneous symmetry breaking and UV fixed point of the three-dimensional $U(N)^3$ fermionic models at large-N.

- D. Benedetti, N. Delporte, S. Harribey and R. Sinha, *Sextic tensor field theories in rank* 3 *and* 5, *JHEP* **06** (2020) 065 [1912.06641].

  We introduced two different multiscalar models with sextic interactions, with $U(N)^3$ or $O(N)^5$ symmetry. In the first case we find a melonic fixed point and we study its CFT data.

- D. Benedetti and N. Delporte, *Remarks on a melonic field theory with cubic interaction*, *JHEP* **04** (2021) 197 [2012.12238].

  We considered a multiscalar model with $SO(3)$ symmetry and cubic interactions, admitting a melonic limit (as the size of the $SO(3)$ irreducible representations goes to infinity) despite being neither a tensor model nor a random-coupling model.

Chapter 1

Introduction

Quantum field theory (QFT) is the pillar of fundamental physics, providing the framework for the Standard Model of particle physics, as well as its extensions. Even current approaches to quantum gravity, such as string theory, asymptotic safety, and virtually any approaches based on a path integral, rely heavily on the methods and ideas of QFT. Moreover, in the Euclidean version, much of the QFT formalism applies also to statistical physics, in particular as an effective language for the theory of critical phenomena. It is thus not surprising that exploring every possible corner of the QFT formalism is a very active field of research, and it has been so since several decades.

Among the many ideas and methods elaborated within the QFT framework, the renormalization group (RG) [1, 2] occupies a special place. It was developed through a cross-fertilization of ideas between statistical and high-energy physics, leading to the modern understanding both of the theory of critical phenomena, and of the relation between fundamental and effective field theories. One of its most insightful outcomes is the idea that a special set of QFTs, the fixed points of the RG flow, have a privileged status, as they define scale-invariant QFTs. Any other, non scale-invariant, QFT is then viewed as a combination of relevant (unstable towards the infrared) and irrelevant (stable) perturbations of such fixed points. In practice, we are only able to define such perturbations when the fixed-point represents a soluble theory, i.e. a theory for which we know how to compute all the correlators. Unfortunately, there are not so many exactly-soluble interacting theories which are available to us, hence we usually define QFTs as perturbations of the free theory (Gaussian fixed point).

For the so-defined QFTs, establishing the existence of interacting fixed points is a major challenge, as these might lie far from the Gaussian fixed point, where it becomes difficult to control the perturbative expansion. One recent approach, known as conformal bootstrap, bypasses the problem by exploiting the fact that, rather generically, the scale invariance of RG fixed points is promoted to conformal invariance,[1] hence we expect a fixed point theory to be described by a conformal field theory (CFT). Therefore, in the conformal bootstrap, one tries to find directly such CFTs by constrining the space of all possible CFT data with self-consistency equations, in many cases with formidable results [5].

More traditional approaches to interacting fixed points are based on analytically continuing some parameter of the QFT, so that one can reach a limit in which the interacting fixed point is under control. For example, by analytically continuing the spacetime dimension d, one can go near the

[1] A full-fledged theorem in this sense has only been proved in two dimensions, and under perhaps too restrictive conditions (in particular unitarity) [3] (see also the review [4]).

critical dimension d_c, so that the nontrivial fixed point becomes very close to the Gaussian fixed point [6]. In this case, one uses $\epsilon = d_c - d$ as an expansion parameter, and the challenge is to reach ϵ of order one. A similar idea consists in analytically continuing the number of field components N to reach the large-N limit, where often the problem of studying nontrivial fixed points becomes tractable [7]. In a second step, one introduces corrections, leading to an expansion in powers of $1/N$, and again the challenge is to reach finite N.

One intuitive reason why we can anticipate simplifications to occur in the large-N limit is based on the central limit theorem of probability theory, according to which one expects that singlet composite operators, i.e. sums of products of fundamental fields that are invariant under the symmetry group of the model, will have small fluctuations as compared to the original fields [8]. Such idea is realized very explicitly in the case of vector models, i.e. models in which the original fields form a vector representation of the symmetry group (e.g. the fundamental representation of $O(N)$), as in that case we have only few independent invariants and we are able to construct an effective theory for such collective fields (either via intermediate field [9], change of variables [10, 11], or source method [12]). Another perspective on the large-N simplification is given by the behavior of Feynman diagrams. For vector models, the Feynman diagrams that typically dominate at large N are the so called cactus diagrams (Fig. 1.1), i.e. trees of bubbles, which can easily be resummed, as the bubble amplitudes factorize. The underlying tree structure becomes evident in the intermediate field representation, in which the $1/N$ expansion reduces to a loop expansion [9].

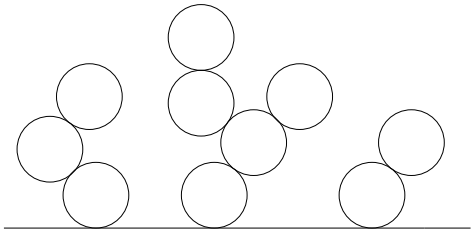

Figure 1.1: A cactus two-point diagram for a model with quartic interactions. A bubble attached by a vertex to an edge is often called *tadpole* or *snale*.

The restriction to cactus diagrams carries drastic simplifications, for example leading to a one-loop structure of the RG beta functions, and to a vanishing anomalous dimension for the fundamental fields. Nevertheless, it has served as a very instructive limit case, and besides the application to studying nontrivial infrared fixed points (e.g. [7, 13, 14]), the large-N limit of fields in the vector representation has been used to tackle many problems, among which nonperturbative aspects of spontaneous symmetry breaking and dynamical mass generation [15, 16], the ultraviolet limit of nonrenormalizable theories [17, 18], and more recently an holographic approach to higher-spin theory [19, 20].

The large-N limit becomes more intricate when the fields form a higher-dimensional representation of the group, or when the symmetry group itself is not maximal (e.g. it is smaller than $O(N)$, in the case of N fields). The most physically relevant example is arguably that of fields in the adjoint representation of $SU(N)$, corresponding to Yang-Mills theory. As realized by 't Hooft [21], the matrix nature of the fundamental fields is such that the large-N limit restricts the perturbative expansion to planar diagrams. This observation has had a huge impact on theoretical physics research, with applications to quantum chromodynamics, statistical models, random surfaces, string theory and AdS/CFT duality (e.g. [22, 23]). One notices that the planar limit of a QFT is still very complicated: although much less than all diagrams, the planar ones are still many, with arbitrary number of (non

factorizable) loops, and essentially impossible to resum. Things are of course easier in zero dimensions, i.e. for random matrix models, relevant to two-dimensional quantum gravity and string theory [24], in which case many models are solvable in the large-N limit [25]. However, in general the planar limit of higher-dimensional QFTs remains far from solvable, unless extra ingredients are brought in, such as maximal supersymmetry, which in the case of $\mathcal{N} = 4$ super-Yang-Mills leads to vanishing beta functions and integrability [26].

While the large-N limit of fields in the vector and matrix representations has been studied and used to a large extent, higher-dimensional tensor representations have been seriously considered only very recently. Random tensor models have actually been introduced in the early 1990's as a generalization of matrix models in an attempt to construct a higher-dimensional theory of quantum gravity by summing over simplicial manifolds [27, 28], but for long time their large-N limit was not understood. With hindsight, the reason for such a situation was twofold: from a sociological point of view, the simplicial approach to quantum gravity was by far not the most popular, and the few who studied it by Monte Carlo simulations found discouraging results [29–31], thus the large-N limit of tensor models was simply not much investigated; from a technical point of view, the original models were based on tensors in a reducible representation of the $O(N)$ group, for which in fact the large-N limit is ill-defined. The state of affairs changed drastically around 2010, when Gurau discovered that a particular class of models with several interacting tensors, called colored tensor models, admitted a large-N limit dominated by melonic diagrams [32–35] (see example in Fig. 1.2; a precise description will be given later on). Subsequently, the melonic limit has been found to be quite general, with several other versions of tensor models having such limit, in particular simpler models involving a single tensor [36–39], even including models in tensor representations of the $O(N)$ group, as long as restricted to irreducible representations [40–43].

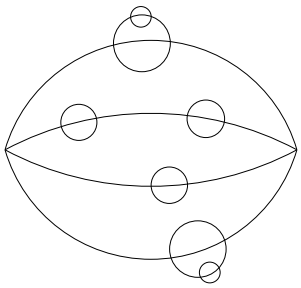

Figure 1.2: An example of melonic vacuum diagram for a model with quartic interactions, obtained from a fundamental melon with two vertices, by repeated insertions of melonic two-point functions (or sunset diagrams).

The discovery of the large-N limit of tensor models did not change the status of simplicial quantum gravity, because, consistently with numerical simulation [29], the dominance of melonic diagrams corresponds to a branched polymer phase [35, 44, 45], with no interesting large-scale limit. However, it marked a significant development from a mathematical physics perspective, showing the existence of a completely new large-N limit, dominated by a combinatorial class of diagrams of a new type. Moreover, one might have expected that increasing the number of indices of the fields the complexity of the limit would have increased as well. It turns out that this is not the case, as melonic diagrams are a small subset of all the planar diagrams, with a precise recursive structure. The melonic limit is therefore much simpler than the planar limit. At the same time, melonic diagrams are different,

and in some sense more complicated, than cactus diagrams. Therefore, they open the door to the possibility of a new tractable limit in QFT.

The first realization that such a new (melonic) large-N limit could provide an interesting tool for building CFTs came from an independent route. In 2016, a revised old model of random magnets came into the limelight as a possible simple model of holography: the Sachdev-Ye-Kitaev (SYK) model [46–49] (see also [50–52] for reviews). This is a quantum mechanical model of N Majorana fermions with a q-body interaction ($q > 2$) mediated by a random tensor coupling. One of the main features of the model is that melonic diagrams dominate in the large-N limit [53, 54], implying a closed Schwinger-Dyson equation for the two point function, that can be solved exactly in the infrared limit, with a conformal solution. The fact that in the SYK model the random tensor appears as a random coupling means that one is dealing with a system having quenched disorder, which in turn means that it is not a model for a fundamental theory and that it is not possible to get rid of the non-singlet states by gauging its global symmetry group (as suitable for the AdS/CFT correspondence), as this only emerges after quenching. However, as first noticed by Witten [55], one can overcome such problems by choosing the Majorana fermions themselves to be in a tensor representation of a global symmetry group, as in the original colored tensor model [33–35]. In this way, one obtains proper quantum mechanical models with all the interesting features of the SYK model, minus the quenching. A simpler model was proposed in [56], with fields in the tri-fundamental of $O(N)^3$, for which the melonic dominance was proven in [38], and several other works on SYK-like tensor models have then followed [57–68].

Once the step from zero to one dimension is done, i.e. from purely combinatorial models to quantum mechanics, it seems only natural to move on to even higher dimensions, i.e. to QFT. And in fact, several higher-dimensional versions both of the SYK model and of tensor models have been explored [56, 69–77]. And this will be the main subject of this thesis, of course with a strong focus on the author's own work, because of the purpose of the manuscript. For a review with a different focus, see [78].

Plan of the thesis. We will begin in Chapter 2 with a brief review of the combinatorial aspects of the new type of large-N limit at the heart of this work, exemplified by few concrete models: the $O(N)^3$ model, the rank-3 symmetric traceless or antisymmetric tensor models, and the $U(N)^2 \times O(D)$ model. We will keep the presentation as minimal and streamlined as possible, in particular with no proofs of the combinatorial results, for which we refer to the original papers. See also [79] for the general combinatorial details on random tensors.

Chapter 3 contains a review of the construction of the two-particle irreducible (2PI) effective action and its large-N limit, in the $O(N)$ model, SYK model, and $O(N)^3$ tensor model. The 2PI formalism is a particularly well-suited tool for melonic theories, as in the large-N limit we can write the full 2PI effective action in a finite number of terms, something which is very unusual for a generating functional of an interacting QFT. It will then allows us to derive Schwinger-Dyson equations for two-point and four-point functions in an easy way, as well as study the free energy, derive an effective field theory for the infrared would-be gauge modes, and possibly it might provide a link to holography thanks to its bilocal nature [80, 81].

In Chapter 4, we will present an overview of what the melonic limit can achieve in a QFT, mostly concentrating on a case study: the long-range $O(N)^3$ model with quartic interactions, in dimension $1 < d < 4$. The melonic limit leads to interacting fixed points, describing interesting CFTs, of which we are able to compute nonperturbatively several elements, such as the two-point function, the

Bethe-Salpeter kernel, the conformal dimensions of an infinite tower of operators, and the sphere free energy. We also review a general result on the instability of CFTs with an operator of complex scaling dimension $d/2 + \mathrm{i}\, r$, with $r \in \mathbb{R}$, as this appears in some melonic CFTs.

In Chapter 5 we will wrap up with some conclusions and an outlook on some open directions.

Chapter 2

Melonic limit: combinatorial aspects

In constructing a large-N limit, symmetries play a crucial role, and in particular different representations of a symmetry group in general lead to different limits. Here, the variable N will be related to the number of fields components, and by symmetry group we mean the group of field transformations, forming a representation of an abstract group, under which the action of the model is invariant. Of special interest to us is the case of tensor representations of an internal global symmetry group. Spacetime symmetries will play a usual role in partially constraining correlation functions, but are irrelevant for the definition of the large-N limit itself.

So what do we mean by fields in a tensor representation? In order to fix ideas, let us consider, as in most of this thesis, scalar fields in flat d-dimensional spacetime, in Euclidean signature. We say that such fields form a representation of a group $\mathcal{G}$ if they collectively form the components (in some basis) of a section of a (trivial) fiber bundle, with $\mathbb{R}^d$ as base space and a vector space V as fiber, such that there exists a group homomorphism from $\mathcal{G}$ to $GL(V)$, the general linear group on V. Vector models, correspond to the case of $\mathcal{G}$ being a simple Lie group, and V corresponding to the so-called *fundamental representation*, also known as standard or defining representation, i.e. the smallest faithful representation of the group. For example, scalar fields in the fundamental representation of $O(N)$ are N real scalars $\varphi_a(x)$, with $a = 1 \dots N$, transforming as

$$\varphi_a(x) \to R_{ab}\varphi_b(x) \,, \qquad R \in O(N) \,, \tag{2.0.1}$$

where R is an orthogonal $N \times N$ matrix, and summation over repeated indices is implicit. The $O(N)$ model is defined by an action invariant under such transformation, and therefore we say that its fields are in the fundamental representation of $O(N)$.

When it comes to tensor fields, we will distinguish two cases: tensor representations of a simple Lie group $\mathcal{G}$, and fundamental representations of a direct product $\prod_{i=1}^r \mathcal{G}_i$ of simple Lie groups $\mathcal{G}_i$. In the latter case, a rank-r tensor field[1] is essentially a function $\varphi : \mathbb{R}^d \to \otimes_{i=1}^r V_i$, where V_i is the vector space corresponding to the fundamental representation of the group $\mathcal{G}_i$. We denote its components as $\varphi_{a_1 \dots a_r}(x)$, with $x \in \mathbb{R}^d$ and $a_i = 1 \dots N_i$, where $N_i = \dim(V_i)$, hence the group acts by the transformation rule:

$$\varphi_{a_1 \dots a_r}(x) \to \left(\prod_{i=1}^r R^{(i)}_{a_i b_i} \right) \varphi_{b_1 \dots b_r}(x) \,, \tag{2.0.2}$$

[1] Notice that in the mathematical literature the *rank* of a tensor has typically a different meaning, generalizing that of rank of a matrix. In physics, it is instead quite common to refer to the number of indices of the tensor as rank. Whenever we will use the word rank here, we will mean it in the physics usage.

with the matrix $R^{(i)}$ belonging to the fundamental representation of the group $\mathcal{G}_i$. Notice that even if we have r copies of the same group, $\mathcal{G}_i = \mathcal{G}$ for $i = 1, \ldots, r$, the matrices $R^{(i)}$ can represent different elements of it. When these are also restricted to be all equal, then we have a tensor representation of the group $\mathcal{G}$:

$$\varphi_{a_1 \ldots a_r}(x) \to \left(\prod_{i=1}^{r} R_{a_i b_i} \right) \varphi_{b_1 \ldots b_r}(x) \, . \tag{2.0.3}$$

However, this is in general a reducible representation, i.e. it can be decomposed in irreducible representations, $\mathcal{G}$-invariant linear subspaces of V which cannot be decomposed further. For example, for $r = 2$ and $\mathcal{G} = O(N)$, the field $\varphi_{a_1 a_2}(x)$ can be decomposed in a trace part, which is invariant (i.e. it is the trivial representation), a symmetric traceless part, $\varphi_{a_1 a_2}(x) + \varphi_{a_2 a_1}(x) - \frac{2}{N} \delta_{a_1 a_2} \varphi_{bb}(x)$, and an antisymmetric part, $\varphi_{a_1 a_2}(x) - \varphi_{a_2 a_1}(x)$. At $r = 3$, the decomposition includes three traces transforming in the fundamental, a totally symmetric traceless tensor, a totally antisymmetric tensor, and two tensors with mixed symmetry. We will not need more than this here.

The cases with $r = 1$ and $r = 2$ are special, and we refer to them as vector and matrix cases, respectively. In this context we reserve the word *tensor* for the case $r \geq 3$, in contrast with standard usage in several areas of physics, such as general relativity and electrodynamics, where objects with two (tangent space) indices are also referred to as tensors, but in line with the fact that for random matrix models the word tensor has never been traditionally used.

2.1 Model building and melonic limit: $O(N)^3$ models

In this section, we will restrict our focus on the arguably simplest models, that is, those based on fields in the fundamental representation of $O(N)^3$. In other words, the fundamental field is a rank-3 field $\varphi_{abc}(x)$ transforming as[2]

$$\varphi_{abc}(x) \to R^{(1)}_{aa'} \, R^{(2)}_{bb'} \, R^{(3)}_{cc'} \, \varphi_{a'b'c'}(x) \, , \tag{2.1.1}$$

with $R^{(i)}$, $i \in \{1, 2, 3\}$ being distinct orthogonal matrices. To fix ideas, we will also assume here that $\varphi_{abc}(x)$ is a scalar field (real in this case, and complex if $O(N)$ is replaced by $U(N)$).

As usual, a specific model is defined by the (Euclidean) spacetime dimension d, and a choice of invariant action, with which to construct perturbatively the partition function[3]

$$Z[J] = e^{W[J]} = \mathcal{N} \int [d\varphi] \, e^{-S[\varphi] + \int_x J_{abc}(x) \varphi_{abc}(x)} \, , \tag{2.1.2}$$

with $W[J]$ being the generating function of connected n-point functions, $W[0]$ the free energy of the model, and $\mathcal{N}$ a normalization that is fixed below together with the measure $[d\varphi]$.

In order to define the functional integration measure, and develop a perturbative expansion, we separate the action in a free and an interacting part, as $S[\varphi] = S_{\text{free}}[\varphi] + S_{\text{int}}[\varphi]$. The former is quadratic in the fields,

$$S_{\text{free}}[\varphi] = \frac{1}{2} \int_{x,y} \varphi_{abc}(x) C^{-1}(x, y) \varphi_{abc}(y) \, , \tag{2.1.3}$$

[2]To be precise, this is not a faithful representation of $O(N)^3$, but only of $O(N)^3/\mathbb{Z}_2^2$, where $\mathbb{Z}_2^2$ is the subgroup of $O(N)^3$ acting trivially on $\varphi_{abc}(x)$ (the subgroup $\mathbb{Z}_2$ of $O(N)$ is represented by plus and minus the identity matrix). This subtlety plays no role in our analysis and therefore we will generally be cavalier about it.

[3]Here and in the following we denote $\int_x = \int \mathrm{d}^d x$, $\int_{x,y} = \int d^d x d^d y$, and so on in direct space, and $\int_p = \int \frac{\mathrm{d}^d p}{(2\pi)^d}$ in momentum space.

thus defining the Gaussian part of the measure, denoted $d\mu_C[\varphi]$, with covariance $C(x,y)$, which we define to be normalized such that:

$$\begin{aligned}\int d\mu_C[\varphi] \prod_{i=1}^{n} \varphi_{a_i b_i c_i}(x_i) &= \mathcal{N} \int [d\varphi]\; e^{-S_{\text{free}}[\varphi]} \prod_{i=1}^{n} \varphi_{a_i b_i c_i}(x_i) \\ &= \begin{cases} 1 & \text{if } n = 0, \\ 0 & \text{if } n \text{ is odd}, \\ \sum_P \prod_{(i,j)\in P} C(x_i, y_j) \delta_{a_i a_j} \delta_{b_i b_j} \delta_{c_i c_j} & \text{if } n \neq 0 \text{ is even}, \end{cases}\end{aligned} \tag{2.1.4}$$

where P denotes all the pairings of n elements into pairs (i,j) (that is, distinct partitions of the set $1 \dots n$ into subsets of two elements), also known as Wick contractions. See for example [82] for general properties of Gaussian measures.

For $d = 0$ the standard choice is $C = 1$, while the choice of propagator for $d > 0$ will be discussed in the next chapters, and in particular in Sec. 4.1.

For the interacting part we take a polynomial in the fields, without derivatives, restricted by invariance under (2.1.1). The invariance requires that tensor indices in the same position on different tensors be contracted pairwise, implying also that invariants require an even number of fields. For example, the so-called *tetrahedron* invariant is defined as

$$I_{\text{tetrahedron}} = \varphi_{a_1 a_2 a_3} \varphi_{a_1 b_2 b_3} \varphi_{b_1 a_2 b_3} \varphi_{b_1 b_2 a_3} \,. \tag{2.1.5}$$

Given a set of invariants of this sort, we write the interacting part of the action as

$$\begin{aligned} S_{\text{int}}[\varphi] &= \int_x \sum_{b\in\mathcal{I}} \frac{\lambda_b}{2q_b\, N^{\frac{3}{2}(q_b-1)+\rho_b}} I_b \\ &= \int_x \sum_{b\in\mathcal{I}} \frac{\lambda_b}{2q_b\, N^{\frac{3}{2}(q_b-1)+\rho_b}} \delta^{(b)}_{\mathbf{a}_1 \dots \mathbf{a}_{2q_B}} \varphi_{\mathbf{a}_1}(x) \dots \varphi_{\mathbf{a}_{2q_b}}(x) \,. \end{aligned} \tag{2.1.6}$$

Here, $\mathcal{I}$ is a set of labels that distinguishes the different invariants, and we have introduced a condensed notation for the indices, $\mathbf{a}_i = a_{i1} a_{i2} a_{i3}$, and an invariant tensor of rank $6q$, $\delta^{(b)}_{\mathbf{a}_1 \dots \mathbf{a}_{2q}}$, which performs the contraction of tensor indices corresponding to a given invariant. The λ_b are 't Hooft couplings (to be held fixed in the large-N limit), and the scaling in N, in particular the parameters ρ_b, have to be chosen in such a way that the large-N limit exists and it is non-trivial. We will get back to it after having introduced a graphical representation for the perturbative expansion.

The generating functional of connected n-point functions now writes

$$W[J] = \ln \int d\mu_C[\varphi]\; e^{-S_{\text{int}}[\varphi] + \int_x J_{abc}(x) \varphi_{abc}(x)} \,. \tag{2.1.7}$$

The goal of perturbation theory is to evaluate the coefficients of its power series in J (i.e. the connected n-point functions) by expanding the integrand in powers of $S_{\text{int}}[\varphi]$, and then using the defining property of the Gaussian measure (2.1.4). As usual, it is convenient to introduce a graphical representation for the interaction terms and their Wick contractions.

In the Feynman diagram representation, a monomial of order $2q$ in the field is represented by a $2q$-valent vertex; while this is a useful representation for the spacetime integrals arising from Wick contractions because all the fields in a monomial are at the same spacetime point, it clearly misses the tensor structure, and it cannot help us in distinguishing different invariants built out of the same number of fields. To take that into account, two types of representations are typically employed, in which the perturbative expansion is represented by either stranded graphs or edge-colored graphs.

The former is a natural generalization of the ribbon graphs of matrix models, but it can result in rather heavy drawings, as each propagator is represented by three (or more, for higher rank models) parallel lines. It is then more convenient to represent the tensor invariants as *colored graphs* [79]: we represent every tensor field as a node (black and white for φ and $\bar{\varphi}$, respectively, if the field is complex) and every contraction of two indices as an edge. Each edge is assigned a color red, blue, or green (or a label 1, 2, or 3) corresponding to the positions of the indices in the tensor. We call the resulting graphs 3-colored graphs (or sometimes *bubbles*). The three different representations of the tetrahedron invariant (2.1.5) are depicted in Fig. 2.1.

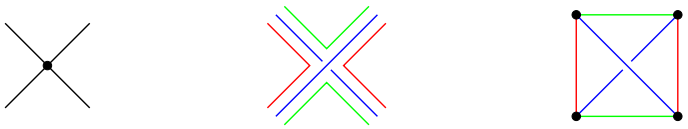

Figure 2.1: The tetrahedral vertex in three different representations; from left to right: the Feynman diagram representation, the stranded representation, and the 3-colored graph representation. In the last two, the colors label the different indices of a tensor.

In the perturbative expansion around the free theory, we represent the free propagators as edges of a new color, connecting two different nodes (the two tensor fields whose Wick contraction leads to that propagator). We choose the black color for the propagator lines, or equivalently, the label 0. When representing the interaction bubbles as 3-colored graphs, the perturbative expansion is then captured by 4-*colored graphs*. We give two examples of 4-colored graphs in Fig. 2.2, to be compared with the respective standard Feynman diagrams in Fig. 2.3, obtained by shrinking the edges[4] of colors from 1 to r. The latter offer a more intuitive representation of Feynman integrals, but the 4-colored graphs

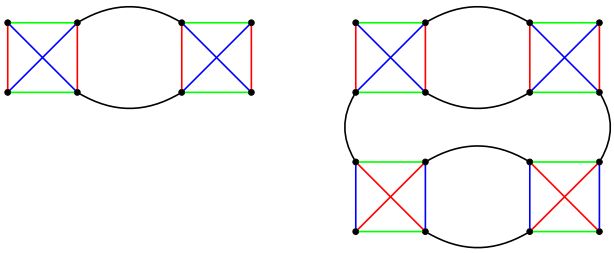

Figure 2.2: Two 4-colored graphs in the perturbative expansion of the four-point function, with tetrahedron interaction vertices drawn in red, blue, and green colors, and propagators drawn in black. The resulting structure of index contractions of the external tensor are equivalent to the pillow (left) and double-trace (right) invariants.

are necessary in order to identify the scaling in N. Indeed, in a 4-colored graph, each propagator identifies all three indices on its two end tensors, whereas each edge of color i identifies only one pair of indices between its end tensors. The indices of color i will then circulate along cycles of alternating color $0i$, which we call *faces*, and each face gives rise to a free sum, resulting in a factor N. The amplitude of a vacuum Feynman diagram $\mathcal{G}$ (i.e. one from the expansion of $W[0]$) thus scales as

$$A(\mathcal{G}) \sim N^{F-\sum_b(\frac{3}{2}(q_b-1)+\rho_b)n_b}\,, \tag{2.1.8}$$

[4]The operation of shrinking a given edge is defined by deleting the edge and identifying its two endpoints.

Figure 2.3: Two Feynman diagrams obtained from the two 4-colored graphs of Fig. 2.2 by shrinking the colored edges. Half-edges are also added to keep track of the external fields.

with F the total number of faces in the associated 4-colored graph and n_b the number of bubbles of the interaction b. The existence of the large-N limit relies on the fact that the power of N is bounded from above for an appropriate choice of ρ_b [38, 79]. Following [38], we take

$$\rho_b = \frac{F(I_b) - 3}{2}\,, \tag{2.1.9}$$

with $F(I_b)$ counting the total number of cycles of alternating colors i and j with $i, j \in \{1, 2, 3\}$ in the 3-colored graph representing the invariant I_b. As shown in [38], this is the optimal choice of scaling leading to a nontrivial large-N limit.

Melonic graphs and melonic diagrams. Melonic k-valent graphs are defined constructively starting from the fundamental melon, i.e. the unique graph built out of two k-valent vertices without forming self-loops (or tadpoles), and then iteratively inserting on any edge a fundamental melonic 2-point graph, i.e. the graph obtained from the fundamental melon by cutting one edge (also known as sunset diagram in the $k = 4$ case), see Fig. 2.4. An example of the final result was given in Fig. 1.2. Notice that melonic k-valent graphs are always bipartite, and edge-colorable with k colors.

Figure 2.4: The *fundamental melon* (left) and the fundamental melonic 2-point diagram (right) for a model with quartic interaction. In this case, the latter is also known as *sunset diagram*, while for higher-order interactions sometimes the name *banana diagrams* is also used [83].

An important result in rank-r tensor models is that if one only allows for interaction bubbles which are melonic r-valent graphs, then in the perturbative expansion the leading order vacuum graphs at large N are melonic $(r+1)$-valent graphs [36]. However, it is important to notice that melonic $(r+1)$-valent graphs do not correspond to melonic Feynman diagrams, i.e. they do not remain melonic after shrinking the edges of colors from 1 to r. From the point of view of the Feynman diagrams, melonic $(r + 1)$-valent graphs reduce to the same type of cactus diagrams appearing in the large-N limit of vector models, and therefore field theories based on such interactions are not expected to lead to very different results than vector models.[5]

Adding non-melonic bubbles, things get more complicated, and possibly more interesting. It was proved in [38] that any $O(N)^3$-invariant interaction bubble can be scaled in such a way that a $1/N$

[5] They can nevertheless lead to new phases with patterns of spontaneous symmetry breaking which are impossible in the vector case [84].

expansion exists, to which it contributes at leading order, and that for some interactions (in that specific example, the quartic tetrahedron interaction (2.1.5)) their leading-order *Feynman diagrams* are melonic. The possibility of restricting the spacetime Feynman diagrams to the melonic type by means of a large-N limit has been a main reason for studying tensor field theories in dimension $d \geq 1$, starting from [56]. In this respect, we mention a few interesting studies on the combinatorial aspects: for interactions of higher order, in [85], the structure of diagrams at first leading orders has been identified; in [39] it was proved that, with tensors of prime rank and for a particular class of complete interactions (i.e. invariants corresponding to a complete graph), the dominant Feynman diagrams are melonic; in [86], the different structures of complete interactions for tensors of odd rank have been classified; in [87], melonic dominance in sextic subchromatic models (rank-3 and a particular rank-4 model) has been shown; lastly, for the $O(N)^3$ model with tetrahedron interaction, all the diagrams contributing at next-to-next-to-leading and next-to-next-to-next-to-leading order have been identified in [88].

Our case study: the quartic model. For concreteness, we concentrate here, and in virtually the whole thesis, on interactions which are at most quartic,[6] resulting in the most studied version of the potential:

$$S_{\text{int}}[\varphi] = \int \mathrm{d}^d x \left(\frac{1}{2} m^{2\zeta} \right. \quad + \frac{\lambda_t}{4N^{3/2}} \quad + \frac{\lambda_p}{12N^2} \sum_{\text{col.perm.}} \quad + \frac{\lambda_d}{4N^3} \left. \right) . \tag{2.1.10}$$

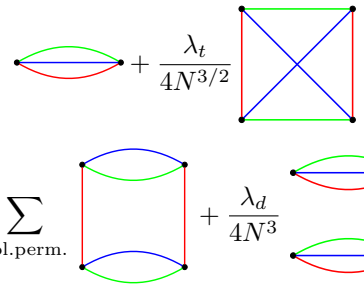

Here, the first invariant is a mass term, while the second is the tetrahedron, which we have already encountered, and which is the only complete interaction of order four; lastly, the third and fourth invariants are known as pillow [92] and double-trace, respectively. The subscripts of the coup[lings come of course from the name of the respective interaction bubbles. Notice that there are actually three pillow invariants, distinguished by the choice of color on the vertical edges: by summing over color permutations (which we have divided by a factor 3 for convenience), with the same coupling λ_p, we enforce a color symmetry on the action, i.e. a permutation group S_3 acting on the indices. In general, bubbles which are composed of one or several connected components are referred to as single-trace or multi-trace, respectively, for analogy with the matrix case, and bubbles I_b for which $\rho_b = 0$ are called *maximally single trace* (MST) [39], as each of their 2-colored subgraphs are connected, i.e. they are like the graph of a matrix single-trace invariant. The mass and tetrahedron invariants are the only MST bubbles in our action.

A sextic model. As an example of a different model, we consider a theory of complex scalars, with $U(N)^3$ invariance, and sextic interactions [93]. The MST invariant leading to melonic diagrams in this case is the complete bipartite graph $K_{3,3}$, resembling a wheel, hence we call this model the *wheel*

[6] Notice also that the number of possible interactions at higher orders grows very fast; for an explicit counting, see [89–91], as well as [61].

model. More explicitly, the latter has the following interacting action:

$$S_{\rm int}[\varphi,\bar\varphi] = \int \mathrm{d}^d x \left(\frac{\lambda_1}{6N^3} + \frac{\lambda_2}{6N^4} + \frac{\lambda_3}{6N^4} + \frac{\lambda_4}{6N^5} + \frac{\lambda_5}{6N^6} \right) , \tag{2.1.11}$$

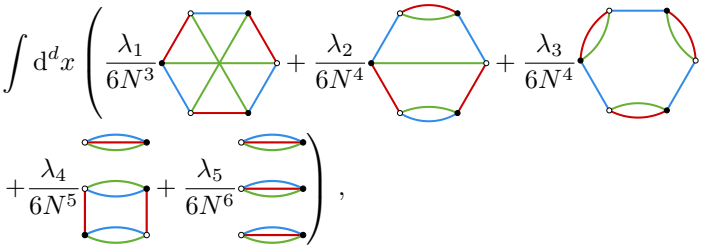

where the optimal scaling (2.1.9) is chosen, and a (normalized) sum over color permutations should be understood, whenever it is non-trivial.

The $1/N$ expansion. For the model with interaction (2.1.10) the $1/N$ expansion was proved in [38]. In order to see it in the simplest possible way, let us first get rid of pillow and double-trace vertices by observing that they can be obtained as radiative corrections from the tetrahedral vertex: the pillow is a one-loop rung (Fig 2.2, left), and the double-trace is a ladder made out of two such rungs with different color inside their loop (Fig 2.2, right). Replacing the pillow and double-trace vertices in a graph by their minimal resolution in terms of tetrahedral vertices one associates with any graph $\mathcal{G}$ a graph $\hat{\mathcal{G}}$ having *only* tetrahedral vertices but the same scaling in N:

$$F(\mathcal{G}) - \frac{3}{2} n_t(\mathcal{G}) - 2n_p(\mathcal{G}) - 3n_d(\mathcal{G}) = F(\hat{\mathcal{G}}) - \frac{3}{2} n_t(\hat{\mathcal{G}}) \,. \tag{2.1.12}$$

Starting from $\hat{\mathcal{G}}$ one can build three *jackets* [33, 38] $\mathcal{J}^i$, i.e. ribbon graphs[7] obtained by ignoring the faces of color $0i$. Each jacket has a non-orientable genus $k(\mathcal{J}^i) \geq 0$ and the number of faces[8] $F(\mathcal{J}^i) = n_t(\hat{\mathcal{G}}) + 2 - k(\mathcal{J}^i)$. As every face belongs to two jackets, the total number of faces of $\hat{\mathcal{G}}$ is

$$F(\hat{\mathcal{G}}) = \frac{3}{2} n_t(\hat{\mathcal{G}}) + 3 - \frac{1}{2} \sum_i k(\mathcal{J}^i) \,. \tag{2.1.13}$$

Denoting $\omega(\mathcal{G}) = \frac{1}{2}\sum_i k(\mathcal{J}^i) \in \frac{1}{2}\mathbb{N}_0$ the *degree* of the original graph $\mathcal{G}$, the scaling with N of a connected vacuum graph is

$$A(\mathcal{G}) \sim N^{3-\omega(\mathcal{G})} \,, \tag{2.1.14}$$

and therefore the free energy $W[0]$, divided by N^3, has an expansion in powers of $1/\sqrt{N}$.

Lastly, following the proofs in [35, 38, 56], one can show that $\mathcal{G}$ has degree zero if and only if $\hat{\mathcal{G}}$ is a melonic Feynman diagram (i.e. it is melonic on color-0 edges). In few sentences, the proof goes as following: first, one notices that from the definition of degree it follows that $\omega(\mathcal{G}) = 0$ if and only if all the jackets are planar; next, one proves that if $\omega(\mathcal{G}) = 0$ then there exists at least one face of length two, i.e. for some color i there are two vertices belonging to a cycle of color $0i$ passing through exactly two propagators (lines of color 0), and no faces of length one or three; lastly, one shows that the graph is two-particle reducible on two pairs of the four remaining edges coming out of the two vertices of the face of length two (see Fig. 2.5), and by iteration (on the graphs G_1 and G_2 of Fig. 2.5, that are also leading-order two-point diagrams) a melonic structure is uncovered .

By such argument, the leading order diagrams are melonic *after* substituting all the pillows and double-trace vertices by their minimal realizations in terms of the tetrahedral vertex. In terms of the

[7] The ribbon graphs are made evident in the stranded representation, where one replaces each black line and vertex by three parallel red, green, and blue lines: a jacket $\mathcal{J}^i$ is then obtained by simply deleting color i.

[8] It is at this point that one uses the fact that $\hat{\mathcal{G}}$ has only tetrahedral vertices. This construction is slightly more complicated on the original graph $\mathcal{G}$, as the jackets of $\mathcal{G}$ are not necessarily connected [38].

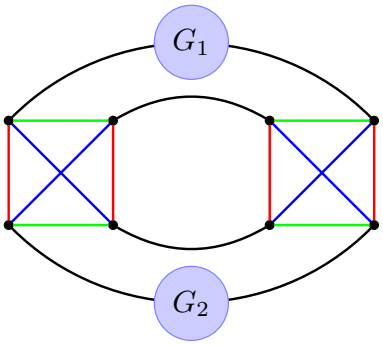

Figure 2.5: A face of length two (the internal black and red cycle) in a leading-order diagram, with its two-particle reducible structure.

original interactions in $\mathcal{G}$, one gets *melon-tadpole* diagrams [41], that is, diagrams obtained by iterated insertions of melons or tadpoles into melons or tadpoles, see Fig. 2.6. Observe that all the tadpoles are based on either pillow or double-trace vertices, while the end vertices of the melons are tetrahedral.

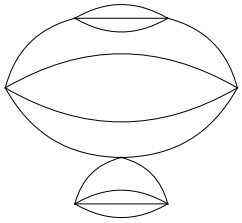

Figure 2.6: An example of melon-tadpole diagram, where all the invariants have been shrunk to point-like vertices.

2.2 The symmetric traceless and antisymmetric tensor models

In this section, we will review the case of combinatorial models with symmetric traceless and antisymmetric tensors. Such models might naively seem the simplest choice to start with, but they are actually among the most complicated ones. The fact that also these models admit a melonic large-N limit [40, 41] was understood only several years later than for the colored tensor models [32–35]. This was partially due to the fact that the first tensor models, introduced in [27, 28], were built on tensors of the type $S_{abc} + \mathrm{i}\, A_{abc}$, where S and A are totally symmetric and antisymmetric tensors, respectively, and they were known to have "bad tadpoles" (see [41]), whose proliferation would arbitrarily increase the power in N of a diagram, thus leading to no new interesting large-N limit. A breakthrough came with the imposition of a tracelessness condition on the symmetric tensors [40], which a posteriori seems rather natural: a general rank-3 symmetric tensor contains traces, which are in the fundamental representation, and therefore tend to favor tadpoles. The formal proof for the melonic limit of symmetric traceless and antisymmetric tensors was then given in [41], and later generalized to the case of mixed symmetry irreducible representations in [42]. We review here the basic ideas and main results of [41], without proofs, as they are rather long and technical.

Let us first consider real rank-3 tensors having no symmetry property under permutation of their indices, thus having N^3 independent components, and transforming in the direct product of three copies of the fundamental representation of the orthogonal group $O(N)$:[9]

$$T_{a_1a_2a_3} \to T'_{a_1a_2a_3} = (O\cdot T)_{a_1a_2a_3} := \sum_{b_1,b_2,b_3} O_{a_1b_1} O_{a_2b_2} O_{a_3b_3} T_{b_1b_2b_3} \ , \qquad O \in O(N) \ . \tag{2.2.1}$$

Although similar to the models built out of the fundamental representation of $O(N)^3$ of the previous section, a tensor model built upon (2.2.1) differs from them in an important aspect: all the indices of the tensor transform with the same orthogonal matrix, hence one can build invariants in which an index in the first position on a tensor is contracted with an index in another position, say the third position, on another tensor, or even on the same tensor.

We denote $\mathbf{1}$ the identity operator in the space of tensors $\mathbf{1}_{a_1a_2a_3,b_1b_2b_3} = \delta_{a_1b_1}\delta_{a_2b_2}\delta_{a_3b_3}$, and:

$$T\mathbf{1}T \equiv \sum_{\substack{a_1,a_2,a_3\\ b_1,b_2,b_3}} T_{a_1a_2a_3} \mathbf{1}_{a_1a_2a_3,b_1b_2b_3} T_{b_1b_2b_3} \ , \qquad \partial_T \mathbf{1} \partial_T \equiv \sum_{\substack{a_1,a_2,a_3\\ b_1,b_2,b_3}} \frac{\partial}{\partial T_{a_1a_2a_3}} \mathbf{1}_{a_1a_2a_3,b_1b_2b_3} \frac{\partial}{\partial T_{b_1b_2b_3}} \ .$$

The Gaussian integral with covariance $\mathbf{1}$, can be represented as a differential operator [79, 94]; for example, the free 2-point function is written as:

$$\langle T_{a_1a_2a_3} T_{b_1b_2b_3} \rangle_0 = \int [dT]\, e^{-\frac{1}{2}T\mathbf{1}T}\, T_{a_1a_2a_3} T_{b_1b_2b_3} = \left[e^{\frac{1}{2}\,\partial_T \mathbf{1} \partial_T}\, T_{a_1a_2a_3} T_{b_1b_2b_3} \right]_{T=0} = \mathbf{1}_{a_1a_2a_3,b_1b_2b_3} \ ,$$

and its full contraction gives $\langle T\mathbf{1}T\rangle_0 = N^3$. The generic tensor model with tetrahedral interaction is defined by the action:

$$S(T) = \frac{1}{2} \sum_{a_1,a_2,a_3} T_{a_1a_2a_3} T_{a_1a_2a_3} - \frac{\lambda}{4N^{3/2}} \sum_{a_1 \dots a_6} T_{a_1a_2a_3} T_{a_3a_4a_5} T_{a_5a_2a_6} T_{a_6a_4a_1} \ , \tag{2.2.2}$$

where the sign of the coupling constant follows the usual conventions in matrix models [24]. The explicit power of N in the interaction term is well known in tensor models and it is the only one which

[9] Here we use the symbol T for the tensor, rather than φ, as this is more standard in $d = 0$.

can lead to an interesting large N limit [38, 40, 79]. The partition function and the (appropriately normalized) first derivative of the free energy are:

$$Z_{\mathbf{1}}(\lambda) = \int [dT]\; e^{-S(T)} = \left[e^{\frac{1}{2}\,\partial_T \mathbf{1} \partial_T}\; e^{\frac{\lambda}{4N^{3/2}} \sum_{a_1 \dots a_6} T_{a_1 a_2 a_3} T_{a_3 a_4 a_5} T_{a_5 a_2 a_6} T_{a_6 a_4 a_1}} \right]_{T=0} ,$$
$$F_{\mathbf{1}}(\lambda) = \frac{4}{N^3} \lambda \partial_\lambda \ln Z_{\mathbf{1}}(\lambda) . \tag{2.2.3}$$

In order to simplify the combinatorics it is convenient to work with $F_{\mathbf{1}}(\lambda)$, rather than the free energy $\ln Z_{\mathbf{1}}(\lambda)$, but of course the latter inherits a large-N expansion from the former, once we have established that.

As discussed at the beginning of this Chapter, unlike the fundamental representation of $O(N)^3$, which is irreducible, the direct product of three copies of the fundamental representation of $O(N)$ is a reducible representation. Therefore, a generic tensor transforming as in (2.2.1) can be decomposed in irreducible components. This is achieved by removing its traces, and decomposing the rest in terms of irreducible representations of the symmetric group $\mathfrak{S}_3$, which commutes with the action of $O(N)$. The result is a decomposition of $T_{a_1 a_2 a_3}$ into the following irreducible objects: a completely symmetric and traceless tensor, a completely antisymmetric one, two tensors with mixed symmetry, and three lower-rank tensors (the traces, which in our rank-3 case correspond to vector representations). Under such a decomposition, the quadratic part of the action (2.2.2) partially diagonalizes[10], while the quartic interaction leads to a mixing between the various irreducible components. From the point of view of model building, the traces lead to hybrid models, mixing different ranks, such as the models studied in [95], and they would require a different scaling in N. The tensors with mixed-symmetry have been considered in [42], but here we will restrict to the completely symmetric or antisymmetric components. The two can mix in the quartic interaction resulting in a term with two antisymmetric and two symmetric tensors; however, for the sake of simplicity, we will not consider possible mixing between irreducible components, and we will deal with either *completely symmetric and traceless* or *completely antisymmetric* tensors.

We denote $\mathbf{A}$ the orthogonal projector on antisymmetric tensors, and $\mathbf{\Sigma}$ the orthogonal projector on symmetric traceless tensors, and generically $\mathbf{P} = \mathbf{A}, \mathbf{\Sigma}$ one of the two projectors. The tensor models for symmetric traceless and antisymmetric tensors with tetrahedral interaction are obtained from the generic model of Eq.(2.2.3) by allowing the propagation of only the antisymmetric (respectively symmetric traceless) modes of the tensor:[11]

$$F_{\mathbf{P}}(\lambda) = \frac{4}{N^3} \lambda \partial_\lambda \ln \left\{ \left[e^{\frac{1}{2}\,\partial_T \mathbf{P} \partial_T}\; e^{\frac{\lambda}{4N^{3/2}} \sum_{a_1 \dots a_6} T_{a_1 a_2 a_3} T_{a_3 a_4 a_5} T_{a_5 a_2 a_6} T_{a_6 a_4 a_1}} \right]_{T=0} \right\} . \tag{2.2.4}$$

Because only the projected modes $\mathbf{P}T$ propagate, one can either take Eq.(2.2.4) as definition and consider that the tensor T still has no symmetry property under permutation of its indices, or one can change variables to $P = \mathbf{P}T$ and write equivalently:

$$F_{\mathbf{P}}(\lambda) = \frac{4}{N^3} \lambda \partial_\lambda \ln \left\{ \left[e^{\frac{1}{2}\,\partial_P \mathbf{P} \partial_P}\; e^{\frac{\lambda}{4N^{3/2}} \sum_{a_1 \dots a_6} P_{a_1 a_2 a_3} P_{a_3 a_4 a_5} P_{a_5 a_2 a_6} P_{a_6 a_4 a_1}} \right]_{P=0} \right\}$$
$$\frac{\partial}{\partial P_{a_1 a_2 a_3}} P_{b_1 b_2 b_3} \equiv \mathbf{P}_{a_1 a_2 a_3, b_1 b_2 b_3} , \tag{2.2.5}$$

[10] Each of the two degenerate sectors of the two tensors with mixed symmetry and of the three traces remain internally mixed.

[11] This is equivalent to giving an infinite mass to the orthogonal modes $(\mathbf{1} - \mathbf{P})T$ of the tensor.

where this time the tensor P is antisymmetric or symmetric traceless. Observe that the second line is a definition.

The $1/N$ expansion of the symmetric traceless and respectively antisymmetric tensor model in rank 3 with tetrahedral interaction is encoded in the following theorem, the main result of [41]:

Theorem 1. *We have (in the sense of perturbation series):*

$$F_{\mathbf{P}}(\lambda) = \sum_{\omega \in \mathbb{N}/2} N^{-\omega} F_{\mathbf{P}}^{(\omega)}(\lambda) \, .$$

The nontrivial part is to show that the degree ω is non-negative. In order to prove that, we first need to improve the naive perturbative expansion by performing a resummation of tadpole and melon insertions. That is, one replaces the interaction term by a normal ordered one, and the propagator by a resummed one:

$$F_{\mathbf{P}}(\lambda) = \frac{4}{N^3} \lambda \partial_\lambda \ln \left\{ \left[e^{\frac{1}{2} K(\lambda,N) \partial_T \mathbf{P} \partial_T} \; e^{\frac{\lambda}{4N^{3/2}} :\sum_{a_1 \dots a_6} T_{a_1 a_2 a_3} T_{a_3 a_4 a_5} T_{a_5 a_2 a_6} T_{a_6 a_4 a_1} :_{K(\lambda,N)}} \right]_{T=0} \right\} . \tag{2.2.6}$$

Here $K(\lambda, N)$ is a renormalized covariance solving a quartic equation. For N large and λ small enough, such equation admits[12] a solution $K(\lambda, N)$, which is a series in both λ and $N^{-1/2}$, uniformly bounded in both N and λ, such that $\lim_{N\to\infty} K(\lambda, N)$ is the generating function of the 4-Catalan numbers, and

$$\lim_{\lambda \to 0} \left[\lim_{N \to \infty} K(\lambda, N) \right] = 1 \, .$$

The subtracted interaction $: T^4 :_K$ is "Wick ordered" up to second order in λ with respect to the measure with covariance $K\mathbf{P}$. The perturbative expansion generates now Feynman graphs with no tadpoles and no melons. As $K(\lambda, N)$ is itself a series in $N^{-1/2}$, the $1/N$ expansion in Theorem 1 follows from the following Proposition, whose proof is the most tedious part of [41]:

Proposition. *Let $\hat{\mathcal{S}}$ be a connected stranded graph with no tadpoles and no melons. Then $\omega(\hat{\mathcal{S}}) \geq 0$.*

In a second stage, one can prove that the model is dominated by melon diagrams:

Theorem 2. *The leading order contribution $F_{\mathbf{P}}^{(0)}(\lambda)$ is a sum over melonic stranded maps.*

We refer again to [41] for the proof of this theorem.

[12] It is at this stage that the $1/N$ expansion fails for a symmetric tensor with no tracelessness condition: such a function $K(\lambda, N)$ does not exist in that case.

2.3 $U(N)^2 \times O(D)$ multi-matrix models

An alternative point of view on tensor models has been advocated in [96], and further studied in [39, 97–102]. The main idea is that considering rank-3 tensors with two indices associated to a vector space of dimension N and the third one to another space of dimension D, we can think of such "rectangular" tensors as a collection of D matrices of size $N \times N$. This offers the possibility of a link to string theory, where the number of bosonic matrices usually corresponds to the number of space dimensions transverse to the D-branes. In such setting, the matrix theory typically has a global $O(D)$ symmetry, and therefore it becomes possible to consider simultaneously the planar large-N limit, and the large-D limit. The latter could serve as an implementation string theory of the large dimension limit in general relativity [103]. However, as observed in [96], in order to obtain an interesting large-D limit, one should borrow the scaling of couplings from the $O(N)^3$ model [38], appropriately redistributed in terms of N and D.

Besides the string theory interpretation, the introduction of the new parameter D is interesting from a combinatorial perspective, and it might find new applications also in QFT. Clearly, the simultaneous large-N and large-D limit coincides with the large-N limit of tensor models; however, the subleading orders are now arranged in a two-parameters series, in $1/N$ and $1/D$, therefore providing more control on the classification of the perturbative diagrams. This possibility was exploited in [100], whose main ideas and results will now be reviewed.

We consider an O(D)-invariant complex matrix model in zero dimension. The basic degrees of freedom are given by D complex matrices X_μ of size $N \times N$: $(X_\mu)_{ab} = X_{\mu ab}$ with $1 \leq \mu \leq D$ and $1 \leq a, b \leq N$. Remark that writing the matrices X_μ in terms of their components $X_{\mu ab}$ makes it evident that we can think of them as the components of a rank-3 tensor with indices having different ranges. A fundamental quantity to be determined is the free energy

$$\mathcal{F}(\lambda) = \log \int [dX]\, e^{-S[X,X^\dagger]}\,, \tag{2.3.1}$$

with an action $S[X, X^\dagger]$ to be specified, and a measure $[dX] = \prod_{\mu,a,b} d\mathrm{Re}(X_\mu)_{ab}\, d\mathrm{Im}(X_\mu)_{ab}$. The global symmetry group, under which the action is invariant, is assumed to be $U(N)^2 \times O(D)$, with the following transformation law

$$X_\mu \to X'_\mu = O_{\mu\mu'} U_{(L)} X_{\mu'} U^\dagger_{(R)}\,, \tag{2.3.2}$$

where O is an orthogonal matrix in $O(D)$, while $U_{(L)}$ and $U_{(R)}$ are two independent unitary matrices in two distinct copies of the group $U(N)$, which we call left and right, respectively. As a result, the two matrix indices (which we omitted in Eq.(2.3.2) and in the following, as standard matrix multiplication is assumed) are distinguishable because they transform with respect to two distinct $U(N)$ groups.

Models of this type have been studied in [39, 96–99]. Here, we focus on the following invariant action:

$$S[X, X^\dagger] = ND\Big(\mathrm{Tr}\big[X^\dagger_\mu X_\mu\big] - \frac{\lambda}{2}\sqrt{D}\ \mathrm{Tr}\big[X^\dagger_\mu X_\nu X^\dagger_\mu X_\nu\big]\Big)\,, \tag{2.3.3}$$

where the interaction term is of the tetrahedral type we encountered in previous sections. The coupling constant λ has been scaled in such a way that it is kept fixed as $N, D \to +\infty$. Indeed, this is the right scaling so as to obtain well-defined large N and large D expansions [96], as further detailed below.

The perturbative expansion in λ of the free energy $\mathcal{F}(\lambda)$ admits as usual a graphical representation in terms of Feynman graphs. These Feynman graphs can be represented in three equivalent ways:

- as connected 4-regular directed orientable maps (with self-loops/tadpoles and multiple edges allowed) such that: each vertex has two outgoing and two ingoing half-edges, and furthermore, the two outgoing (resp. two ingoing) half-edges appear on opposite sides of the vertex (see Figure 2.7, left panel);

- as connected 4-regular directed orientable stranded graphs, obtained from the above representation upon replacement of each edge by a triple of parallel strands: two external and one internal, as illustrated in the top right corner of Figure 2.7. The external strands carry the indices of the two U(N) symmetry groups, and can therefore be distinguished. An external strand is called *left* (resp. *right*) if it is on the left (resp. right) side, with respect to the orientation, of an edge connecting two half-edges. Besides, the internal strand corresponds to the O(D) symmetry group. The contraction pattern of the three types of strands at each vertex follows from the structure of the tetrahedral interaction (see Figure 2.7, right panel). It is such that a strand of a given type (left, right, or internal) is always connected to another strand of the same type. In a Feynman graph, the strands are closed into loops. The loops made out of external strands correspond to the faces of the underlying 4-regular map, and together form a ribbon graph; we call them *L- or R-faces*, depending on whether they are constituted of left or right strands. As for the loops made out of internal strands, we will call them *straight faces* or O(D)*-loops*.

- as connected 4-colored graphs, obtained in the usual way as in tensor models [79]. From this perspective, the Feynman graphs can also be viewed as dual to discretizations of three-dimensional pseudo-manifolds, but these are in general non-orientable [104].

This results in a nice geometric interpretation of the Feynman graphs. First, as in similar one-matrix models, the ribbon structure generated by the propagation of U(N)^2 indices is dual to quadrangulated orientable surfaces of arbitrary genus. Second, as the result of the O(D) symmetry, these surfaces are decorated by specific patterns of cycles, referred to as O(D)-loops, which only intersect at vertices. In this combinatorial space, the statistical properties of the genus are controlled by the large-N limit, while the proliferation of O(D)-loops – captured by a second integer number [96] that we call the grade – is directly tied to the large-D limit. This already suggests that, by suitably correlating the two limits, one might be able to balance the interactions between topological (genus) and combinatorial (O(D)-loops) aspects, in such a way that the model is driven to different universality classes in the continuum.

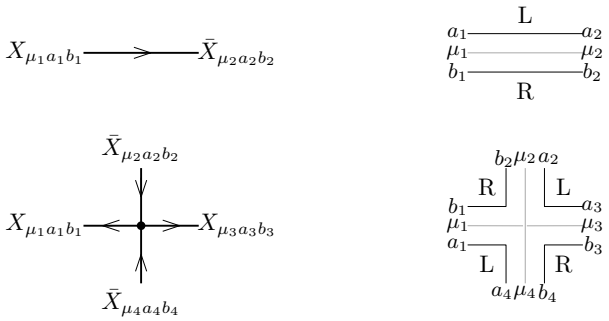

Figure 2.7: Propagator and vertex in the map (left) and stranded graph (right) representations. For simplicity, the edge orientations are left implicit in the stranded representation (note however that fixing the orientation is equivalent to choosing R and L sides).

As first shown in [96], the free energy has a double expansion in $1/N$ and $1/\sqrt{D}$, reading:

$$\mathcal{F}(\lambda) = \sum_{g\in\mathbb{N}} N^{2-2g} \sum_{\ell\in\mathbb{N}} D^{1+g-\frac{\ell}{2}} \mathcal{F}_{g,\ell}(\lambda)\,. \tag{2.3.4}$$

In this expression, $g \in \mathbb{N}$ is the *genus* of the Feynman graphs, which corresponds to the genus of the 4-regular maps, or equivalently, to the genus of the corresponding $U(N)^2$ ribbon graphs. It is defined through Euler's relation

$$2-2g = -e+v+f_L+f_R = -v+f\,, \tag{2.3.5}$$

where e is the number of edges or propagators, v is the number of vertices ($e = 2v$ since the maps are 4-regular), f_L (resp. f_R) is the number of L-faces (resp. R-faces) and $f = f_L + f_R$. The quantity $\ell \in \mathbb{N}$ is another parameter associated with the Feynman graphs; it is related to the *index* (see below), which was defined in full generality in [39]. In the present case, the parameter ℓ is given by:

$$\frac{\ell}{2} = 2 + v - \frac{1}{2}f - \varphi\,, \tag{2.3.6}$$

where φ is the number of straight faces or $\mathrm{O}(D)$-loops. It can also be expressed, using Eq. (2.3.5), as

$$\frac{\ell}{2} = 1 + g + \frac{1}{2}v - \varphi\,. \tag{2.3.7}$$

As seen from Eq. (2.3.4), the parameter ℓ introduces an extra grading in the standard genus expansion of matrix models. We therefore refer to it as the *grade*.[13]

The fact that the grade is non-negative is made evident by rewriting it as

$$\frac{\ell}{2} = g_L + g_R\,, \tag{2.3.8}$$

where g_L (resp. g_R) is the genus of the ribbon graph obtained from a Feynman graph in the stranded representation, by deletion of the L (resp. R) strands. Since $g_i \in \frac{\mathbb{N}}{2}$ for $i = L, R$ (the corresponding ribbon graphs are not necessarily orientable), it follows that $\ell \in \mathbb{N}$.

Another important combinatorial quantity is the *degree* [37, 38]:

$$\omega = g + \frac{\ell}{2}\,, \tag{2.3.9}$$

a close relative of the *Gurau degree* [33, 34], also known as the *index* in the more general context of [39]. For $D = N$, we recover the large N structure of $\mathrm{U}(N)^2 \times \mathrm{O}(N)$ [37] and $\mathrm{O}(N)^3$ [38] tensor models that we encountered in (2.1.14):

$$\mathcal{F}(\lambda) = \sum_{\omega\in\frac{\mathbb{N}}{2}} N^{3-\omega} \mathcal{F}_{\omega}(\lambda)\,. \tag{2.3.10}$$

Using equations (2.3.5) and (2.3.6), the degree can also be written as

$$\omega = 3 + \frac{3}{2}v - f - \varphi\,, \tag{2.3.11}$$

which does not refer to two-dimensional topology and coincides with the familiar expression found in the tensor models literature.

[13] Notice that the parameter ℓ was called index in [96], while this name was used for a different quantity in [39]. In order to avoid confusion, here we introduce a new name for it.

We wish to reorganize (2.3.4) as

$$\mathcal{F}(\lambda) = \sum_{g\in\mathbb{N}} \left(\frac{N}{\sqrt{D}}\right)^{2-2g} \sum_{\ell\in\mathbb{N}} D^{2-\frac{\ell}{2}} \mathcal{F}_{g,\ell}(\lambda)\,, \tag{2.3.12}$$

from which it is evident that if we keep

$$M := \frac{N}{\sqrt{D}} \tag{2.3.13}$$

fixed as we take $N \to \infty$ and $D \to \infty$, we obtain

$$\lim_{\substack{N,D\to\infty \\ M<\infty}} \frac{1}{D^2}\mathcal{F}(\lambda) = \sum_{g\geq 0} M^{2-2g}\mathcal{F}_{g,0}(\lambda) \equiv \mathcal{F}^{(0)}(M,\lambda)\,. \tag{2.3.14}$$

In other words, by allowing $D \neq N$, but keeping the ratio (2.3.13) fixed, we have a *double-scaling limit* that selects Feynman graphs with $\ell = 0$, but of arbitrary genus. Since such graphs are much less than all the possible graphs, they can lead to a summable series.

As usual, we are interested in determining the critical point λ_c, which we do not expect to depend on g, and the critical exponent $\gamma(g)$, associated to a non-analytic behavior of the free energy such as $\mathcal{F}_{g,0}(\lambda)_{\text{crit}} \sim (\lambda - \lambda_c)^{2-\gamma(g)}$. Determining the critical properties of the model is interesting both from the combinatorial and physical point of view: from the critical point and critical exponent we can infer the asymptotic number of graphs for large number of vertices, which is a standard objective in combinatorics; and from the physical point of view, the critical model determines the continuum limit of the geometrical objects dual to the Feynman graphs, as in the limit $\lambda \to \lambda_c$ the average number of vertices typically diverges [24].

In principle, we could use $\mathcal{F}^{(0)}(M,\lambda)$ as a generating function for $\mathcal{F}_{g,0}(\lambda)$, and use the latter to define a continuum limit at fixed g. However, since we expect λ_c to be genus-independent, we can also find a combination of M and $\lambda - \lambda_c$ to keep fixed for a *triple-scaling limit*. More precisely, if $\gamma(g) = a + bg$, then we have

$$\lim_{\substack{M\to\infty \\ \lambda\to\lambda_c^-}} \frac{1}{M^2(\lambda-\lambda_c)^{2-a}}\mathcal{F}^{(0)}(M,\lambda) = \sum_{g\in\mathbb{N}} \kappa^{2g} f_g\,, \tag{2.3.15}$$

with $\kappa^{-1} = M(\lambda - \lambda_c)^{b/2}$ fixed. Since the large-D limit selects for each genus g a subset of diagrams, we expect that the series in Eq. (2.3.15) will have an improved convergence with respect to the usual double-scaling limit of matrix models, which is not even Borel summable [24]. In fact, we find that the triple-scaling limit leads to a series with a finite radius of convergence [100].

The main results of [100] are quite technical, requiring definitions of schemes [105,106], separating and non-separating dipoles, and so on. Here, we limit ourselves to briefly summarizing the main findings in words, and we refer to the original paper for details.

The first main result is the complete recursive characterization of Feynman graphs with vanishing grade and arbitrary genus, which are precisely the ones that survive in a double-scaling limit where N and D are sent to infinity while keeping the ratio N^2/D finite.

Restricting attention to a particular subclass of graphs – the *dominant* graphs – which govern the critical regime of this double-scaled theory, we established that they have a plane binary tree structure. As a result, their partition function (which we obtain through a triple-scaling of the multi-matrix model, as described above) has a critical point dominated by large trees, which however describe orientable surfaces with a large genus, associated to the number of leaves of the tree. The expectation value of the genus (or equivalently the size of the trees) diverges at criticality, and even

though its samples look naively quite different from a tree, this ensemble converges in the continuum limit to the universality class of branched polymers.

Besides the free energy, which can be viewed as the generating function of vacuum diagrams with v vertices, it is quite natural in combinatorics to consider other generating functions, with further restrictions. Restricting to the class of 3-edge connected graphs, also known in physics as two-particle irreducible (2PI) graphs, forbids tadpoles and triple edges. On top of being an interesting class of diagrams from the combinatorial point of view, the 2PI restriction is also natural in the context of two-dimensional quantum gravity, where tadpoles and multiple edges are viewed as dual to degenerate quadrangulations [107]. Surprisingly, with such a restriction in the triple-scaling limit, we found a very different critical behavior, falling in the universality class of Liouville quantum gravity (or, in other words, the Brownian sphere) [108–111]. This change of universality class resulting from the 2PI condition is an interesting new feature, not shared by the usual large-N limit, which in contrast displays universality under such type of change of ensembles [112].

We finally note that, while some of the questions and results above are tied to the random-geometric context, the general characterization of higher-genus leading-order Feynman graphs might be of broader interest. In higher dimension, it might for instance provide an opportunity to embed the melonic regime of SYK-like tensor/matrix quantum-mechanical models and large-N tensor quantum field theory, into a genus expansion tractable enough to allow explicit computations (of e.g. quantum corrections to operator dimensions).

Chapter 3

2PI formalism

As discussed in the introduction, a great boost for studying for studying QFTs with a melonic limit came from the SYK model and the realization that tensor models provide a valid alternative to it, notably without the quenched disorder [55].

While they coincide at leading order, the SYK model and its tensor analogues are quite different at subleading orders [53]. Moreover, tensor field theories have many more covariant and invariant (or singlet) operators [61, 80, 89, 90]. This has rather drastic consequences: one-dimensional tensor models display a large number of light modes in the infrared [61, 62] which are absent in the SYK model. In order to study these modes, and possibly to better understand the holographic dual of such theories, it would be useful to have a bilocal reformulation of the theory. In fact, while the construction of the bilocal action in the SYK model is a standard procedure for disordered systems such as spin glasses [113,114], it is not tied to disorder and it can also be understood in a more general context as a special case of the collective field method [10]. However, until now, no collective field formulation has been found for tensor models (except in the few cases in which an intermediate field representation is possible, but which do not have SYK-type behavior [73], or for a chosen subset of invariants [80, 81]): in [62] a bilocal action is *postulated* but not derived, while in [61] the existence of the new light modes is inferred from other arguments; in [115] a bilocal action is proposed for the Gurau-Witten model [32, 55], but it leads to wrong Schwinger-Dyson equations. Actually, one can expect that no simple and exact reformulation of tensor models is possible in terms of few collective variables because the collective field method of [10] is based on the idea that one could rewrite a theory with a certain symmetry directly in terms of its invariants; but while vector models have only one possible invariant (and its derivatives), and matrix models can be reduced to eigenvalues, which are much less than the original number of variables, tensor models have a much larger number of invariants and no useful reduction to eigenvalues is available so far. Furthermore, for vector models the collective field reformulation reduces the large-N expansion to a simple saddle-point (or loop) expansion, which we do not expect to be the case for tensor models.

In [116] we have proposed to use the two-particle irreducible (2PI) effective action formalism [12] (see [117] for a modern review) for tensor models and showed that it provides a useful version of the bilocal reformulation. The 2PI formalism has been applied to a variety of problems (see for example [118–121] and references therein) and it has been shown to be well suited for a $1/N$ expansion in the case of the $O(N)$ model [122, 123]. Nevertheless, it is not a very standard QFT topic, and therefore we will concisely review it in Sec. 3.1, together with its large-N expansion for the $O(N)$ model in Sec. 3.2. The connection to the collective field formalism is in this case straightforward, as

we will explain in Sec. 3.2.1.

In order to elucidate the usefulness of the 2PI effective action it is worthwhile to apply it to the SYK model first, as we will do in Sec. 3.3. It turns out that the 2PI reformulation reproduces exactly the results of [49,124–126], up to the same order in $1/N$ *without using the replica method*, i.e. without using the trick in Eq. (3.3.19). This being said, the 2PI reformulation in the SYK model has its own drawbacks:

- it requires to know explicitly the graphs contributing to each order in $1/N$. While this is exogenous to the formalism, hence not very aesthetically pleasing, the graph analysis has already been done and we are able to use this information to write the 2PI action up to the same order as the usual replica based bilocal action.
- it also fails at higher enough orders in $1/N$. This has nothing to do with replicas, although it happens at the same order at which the replica diagonal ansatz breaks down: it has to do with the lack of commutation between going on shell and taking quenched averages (this will be explained in Sec. 3.3).

The main lesson to be drawn from the 2PI reformulation of the SYK model is that the leading and next-to-leading orders in the $1/N$ expansion of the model are exactly the leading order and first loop correction in a loop expansion of the bilocal theory of [49, 124, 126]. This structure *does not survive* at higher orders: the $1/N$ expansion is a loop expansion in the annealed version of the model, but not in the quenched one.

The main point of [116] is however that the 2PI formalism becomes much more useful in the tensor case, where the issues with the quenched average are absent, and where we do not yet have an alternative collective field reformulation. Among other things, its application to the Carrozza-Tanasa-Klebanov-Tarnopolsky model [38, 56] puts on a firmer ground the result of [62] by showing that the bilocal action that they postulated is in fact the leading-order 2PI effective action. Furthermore, in the Gurau-Witten model, which we will not review here, we are able to expand the action up to fourth order in the $1/N$ expansion, highlighting a similar structure among the three subleading terms: they all have the form of a logarithm of a determinant, hence they can be interpreted as Gaussian integrals over bilocal fields. Surprisingly, all such terms can be interpreted as the one-loop correction of an auxiliary bilocal effective action.

3.1 General construction

Let us review the definition and properties of the 2PI effective action [12]. For practical purposes, we consider a theory of real bosonic scalar fields $\varphi_{\mathbf{a}}$ with classical action $\mathbf{S}[\varphi]$, where in order to keep a compact notation the index $\mathbf{a}$ denotes both a space time point and representation indices.[1] In order to simplify notation, we will sometimes omit the arguments of functionals, and therefore, to avoid confusion with independent variables, we will denote functionals by capital boldface letters. Sums, products, Kronecker deltas and traces include both flavor indices and space time points, and repeated indices are summed. We define:

$$\mathbf{W}[j,k] = \ln \int [d\varphi]\ \exp\left\{ -\mathbf{S}[\varphi] + j_{\mathbf{a}}\varphi_{\mathbf{a}} + \frac{1}{2}\varphi_{\mathbf{a}} k_{\mathbf{ab}} \varphi_{\mathbf{b}} \right\}, \tag{3.1.1}$$

[1] For example, vector indices a when the fields form a vector representation of some group, and a triplet abc for a rank-3 tensor. Later on, when useful, we will make the distinction between space time points and other indices explicit, writing for example $\varphi_{\mathbf{a}} = \varphi_a(x)$.

which is the generating functional of connected moments of a theory with shifted inverse covariance $\frac{\delta^2 \mathbf{S}}{\delta\varphi_{\mathbf{a}}\delta\varphi_{\mathbf{b}}}[0] - k_{\mathbf{ab}}$. Observe that $\mathbf{W}[j,k]$ depends only on the symmetric part of $k_{\mathbf{ab}}$ which then is assumed to be symmetric in its indices. Therefore:

$$\frac{\delta k_{\mathbf{ab}}}{\delta k_{\mathbf{mn}}} = \frac{1}{2}\mathcal{S}_{\mathbf{ab;mn}} \ , \tag{3.1.2}$$

where we have introduced the projector on symmetric matrices:[2]

$$\mathcal{S}_{\mathbf{ab;mn}} = \frac{1}{2}(\delta_{\mathbf{am}}\delta_{\mathbf{bn}} + \delta_{\mathbf{an}}\delta_{\mathbf{bm}}) \ . \tag{3.1.3}$$

To avoid cluttering, we will denote sometimes the functional derivatives as subscripts:

$$\mathbf{W}_{j_{\mathbf{a}}}[j,k] \equiv \frac{\delta \mathbf{W}}{\delta j_{\mathbf{a}}}[j,k], \qquad \mathbf{W}_{k_{\mathbf{ab}}}[j,k] \equiv \frac{\delta \mathbf{W}}{\delta k_{\mathbf{ab}}}[j,k] \ . \tag{3.1.4}$$

Using two independent sources in (3.1.1) has the advantage that one obtains several expressions for the correlations of the theory in terms of derivatives of the generating functions, which gives a certain redundancy in the description of the theory in this language: derivatives with respect to $k_{\mathbf{ab}}$ are related to repeated derivatives with respect to $j_{\mathbf{a}}$, the examples of one and two k-derivatives being explicitly worked out below. Such relations could be used as consistency checks for truncations of the generating functional which are performed in some approximation schemes where there is no small parameter, but such checks will not be needed for more systematic approximation schemes, such as the $1/N$ expansion that we are interested in here. In the following, we will use as much as possible only derivatives with respect to the bilocal source to express the interesting correlations, hence we will often put the local source on shell very early on. Alternatively one could start from the beginning by introducing only the bilocal source k. This has the drawback that not all the correlations of the theory can be obtained from the generating functional. However, all the ones which interest us in this review can.

1-point and 2-point functions. We denote $\mathbf{\Phi}$ and $\mathbf{G}$ the connected 1-point and 2-point functions of the theory with sources j and k:

$$\mathbf{\Phi}_{\mathbf{a}}[j,k] = \mathbf{W}_{j_{\mathbf{a}}}[j,k] \ , \tag{3.1.5}$$

$$\mathbf{G}_{\mathbf{ab}}[j,k] = \mathbf{W}_{j_{\mathbf{a}}j_{\mathbf{b}}}[j,k] = 2\mathbf{W}_{k_{\mathbf{ab}}}[j,k] - \mathbf{W}_{j_{\mathbf{a}}}[j,k]\mathbf{W}_{j_{\mathbf{b}}}[j,k] \ . \tag{3.1.6}$$

We are generally interested in the connected 1-point and 2-point functions of the theory without sources, for which we introduce the following notation:

$$\mathbf{\Phi}_{\mathbf{a}}[0,0] = \langle\varphi_{\mathbf{a}}\rangle_{\text{conn}} \equiv \underline{\phi}_{\mathbf{a}} \ , \qquad \mathbf{G}_{\mathbf{ab}}[0,0] = \langle\varphi_{\mathbf{a}}\varphi_{\mathbf{b}}\rangle_{\text{conn}} \equiv \underline{G}_{\mathbf{ab}} \ . \tag{3.1.7}$$

Notice that $\mathbf{G}_{\mathbf{ab}}$ (hence in particular $\underline{G}_{\mathbf{ab}}$) is symmetric in its indices.

For a free theory with covariance C we obtain:

$$\mathbf{W}^C[j,k] = -\frac{1}{2}\,\mathrm{Tr}[\ln(C^{-1}-k)] + \frac{1}{2}j_{\mathbf{a}}\left(C^{-1}-k\right)^{-1}_{\mathbf{ab}} j_{\mathbf{b}} \ . \tag{3.1.8}$$

and as a consequence:

$$\mathbf{\Phi}^C_{\mathbf{a}}[j,k] = \left(C^{-1}-k\right)^{-1}_{\mathbf{ab}} j_{\mathbf{b}} \ , \qquad \mathbf{G}^C_{\mathbf{ab}}[j,k] = \left(C^{-1}-k\right)^{-1}_{\mathbf{ba}} \ . \tag{3.1.9}$$

[2] In the case of Grassmann fields (for which we will typically use the letters ψ and Ψ instead of φ and ϕ) $k_{\mathbf{ab}}$ is antisymmetric, hence the derivative evaluates to the antisymmetric projector: $\mathcal{A}_{\mathbf{ab;mn}} = \frac{1}{2}(\delta_{\mathbf{am}}\delta_{\mathbf{bn}} - \delta_{\mathbf{an}}\delta_{\mathbf{bm}})$.

Let $\{\mathbf{J_a}[\phi,G],\mathbf{K_{ab}}[\phi,G]\}$ be the inverse of $\{\mathbf{\Phi_a}[j,k],\mathbf{G_{ab}}[j,k]\}$. For a free theory they are:

$$\mathbf{J}^C_{\mathbf{a}}[\phi,G]=(G^{-1})_{\mathbf{ab}}\phi_{\mathbf{b}}\ ,\qquad \mathbf{K}^C_{\mathbf{ab}}[\phi,G]=(C^{-1})_{\mathbf{ab}}-(G^{-1})_{\mathbf{ab}}\ .$$

The 1- and 2-point functions $\underline{\phi}$ and $\underline{G}$ are then determined implicitly by the equations:

$$\mathbf{J_a}[\underline{\phi},\underline{G}]=0,\qquad \mathbf{K_{ab}}[\underline{\phi},\underline{G}]=0\ , \tag{3.1.10}$$

and for the free theory we get $\underline{\phi}^C=0,\underline{G}^C=C$.

4-point function. The second derivative of $\mathbf{W}$ with respect to k is:

$$\mathbf{W}_{k_{\mathbf{ab}}k_{\mathbf{cd}}}=\frac{1}{2}\mathbf{G_{ab};}_{k_{\mathbf{cd}}}+\frac{1}{2}\mathbf{\Phi_a}_{;k_{\mathbf{cd}}}\mathbf{\Phi_b}+\frac{1}{2}\mathbf{\Phi_a\Phi_b}_{;k_{\mathbf{cd}}}\ . \tag{3.1.11}$$

Assuming that odd correlators $\mathbf{W}_j$ and $\mathbf{W}_{kj}$ vanish at $j=0$, we obtain:

$$\sum_{\mathbf{cd}}\mathbf{W}_{k_{\mathbf{ab}}k_{\mathbf{cd}}}[j=0,k=0]\ \mathbf{K_{cd};}_{G_{\mathbf{mn}}}[\underline{\phi}=0,\underline{G}]=\frac{1}{2}\frac{\delta G_{\mathbf{ab}}}{\delta G_{\mathbf{mn}}}=\frac{1}{2}S_{\mathbf{ab;mn}}\ . \tag{3.1.12}$$

The connected 4-point function is the fourth derivative $\mathbf{W}_{j_{\mathbf{a}}j_{\mathbf{b}}j_{\mathbf{c}}j_{\mathbf{d}}}[0,0]$. It can be re expressed using derivatives with respect to k, as several relations exist between derivatives of $\mathbf{W}[j,k]$ with respect to j and k. The simplest one which is obtained by noticing that deriving the partition function $\exp\{\mathbf{W}[j,k]\}$ once with respect to k we obtain (one half times) the same result as deriving twice with respect to j:

$$(\mathbf{W}_{j_{\mathbf{a}}j_{\mathbf{b}}}+\mathbf{W}_{j_{\mathbf{a}}}\mathbf{W}_{j_{\mathbf{b}}}-2\mathbf{W}_{k_{\mathbf{ab}}})e^{\mathbf{W}}=0\ , \tag{3.1.13}$$

leading to Eq. (3.1.6). Deriving this equality either one more time with respect to k or two more times with respect to j, and combining the results we obtain a long relation, which simplifies considerably in a symmetric phase $\underline{\phi}=0$:

$$\mathbf{W}_{k_{\mathbf{ab}}k_{\mathbf{cd}}}[0,0]=\frac{1}{4}\Big(\mathbf{W}_{j_{\mathbf{a}}j_{\mathbf{b}}j_{\mathbf{c}}j_{\mathbf{d}}}+\mathbf{W}_{j_{\mathbf{a}}j_{\mathbf{c}}}\mathbf{W}_{j_{\mathbf{b}}j_{\mathbf{d}}}+\mathbf{W}_{j_{\mathbf{a}}j_{\mathbf{d}}}\mathbf{W}_{j_{\mathbf{b}}j_{\mathbf{c}}}\Big)_{j,k=0}\equiv\frac{1}{4}\mathcal{F}_{(\mathbf{a},\mathbf{b});(\mathbf{c},\mathbf{d})}\ . \tag{3.1.14}$$

We have thus obtained an explicit relation between the derivatives of $\mathbf{W}$ (on shell) with respect to the k and j sources, as advertised before. The function $\mathcal{F}_{(\mathbf{a},\mathbf{b});(\mathbf{c},\mathbf{d})}$ is the full 4-point function minus the contribution of the disconnected channel $(\mathbf{a},\mathbf{b})(\mathbf{c},\mathbf{d})$. For example, in the free theory we obtain from (3.1.6) and (3.1.9):

$$\mathbf{W}^C_{k_{\mathbf{ab}}k_{\mathbf{cd}}}[0,0]=\frac{1}{2}C_{\mathbf{bm}}C_{\mathbf{ma}}S_{\mathbf{mn;cd}}=\frac{1}{4}(C_{\mathbf{bc}}C_{\mathbf{da}}+C_{\mathbf{bd}}C_{\mathbf{ca}})\ . \tag{3.1.15}$$

2PI effective action. We define the *2PI effective action* as the double Legendre transform of $\mathbf{W}[j,k]$:

$$\mathbf{\Gamma}[\phi,G]=-\mathbf{W}[\mathbf{J},\mathbf{K}]+\mathbf{J_a}\phi_{\mathbf{a}}+\frac{1}{2}\phi_{\mathbf{a}}\mathbf{K_{ab}}\phi_{\mathbf{b}}+\frac{1}{2}\,\mathrm{Tr}[G\mathbf{K}]\ . \tag{3.1.16}$$

Deriving (3.1.16) with respect to ϕ and G, we obtain the two identities:

$$\mathbf{\Gamma}_{\phi_{\mathbf{a}}}[\phi,G]=\mathbf{J_a}[\phi,G]+\mathbf{K_{ab}}[\phi,G]\phi_{\mathbf{b}}\ ,\qquad \mathbf{\Gamma}_{G_{\mathbf{ab}}}[\phi,G]=\frac{1}{2}\mathbf{K_{ba}}[\phi,G]\ . \tag{3.1.17}$$

Furthermore, $\mathbf{\Gamma}_{GG}[\phi,G]=\frac{1}{2}\mathbf{K}_G[\phi,G]$ which, combined with Eq. (3.1.12) and (3.1.14), yields for a theory in the symmetric phase:

$$\mathcal{F}_{(\mathbf{a},\mathbf{b});(\mathbf{c},\mathbf{d})}\mathbf{\Gamma}_{G_{\mathbf{cd}}G_{\mathbf{mn}}}[0,\underline{G}]=\mathcal{S}_{\mathbf{ab;mn}}\ . \tag{3.1.18}$$

As usual we get back to $\mathbf{W}[j,k]$ by means of a new Legendre transform:

$$\mathbf{W}[j,k] = -\mathbf{\Gamma}[\mathbf{\Phi},\mathbf{G}] + j_{\mathbf{a}}\mathbf{\Phi}_{\mathbf{a}} + \frac{1}{2}\mathbf{\Phi}_{\mathbf{a}}k_{\mathbf{ab}}\mathbf{\Phi}_{\mathbf{b}} + \frac{1}{2}\,\mathrm{Tr}[\mathbf{G}k]\;, \tag{3.1.19}$$

where the functionals $\mathbf{\Phi}[j,k], \mathbf{G}[j,k]$ are determined by solving:

$$\mathbf{\Gamma}_{\phi}[\mathbf{\Phi},\mathbf{G}] = j + k\mathbf{\Phi}\;, \qquad \mathbf{\Gamma}_{G}[\mathbf{\Phi},\mathbf{G}] = \frac{1}{2}k\;. \tag{3.1.20}$$

The 2PI effective action has a number of interesting features [12, 117] (see also [116] for more details):

1. The solution of the equations of motion $\mathbf{\Gamma}_{\phi} = 0, \mathbf{\Gamma}_{G} = 0$ is $\underline{\phi}, \underline{G}$, which are the connected 1- and 2-point functions of the theory.

2. It can be evaluated in a loop expansion. Putting in evidence the tree-level and one-loop terms, and discarding a constant term, we obtain:[3]

$$\mathbf{\Gamma}[\phi,G] = \mathbf{S}[\phi] + \frac{1}{2}\,\mathrm{Tr}[\ln G^{-1}] + \frac{1}{2}\,\mathrm{Tr}[G_0^{-1}G] + \mathbf{\Gamma}_2[\phi,G]\;, \tag{3.1.21}$$

   where $G_0 = (\mathbf{S}_{\phi\phi}[\phi])^{-1}$ is the free covariance of the theory around the field configuration ϕ and $\mathbf{\Gamma}_2[\phi,G]$ starts at two loops.

   In the free theory of covariance C, the one loop result is exact, and therefore we have:

$$\mathbf{\Gamma}_{\mathrm{free}}[\phi,G] = \frac{1}{2}\phi_{\mathbf{a}}C^{-1}_{\mathbf{ab}}\phi_{\mathbf{b}} + \frac{1}{2}\,\mathrm{Tr}[\ln G^{-1}] + \frac{1}{2}\,\mathrm{Tr}[C^{-1}G]\;, \tag{3.1.22}$$

   and it can be easily verified that (3.1.18) holds.

3. The equations of motion of (3.1.21) with respect to G write:

$$\frac{\delta\mathbf{\Gamma}[\phi,G]}{\delta G_{\mathbf{ab}}} = 0 \quad \Leftrightarrow \quad (G^{-1})_{\mathbf{ab}} = (G_0^{-1})_{\mathbf{ab}} + 2\frac{\delta\mathbf{\Gamma}_2[\phi,G]}{\delta G_{\mathbf{ab}}}\;, \tag{3.1.23}$$

   As G_0 is the free covariance of the theory (in the presence of a background field ϕ, and G is the connected two point function, it follows from the standard Schwinger-Dyson equation $G^{-1} = G_0^{-1} - \Sigma$ (Fig. 3.1) that

$$\Sigma_{\mathbf{ab}}[\phi,G] = -2\frac{\delta\mathbf{\Gamma}_2[\phi,G]}{\delta G_{\mathbf{ab}}}\;. \tag{3.1.24}$$

   must be identified with the self-energy Σ of the model, which is the sum of amputated one-particle-irreducible (1PI) two point diagrams.

Figure 3.1: Usual diagrammatic interpretation of the Schwinger-Dyson equations for the two-point function G. The self-energy Σ is a sum of 1PI two-point diagrams. On the right-hand side, each line represents a free propagator G_0.

[3] For complex or Grassmann fields, a similar expression holds, but with the functional trace terms multiplied by an extra factor 2 for the complex case and by a minus sign for the Grassmann case.

4. $\mathbf{\Gamma}_2[\phi, G]$ is given by (minus) the sum of all the two-particle irreducible (2PI) vacuum diagrams (i.e. diagrams that do not disconnect when cutting open any two edges) with vertices given by the effective interaction $\mathbf{S}_{\rm int}[\phi, \varphi]$, the part of $\mathbf{S}[\phi + \varphi]$ containing powers of φ higher than two, and effective propagators G. This is can be understood in the following way. It is clear that if $\mathbf{\Gamma}_2[\phi, G]$ is a sum of 2PI diagrams, then $-2\frac{\delta \mathbf{\Gamma}_2}{\delta G} = \Sigma$ is a sum of 1PI diagrams, because cutting one edge from 2PI diagrams (i.e. deriving with respect to G) weakens their irreducibility. Moreover, since here the self-energy $\Sigma[\phi, G]$ is given by a sum of diagrams with full propagator G, rather than bare propagator G_0, no two-point subdiagrams are included in it. Therefore, if a general diagram in $\Sigma[\phi, G]$ disconnects by cutting two edges, necessarily each of the two components must be connected to one of the two external points, otherwise one of the two components would be a two-point subdiagram of $\Sigma[\phi, G]$. And since $\mathbf{\Gamma}_2[\phi, G]$ is reconstructed from $\Sigma[\phi, G]$ by closing it with an additional edge, it follows that $\mathbf{\Gamma}_2[\phi, G]$ is 2PI.

In summary we can write the schematic expression:

$$e^{-\mathbf{\Gamma}[\phi,G]} = e^{-\mathbf{S}[\phi] - \frac{1}{2}\,\mathrm{Tr}\left[G_0^{-1}G\right] + \frac{1}{2}\,\mathrm{Tr}[\ln G^{-1}]} \int_{2PI} d\mu_G[\varphi]\; e^{-\frac{1}{2}\varphi G^{-1}\varphi - \mathbf{S}_{\rm int}[\phi,\varphi]}\;, \tag{3.1.25}$$

where $d\mu_G[\varphi]$ is a normalized Gaussian measure (see (2.1.4)) with covariance $G_{\mathbf{a},\mathbf{b}}$, and the subscript 2PI reminds us that in the perturbative expansion of the functional integral we only retain 2PI diagrams.

3.2 Large-N expansion of the $O(N)$ model

While the properties listed in the previous section are completely generic, we are now going to introduce the $1/N$ expansion of the 2PI effective action. We will use a classical example [12, 117], the $O(N)$ model, in which N is the number of scalar fields: $\varphi_a(x)$, with $a = 1, \ldots, N$. From now on, we make explicit the vector indices and the space time points. We denote by Tr a trace both on vector indices and a functional trace, i.e. for a matrix-valued bi-local field $F_{ab}(x, y)$ we have

$$\mathrm{Tr}[F] = \int_{x,y} \delta(x - y)\; \mathrm{Tr}[F_{ab}(x, y)] = \int_x F_{aa}(x, x)\;.$$

In the $O(N)$ model, the N scalars are postulated to transform in the fundamental representation of the $O(N)$ group, i.e. as in (2.0.1), and the action is chosen to be invariant under such transformations. More specifically, restricting to quartic interactions, the action is:

$$\mathbf{S}[\varphi] = \frac{1}{2}\int_{x,y} \varphi_a(x) C^{-1}(x, y)\varphi_a(y) + \frac{\lambda}{4!N}\int_x (\varphi_a(x)\varphi_a(x))^2\;, \tag{3.2.1}$$

where $C(x, y)$ is the covariance of the Gaussian functional measure of the free theory. In $d \geq 1$, $C^{-1}(x, y)$ is usually the kernel of a differential operator, e.g. $C^{-1} = -\partial^2 + m^2$.

All the definitions we introduced above for the 2PI effective action apply directly, with:

$$G^{-1}_{0,ab}(x, y) = C^{-1}(x, y)\delta_{ab} + \frac{\lambda}{6N}(\phi_c\phi_c)\delta_{ab}\delta(x - y) + \frac{\lambda}{3N}\phi_a\phi_b\delta(x - y)\;, \tag{3.2.2}$$

$$\mathbf{S}_{\rm int}[\phi, \varphi] = \int_x \left(\frac{\lambda}{6N}\phi_a\varphi_a\varphi_b\varphi_b + \frac{\lambda}{4!N}(\varphi_a\varphi_a)^2\right)\;. \tag{3.2.3}$$

There are two kinds of vertices, a trivalent and a tetravalent one, which we represent in Fig. 3.2. The solid lines track the identification of the indices in the vertex. The dashed edge symbolizes

Figure 3.2: The two vertices from Eq. (3.2.3).

the vertex (in an intermediate field representation it would correspond to the propagator of the Hubbard–Stratonovich field), and the blue dotted halfedge represents the background field ϕ.

The vertices are connected by propagators G which connect the solid half edges into solid edges. An example of a Feynman diagram is presented in Fig. 3.3.

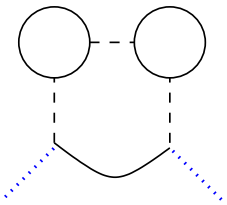

Figure 3.3: An example of a graph with one tetravalent and two trivalent vertices.

In order to construct the $1/N$ expansion, one should take into account the implicit N-dependence due to the presence of N variables. This is done by counting any "single-trace" invariant as contributing with a factor N. There are two types of such invariants in the $O(N)$ model: $\mathrm{Tr}[G^n]$ and $\phi_a(G^n)_{ab}\phi_b$. Taking into account also the explicit factor N^{-1} in the coupling, one immediately finds that the first three terms in the effective action,

$$\mathbf{\Gamma}[\phi, G] = \mathbf{S}[\phi] + \frac{1}{2}\,\mathrm{Tr}[\ln G^{-1}] + \frac{1}{2}\,\mathrm{Tr}[G_0^{-1}G] + \mathbf{\Gamma}_2[\phi, G]\ , \tag{3.2.4}$$

all scale like N, except the contribution from the last term in (3.2.2) which is of order one. Next, one observes that the last term can be expanded as:

$$\mathbf{\Gamma}_2[\phi, G] = \mathbf{\Gamma}_2^{(1)}[\phi, G] + \mathbf{\Gamma}_2^{(0)}[\phi, G] + \mathbf{\Gamma}_2^{(-1)}[\phi, G] + \dots\ , \qquad \text{with}\ \ \mathbf{\Gamma}_2^{(p)}[\phi, G] \sim N^p\ . \tag{3.2.5}$$

This is most easily seen in the symmetric phase, when going partially on shell, i.e. assuming that $\phi_a = 0$ and $G_{ab} \sim \delta_{ab}$ (see [116] for the general case). Whether such a solution is stable or not, and whether there are other stable solutions, will depend on the space dimension. In particular, in $d \leq 2$ spontaneous symmetry breaking of continuous symmetries is impossible [127, 128], hence we do not expect other stable solutions.[4]

From the Feynman rules one obtains a trace over the vector indices of G to some power for each closed loop of the solid strands, hence each such loop should be counted as a factor N. Each vertex brings instead a factor $1/N$. The power counting in N is transparent in a *loop vertex representation* [130] (or *cactus* representation) in intermediate field. The loops of vector indices are contracted into *loop vertices* (of arbitrary degree) and the original Feynman vertices become edges of the intermediate field (the black dashed edges in Fig. 3.3). In this representation the scaling with N of a graph is

[4] However, one should keep in mind that the large-N limit can sometimes lead to an apparently opposite conclusion, as explained for the chiral Gross-Neveu model by Witten [129]. See also [73] for an analogue phenomenon in a tensor-valued version of the Gross-Neveu model.

N^{-E+L} where E is the number of intermediate field edges (i.e. vertices in the original Feynman representation) and L the number of loop vertices. As the graph is connected, the number of loops (or cyclomatic umber) of diagrams in the intermediate field representations is $E - L + 1 = \omega \geq 0$.

It follows that the scaling in N of a graph is $N^{-\omega+1}$, hence the graphs contributing to $\mathbf{\Gamma}_2$ scale at most like N, and they scale like N only if they are trees in the intermediate field. Furthermore, the graphs contributing to $\mathbf{\Gamma}_2[0, G]$ must at the same time be 2PI from the point of view of the original propagators, which translates into the constraint that the tree has no vertices of degree greater than one. Thus only one graph (the double tadpole of Fig. 3.4) contributes at leading order (LO):

$$\mathbf{\Gamma}_2^{(1)}[0, G] = \frac{\lambda}{4!N} \int_x G_{aa}(x, x) G_{bb}(x, x) = N \frac{\lambda}{4!} \int_x G(x, x)^2 \, . \tag{3.2.6}$$

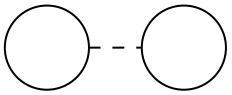

Figure 3.4: The leading order contribution of the large-N expansion in the $O(N)$ model. Shrinking the dashed edge the figure eight of the usual representation is obtained.

The equations of motion of $\mathbf{\Gamma}[0, G]$ at LO lead to the large-N Schwinger-Dyson (SD) equations for the 2-point function:[5]

$$G_{ab}^{-1}(x, y) = \left(C^{-1}(x, y) + \frac{\lambda}{6} G(x, x) \delta(x - y) \right) \delta_{ab} \, . \tag{3.2.7}$$

At next-to-leading order (NLO), we have graphs with $E = L$, always with the 2PI restriction: they are the closed chains of bubbles depicted in Fig. 3.5. The form an infinite family, but thanks to their simple structure they can be summed. In fact, by introducing the kernel

$$\mathcal{K}(x, y) = \frac{\lambda}{6N} G_{ab}(x, y) G_{ba}(x, y) = \frac{\lambda}{6} G(x, y)^2 \, , \tag{3.2.8}$$

we find

$$\mathbf{\Gamma}_2^{(0)}[0, G] = \sum_{n \geq 1} \frac{(-1)^{n+1}}{2n} \operatorname{Tr}[\mathcal{K}^n] = \frac{1}{2} \operatorname{Tr}[\ln(\mathbf{1} + \mathcal{K})] \, . \tag{3.2.9}$$

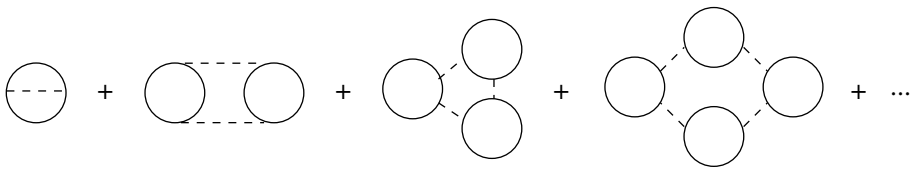

Figure 3.5: The next-to-leading order contribution of the large-N expansion in the $O(N)$ model.

[5] We notice that in $d = 0$ (and fixing for example $C = 1$) the SD equation becomes a simple quadratic equation for G with solution $G = 3(-1 \pm \sqrt{1 + 2\lambda/3})/\lambda$, thus exhibiting a well-known singularity at a negative value of the coupling (e.g. [131]). For $d \geq 1$ instead (with $C^{-1} = -\partial^2 + m^2$), the SD equation simply leads to a renormalization of the mass (a finite one in $d = 1$).

3.2.1 Large-N expansion as the loop expansion of an auxiliary theory

Notice that (3.2.9) looks like the result we would obtain from a standard Gaussian integral with inverse covariance $\mathbf{1}+\mathcal{K}$. It turns out that the large-N expansion for the 2PI effective action of the vector model can indeed be cast as a loop expansion for an auxiliary bilocal theory, as we are now going to show.

Consider the partition function for the vector model, which corresponds to

$$Z = e^{\mathbf{W}[0,0]} = e^{-\mathbf{\Gamma}[\underline{\phi},\underline{G}]} = \int [d\varphi]\, e^{-\mathbf{S}[\varphi]} \,, \tag{3.2.10}$$

with the action (3.2.1). Next, insert in the functional integral the identity:

$$\begin{aligned} 1 &= \int [d\tilde{G}]\delta\left(N\tilde{G}(x,y) - \varphi_a(x)\varphi_a(y)\right) \\ &= \int [d\tilde{G}][d\tilde{\Sigma}]\, e^{-\frac{1}{2}\int_{x,y}\tilde{\Sigma}(x,y)\left(N\tilde{G}(x,y)-\sum_a \varphi_a(x)\varphi_a(y)\right)} \,, \end{aligned} \tag{3.2.11}$$

exploit the delta function to write the interaction in terms of $\tilde{G}$, and then perform the integral over φ:

$$\begin{aligned} Z &= \int [d\varphi][d\tilde{G}][d\tilde{\Sigma}]\, e^{-\mathbf{S}[\varphi]-\frac{1}{2}\int_{x,y}\tilde{\Sigma}(x,y)\left(N\tilde{G}(x,y)-\sum_a \varphi_a(x)\varphi_a(y)\right)} \\ &= \int [d\tilde{G}][d\tilde{\Sigma}]\, e^{-N\left\{\frac{1}{2}\mathrm{Tr}[(C^{-1}-\tilde{\Sigma})\tilde{G}]+\frac{1}{2}\mathrm{Tr}[\ln(\tilde{\Sigma})]+\frac{\lambda}{4!}\int_x \tilde{G}(x,x)^2\right\}} \\ &\equiv \int [d\tilde{G}][d\tilde{\Sigma}]\, e^{-N\mathbf{S}_{\rm eff}[\tilde{G},\tilde{\Sigma}]} \,. \end{aligned} \tag{3.2.12}$$

We have thus rewritten the original functional integral over N (local) variables as an integral over just two (bilocal) variables, and all the dependence on N is now explicit and factored in front of the total action. Therefore, the $1/N$ expansion takes the standard form of a loop (i.e. saddle-point) expansion. We shift the fields to the saddle point value: $\tilde{G}(x,y) = \underline{G}(x,y) + N^{-1/2}g(x,y)$, $\tilde{\Sigma}(x,y) = \underline{\Sigma}(x,y) + N^{-1/2}\sigma(x,y)$. Expanding to second order in g and σ, we find:

$$Z \simeq e^{-N\mathbf{S}_{\rm eff}[\underline{G},\underline{\Sigma}]}\int [dg][d\sigma]\, e^{-\mathbf{S}^{(2)}_{\rm eff}[\underline{G},\underline{\Sigma};g,\sigma]} \,, \tag{3.2.13}$$

where the on-shell effective classical action coincides with the on-shell 2PI effective action at LO:

$$\mathbf{S}_{\rm eff}[\underline{G},\underline{\Sigma}] = \frac{1}{2}\,\mathrm{Tr}[\ln \underline{G}^{-1}] + \frac{1}{2}\,\mathrm{Tr}[C^{-1}\underline{G}] + \frac{\lambda}{4!}\int_x \underline{G}(x,x)^2 \,. \tag{3.2.14}$$

We have also defined the quadratic part of the action:

$$\begin{aligned} \mathbf{S}^{(2)}_{\rm eff}[\underline{G},\underline{\Sigma};g,\sigma] = &-\frac{1}{4}\int_{x_1,x_2,x_3,x_4} \sigma(x_1,x_2)\underline{\mathcal{K}}_4(x_1,x_2;x_3,x_4)\sigma(x_3,x_4) \\ &-\frac{1}{2}\int_{x_1,x_2}\sigma(x_1,x_2)g(x_1,x_2) + \frac{\lambda}{4!}\int_x g(x,x)^2 \,, \end{aligned} \tag{3.2.15}$$

where the kernel is:

$$\underline{\mathcal{K}}_4(x_1,x_2;x_3,x_4) = \frac{1}{2}(\underline{G}(x_1,x_3)\underline{G}(x_2,x_4) + \underline{G}(x_1,x_4)\underline{G}(x_2,x_3)) \,. \tag{3.2.16}$$

Performing the Gaussian integrals we find:

$$\begin{aligned} Z &\simeq \frac{e^{-N\mathbf{S}_{\rm eff}[\underline{G},\underline{\Sigma}]}}{\left(\det\left(\underline{\mathcal{K}}_4\right)\right)^{1/2}}\int [dg]\, e^{-\frac{1}{4}\int_{x_1,x_2,x_3,x_4} g(x_1,x_2)\underline{\mathcal{K}}_4^{-1}(x_1,x_2;x_3,x_4)g(x_3,x_4)-\frac{\lambda}{4!}\int_x g(x,x)^2} \\ &= e^{-N\mathbf{S}_{\rm eff}[\underline{G}]-\frac{1}{2}\mathrm{Tr}[\ln(1+\underline{\mathcal{K}})]} \,, \end{aligned} \tag{3.2.17}$$

where the kernel $\underline{\mathcal{K}}$ in the final result is exactly the one in (3.2.8) evaluated on shell. Notice that due to the interaction being local rather than bilocal (compare with the SYK model in the next section), the 4-point kernel $\underline{\mathcal{K}}_4$ reduces to the 2-point kernel $\underline{\mathcal{K}}$. We have thus recovered the LO and NLO of $\mathbf{\Gamma}[\underline{\phi}, \underline{G}]$ by a standard saddle-point method.

A remark is in order. In $\mathbf{\Gamma}[\underline{\phi}, \underline{G}]$ the on-shell fields should be obtained from the full effective action. As we explained, $\underline{\phi} = 0$ is valid to all orders in the symmetric phase, but the on-shell value $\underline{G}$ receives corrections in $1/N$. Expanding $\mathbf{\Gamma}[0, G] \simeq N\mathbf{\Gamma}^{(1)}[0, G] + \mathbf{\Gamma}^{(0)}[0, G]$, we find an expansion for the solution $\underline{G} = \underline{G}^{(0)} + N^{-1}\underline{G}^{(-1)}$, and therefore, $\mathbf{\Gamma}[\underline{\phi}, \underline{G}] = N\mathbf{\Gamma}^{(1)}[0, \underline{G}^{(0)}] + \mathbf{\Gamma}^{(0)}[0, \underline{G}^{(0)}] + O(N^{-1})$, because $\frac{\delta \mathbf{\Gamma}^{(1)}}{\delta G}[0, \underline{G}^{(0)}] = 0$ by construction.

3.3 2PI effective action for the SYK model

The SYK model is defined in terms of N Majorana fermions in one dimension, with anticommutation relation $\{\psi_a, \psi_b\} = \delta_{ab}$, and with action

$$\mathbf{S}_{\text{SYK}}[\psi] = \int dt \left(\frac{1}{2}\psi_a \partial_t \psi_a + \frac{\mathrm{i}^{q/2}}{q!} J_{a_1 \dots a_q} \psi_{a_1} \dots \psi_{a_q} \right) . \tag{3.3.1}$$

Here, $J_{a_1 \dots a_q}$ is a random totally antisymmetric tensorial coupling, with Gaussian distribution

$$P[J_{a_1 \dots a_q}] \propto \exp\left\{ -\frac{N^{q-1}(J_{a_1 \dots a_q})^2}{2(q-1)!J^2} \right\} \qquad \text{(no sum)} . \tag{3.3.2}$$

We will denote with a bar the average over the disorder:

$$\overline{A[J]} = \int \left(\prod_{a_1 < a_2 < \dots < a_q} [dJ_{a_1 \dots a_q}] P[J_{a_1 \dots a_q}] \right) A[J] . \tag{3.3.3}$$

For example, we have

$$\overline{J_{a_1 \dots a_q} J_{b_1 \dots b_q}} = \frac{q!(q-1)!}{N^{q-1}} J^2 \, \Pi_{a_1 \dots a_q, b_1 \dots b_q} , \tag{3.3.4}$$

where $\Pi_{a_1 \dots a_q, b_1 \dots b_q}$ is the projector on antisymmetric rank-q tensors:

$$\Pi_{a_1 \dots a_q, b_1 \dots b_q} = \frac{1}{q!} \sum_{\sigma \in \mathfrak{S}_q} \epsilon(\sigma) \prod_{i=1}^{q} \delta_{a_i b_{\sigma(i)}} , \tag{3.3.5}$$

with $\mathfrak{S}_q$ the symmetric group on q elements, and $\epsilon(\sigma)$ the sign of the permutation σ.

One deals with the randomness of the coupling by computing quenched averages of intensive quantities, such as the free energy or the entropy, which in general (e.g. for models with short-range interactions) are self-averaging, i.e. in the thermodynamic limit they converge with probability one to their average. In particular, the quenched free energy is

$$-N\overline{F} = \overline{\ln Z} = \int \left(\prod_{a_1 < a_2 < \dots < a_q} [dJ_{a_1 \dots a_q}] P[J_{a_1 \dots a_q}] \right) \ln \int [d\psi] e^{-\mathbf{S}_{\text{SYK}}[\psi]} . \tag{3.3.6}$$

The expansion in Feynman graphs is standard, with the only peculiarity that the quenched average adds on the connected diagrams extra edges representing the covariance (3.3.4).

In the same way as we defined a quenched free energy, we can define the quenched generating functionals of connected, 1PI, and 2PI diagrams, by constructing them in the usual way for each

realization of the disorder and taking the average over disorder at the end. One should be careful with defining the generating functionals in such a way, because for example the averaging procedure does not in general commute with evaluating the effective action on shell. However, for the SYK model it can be shown by an analysis of the diagrams that commutativity holds at LO and NLO, a fact that here we will only show a posteriori by comparison to known results.[6]

We can therefore repeat all the construction of the 2PI effective action as above, with the novel feature that 2PI graphs contributing to $\mathbf{\Gamma}_2$ now have to be averaged over disorder, and that the fermionic nature of the model brings in some minus factors. We have

$$\mathbf{\Gamma}[\Psi, G] = \mathbf{S}_{\rm SYK}[\Psi] - \frac{1}{2}\,\mathrm{Tr}[\ln G^{-1}] - \frac{1}{2}\,\mathrm{Tr}[G_0^{-1}G] + \mathbf{\Gamma}_2[\Psi, G]\,. \tag{3.3.7}$$

In order to simplify the analysis of the large-N limit we directly set $\Psi = 0$, which is again justified by the absence of spontaneous symmetry breaking. By the same reason we could also fix $G_{ab}(x,y) = \delta_{ab}G(x,y)$, although in general it will be more transparent to keep the general expression. After averaging over the disorder all the diagrams lead to different multiple traces of powers of $G_{ab}(t,t')$, and as before we should count each trace as contributing a factor N. We find in this way an expansion of the same type as (3.2.5). Remembering that in the large-N limit the disorder average selects melons [47] (see [53, 54] for rigorous diagrammatic proofs), we find that $\mathbf{\Gamma}_2[0,G]$ at leading order in $1/N$ is given by the fundamental vacuum melon of Fig. 3.6, which is the only 2PI melon graph, with propagators given by G, i.e.:

$$\begin{aligned}\mathbf{\Gamma}_2^{(1)}[0,G] &= -\frac{1}{2q!}\overline{J_{a_1\ldots a_q}J_{b_1\ldots b_q}}\int_{t,t'}\prod_{c=1}^{q}G_{a_c b_c}(t,t') \\ &= -\frac{J^2}{2qN^{q-1}}\int_{t,t'}G_{aa}(t,t')^q = -\frac{J^2N}{2q}\int_{t,t'}G(t,t')^q\,.\end{aligned} \tag{3.3.8}$$

Notice that having chosen a Wick pairing of fermions to give the propagators (in $q!$ ways, thus canceling one of the $1/q!$ factors that come from the vertices), the average over disorder produces many different types of contractions, due to the projector in (3.3.4), but in the second line we have taken the only contraction that contributes at LO. The number of traces (and hence the power of N) is in general

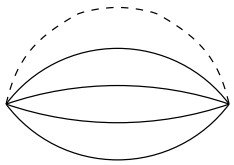

Figure 3.6: The fundamental melon for $q = 4$. The dashed line represents the Wick contraction associated to the quenched average.

given by the number $c(\sigma)$ of cycles in the disjoint cycle decomposition of the permutation σ appearing in the projector. Thus permutations that can be obtained with a single transposition contribute to

[6] Note that in the standard way of obtaining LO and NLO results for the SYK model a replica diagonal ansatz is taken for the bilocal field, which is justified by the fact that for the SYK model quenched and annealed averages coincide at LO and NLO [126, 132]. At NNLO, within the replica method one should take into account interactions between different replicas (i.e. off-diagonal fluctuations of the bilocal field), while in the 2PI formalism one should take into account diagrams that arise when the averaging is done after the on-shell evaluation.

the NLO:

$$\begin{aligned}&\left(-\frac{1}{2q!}\overline{J_{a_1\ldots a_q}J_{b_1\ldots b_q}}\int_{t,t'}\prod_{c=1}^{q}G_{a_cb_c}(t,t')\right)_{\text{NLO}}\\&=-\frac{J^2}{2qN^{q-1}}\binom{q}{2}\int_{t,t'}G_{aa}(t,t')^{q-2}G_{bc}(t,t')G_{cb}(t,t')=-\frac{J^2(q-1)}{4}\int_{t,t'}G(t,t')^q\,.\end{aligned}\tag{3.3.9}$$

The full 2PI effective action at leading order in $1/N$ is thus:

$$\frac{1}{N}\mathbf{\Gamma}[0,G]=-\frac{1}{2}\operatorname{Tr}[\ln G^{-1}]-\frac{1}{2}\operatorname{Tr}[\partial_tG(t,t')]-\frac{J^2}{2q}\int_{t,t'}G(t,t')^q\,,\tag{3.3.10}$$

which coincides with the bilocal action derived in [124] by a change of variables within the replica method. The equivalence with [124] implies in particular that the equations of motion are the same and coincide with the SD equations:[7]

$$G^{-1}(t,t')=\partial_t\delta(t,t')-J^2G(t,t')^{q-1}\,,\tag{3.3.11}$$

and that the Schwarzian action controlling the conformal fluctuations can be derived in a similar fashion as in that paper. We denote the solution of (3.3.11) as $\underline{G}(t,t')$.

Recalling Eq. (3.1.14) and (3.1.18), the second derivative $\mathbf{\Gamma}_{GG}[0,\underline{G}]$ is equal to the inverse of $\mathcal{F}(t_1,t_2,t_3,t_4)$, i.e. of the full 4-point function minus the disconnected channel ($1\to2,3\to4$). Interestingly, such channel is the leading-order (and uninteresting) term in the SYK 4-point function [47,49].[8] Therefore, $\mathbf{\Gamma}_{GG}[0,\underline{G}]$ captures precisely the inverse of the object of interest in SYK. We can compute this from our LO effective action, and recover the corresponding result of the SYK 4-point function given by the sum of the ladder diagrams, see [47–49]. Taking into account that:

$$\frac{\delta G_{34}}{\delta G_{12}}=\frac{1}{2}\left(\delta(t_1-t_3)\delta(t_2-t_4)-\delta(t_1-t_4)\delta(t_2-t_3)\right)\equiv I_-(t_1,t_2;t_3,t_4)\,,\tag{3.3.13}$$

with I the orthogonal projector on antisymmetric functions, and denoting the on-shell four point kernel:

$$\underline{K}(t_1,t_2;t_3,t_4)=-J^2(q-1)\underline{G}(t_1,t_3)\underline{G}(t_2,t_4)\underline{G}(t_3,t_4)^{q-2}\,,\tag{3.3.14}$$

we get:

$$\mathbf{\Gamma}_{G_{34}}=\frac{1}{2}\underline{G}^{-1}(t_4,t_3)+\frac{1}{2}\partial_t\delta(t_3-t_4)-\frac{1}{2}J^2[\underline{G}(t_3,t_4)]^{q-1}\,,\tag{3.3.15}$$

$$\begin{aligned}\mathbf{\Gamma}_{G_{12}G_{34}}&=-\frac{1}{4}\underline{G}^{-1}(t_4,t_1)\underline{G}^{-1}(t_2,t_3)+\frac{1}{4}\underline{G}^{-1}(t_4,t_2)\underline{G}^{-1}(t_1,t_3)\\&\quad+\frac{1}{4}[\delta(t_1-t_3)\delta(t_2-t_4)-\delta(t_1-t_4)\delta(t_2-t_3)][-J^2(q-1)\underline{G}(t_3,t_4)^{q-2}]\\&=-\frac{1}{2}\int_{t,t'}\underline{G}^{-1}(t_1,t)\underline{G}^{-1}(t_2,t')\Big[I_-(1-\underline{K})\Big](t,t';t_3,t_4)\,.\end{aligned}\tag{3.3.16}$$

Inverting the last expression we find:

$$\mathcal{F}(t_1,t_2,t_3,t_4)=\int_{t,t'}\left(\frac{1}{1-\underline{K}}\right)(t_1,t_2,t,t')(-\underline{G}(t,t_3)\underline{G}(t',t_4)+\underline{G}(t,t_4)\underline{G}(t',t_3))\,,\tag{3.3.17}$$

which is precisely the starting point of the computations in [47–49].

[7] Here one should remember that for Majorana fermions $G(t,t')=-G(t',t)$.

[8] As a reminder, the 4-point function we are talking about is:

$$\frac{1}{N^2}\langle\psi_m(t_1)\psi_m(t_2)\psi_n(t_3)\psi_n(t_4)\rangle=G(t_{12})G(t_{34})+\frac{1}{N}\mathcal{F}^{LO}(t_1,t_2,t_3,t_4)+\ldots\,.\tag{3.3.12}$$

The $G(t_{12})G(t_{34})$ part is precisely the channel missing when taking the derivatives as in (3.1.14), and therefore, evaluating this derivative at LO will give us $\mathcal{F}^{LO}$. The latter was computed in [47–49] by conformal methods.

3.3.1 Next-to-leading order action

As in the vector model of the previous section, (3.3.10) will receive corrections at higher orders in $1/N$. We want to show that the NLO correction can be interpreted as the result of performing the Gaussian integral over the fluctuations in the usual bilocal action expanded to quadratic order. In order to do that, we need to understand which 2PI diagrams contribute at NLO, a question that has been addressed in detail in [53] for the colored version of the model, which is a special case of the generalization of the SYK model introduced by Gross and Rosenhaus [133] (see also [115] for a discussion of the same model at NLO). It turns out that similar type of diagrams dominate also the standard SYK model, but have to be accompanied by the twisted melons (3.3.9), which are absent in the colored case.

The NLO 2PI vacuum graphs are thus given by all the periodic ladders with $n \geq 1$ rungs, with or without one twist of the rails, see Fig. 3.7. One should notice that the case $n = 1$ is quite special. First, the case $n = 1$ without twist is 2-particle reducible if $q = 4$, but since it evaluates to zero for any q (because $G(t, t) = 0$ due to the anticommutation of fermions), we can formally include it in the list. On the other hand, the case $n = 1$ with twist corresponds again to a fundamental melon, thus one might think that it is LO rather than NLO. However, this corresponds precisely to the twisted melons in (3.3.9), which therefore can be conveniently grouped with the ladders. Although such ladders form

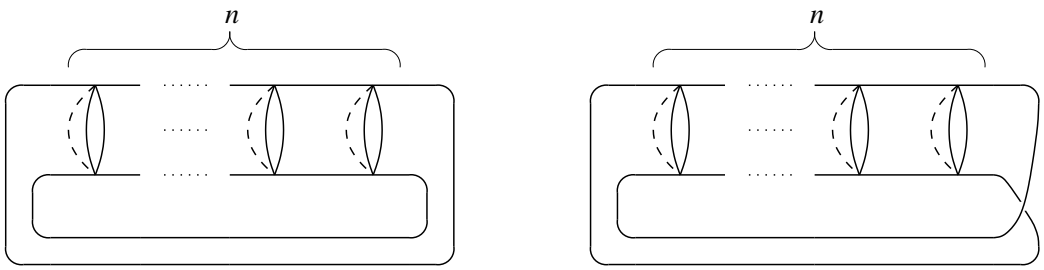

Figure 3.7: NLO contributions with n rungs, without (left) and with (right) twist.

an infinite family of graphs, they can be summed in a similar way as to what we did for the vector case, i.e. by introducing a kernel for the insertion of a rung. One important difference is that now the kernel carries two vertices rather than one, which counts for different combinatorial factors and minus signs in the summation (notice that the kernel below has itself another minus sign, due to the fermionic nature of the theory). More explicitly, we have

$$\mathbf{\Gamma}_2^{(0)}[0, G] = -\frac{1}{2}\sum_{n\geq 0}\frac{1}{n}\,\mathrm{Tr}[\mathcal{K}^n I_-] = \frac{1}{2}\,\mathrm{Tr}[\ln(I_- - \mathcal{K}I_-)]\,, \tag{3.3.18}$$

where I_- and $\mathcal{K}$ are given in (3.3.13) and (3.3.14) (now off-shell), and to obtain the last equality we used the fact that $I_- = I_-^n$ because it is a projector, and $[\mathcal{K}, I_-] = 0$. Evaluating $\mathbf{\Gamma}_2^{(0)}[0, G]$ on the solution of the LO equations of motion, we find that this is the same result that one would obtain by integrating the quadratic fluctuations of the bilocal effective action of [49, 124, 126].

In order to see that, we just have to repeat what we have done for the vector case, with the important difference that due to the disorder one has to use the replica method. The quenched average in the SYK model can be performed using the replica method, at the cost of introducing n replicas of the system, and having to take the non-trivial limit $n \to 0$, which is needed in order to evaluate the quenched free energy:

$$\overline{\ln Z} = \lim_{n\to 0}\partial_n \overline{Z^n}\,. \tag{3.3.19}$$

One finds [126]:

$$\overline{Z^n} = \int \left(\prod_{\alpha\beta} [dG^{\alpha\beta}][d\Sigma^{\alpha\beta}] \right) e^{-N\mathbf{S}_{\text{eff}}[G,\Sigma]} , \tag{3.3.20}$$

where

$$\mathbf{S}_{\text{eff}}[G,\Sigma] = -\frac{1}{2}\widehat{\text{Tr}} \ln(\partial_t - \Sigma) + \frac{1}{2}\sum_{\alpha\beta}\int_{t,t'} \left(\Sigma^{\alpha\beta}(t,t')G^{\alpha\beta}(t,t') - \frac{J^2}{q}(G^{\alpha\beta}(t,t'))^q \right) . \tag{3.3.21}$$

Performing the saddle-point approximation with a replica diagonal ansatz $\underline{G}^{\alpha\beta} = \underline{G}\delta^{\alpha\beta}$, which is valid up to NLO in $1/N$ [126], one arrives at [49]:

$$\overline{\ln Z} = N\left(\frac{1}{2}\,\text{Tr}[\ln \underline{G}^{-1}] + \frac{1}{2}\,\text{Tr}[\partial_t \underline{G}(t,t')] + \frac{J^2}{2q}\int_{t,t'} \underline{G}(t,t')^q \right) - \frac{1}{2}\,\text{Tr}[\ln(I_- - \tilde{\mathcal{K}} I_-)] , \tag{3.3.22}$$

with

$$\tilde{\mathcal{K}}(t_1,t_2;t_3,t_4) = |\underline{G}(t_1,t_2)|^{\frac{q-2}{2}}\, \underline{\mathcal{K}}(t_1,t_2;t_3,t_4)\, |\underline{G}(t_3,t_4)|^{\frac{2-q}{2}} . \tag{3.3.23}$$

Since $\frac{1}{2}\,\text{Tr}[\ln(I_- - \tilde{\mathcal{K}} I_-)] = \frac{1}{2}\,\text{Tr}[\ln(I_- - \underline{\mathcal{K}} I_-)]$, we recover our $\mathbf{\Gamma}[0,\underline{G}]$ up to NLO, as claimed.

Note that the main difference between (3.3.21) with replica-diagonal ansatz and (3.2.12) is that in the SYK model the interaction part of $\mathbf{S}_{\text{eff}}$ is bilocal while in the $O(N)$ model it is local. This is reflected in the fact that the associated fluctuation kernel is truly a 4-point kernel in the SYK case while it is a 2-point kernel in the $O(N)$ case. From a graphical point of view the bilocality in the SYK model originates from the fact that the NLO graphs are ladders, while in the vector model they are chains of bubbles (see Fig. 4.2 later on).

The replica diagonal ansatz used to derive the result above implies that $\overline{\ln Z} = \ln \overline{Z}$, i.e. that quenched and annealed averages coincide (see [132] for a combinatorial proof at LO). Starting at NNLO [126], the two averaging procedures start to differ, or in other words, the replica-symmetric ansatz becomes inaccurate. From the point of view of the 2PI formalism, the complications at NNLO arise from the non-commutativity of averaging over disorder and going on shell, as we discussed before.

3.4 2PI effective action for the $O(N)^3$ model

In this last section we will apply the 2PI formalism the $O(N)^3$ model, or Carrozza-Tanasa-Klebanov-Tarnopolsky (CTKT) model [38, 56], in $d = 0$ and $d = 1$. For an application to the colored tensor model (Gurau-Witten model), we refer to the original paper [116]. It is straightforward to define the 2PI effective action for tensor-valued field theories in d dimensions applying the construction that we reviewed in Sec. 3.1: all the equations before Sec. 3.2 are in fact still valid, with the collective index now corresponding to an r-uple of indices $(a_1 \dots a_r)$ plus the spacetime point. For example, in rank 3 the bilocal field $G_{\mathbf{ab}}$ corresponds to $G_{a_1a_2a_3b_1b_2b_3}(x,y)$, and so on. The presence of several fields is also straightforward to take into account: one simply needs to extend further the meaning of the vector label by including a field index $c = 1 \dots q$, in which case the discrete part of the collective-index $\mathbf{a}$ can still be thought as a vector index, with $\mathbf{a} = 1 \dots M$, with $M = q\prod_{i=1}^r N_i$. The crucial property that characterizes a proper tensor model is the symmetry group: for a vector model the natural symmetry group would be $O(M)$, while for a tensor model this is broken by the choice of interaction down to a smaller group with a natural tensorial interpretation (for example, in our case study, $O(N^3)$ is broken down to $O(N)^3$).

3.4.1 The bosonic CTKT model in $d = 0$

The CTKT model in zero dimensions is defined by the action:

$$\mathbf{S}_{\text{CTKT}}[\varphi] = \frac{1}{2}\varphi_{abc}\varphi_{abc} + \frac{\lambda}{4N^{3/2}}\varphi_{a_1a_2a_3}\varphi_{a_1b_2b_3}\varphi_{b_1a_2b_3}\varphi_{b_1b_2a_3} \ . \tag{3.4.1}$$

As standard, we refer to the location of an index as a color, e.g. the indices a_1 and b_1 in the interaction above are of color 1, and so on.

The perturbative expansion has been detailed in Sec. 2.1. The corresponding 2PI effective action is constructed as as explained in Sec. 3.1, and in particular equation (3.1.21) is still valid, with $\mathbf{S}[\phi] = \mathbf{S}_{CTKT}[\phi]$,

$$\begin{aligned}(G_0^{-1})_{a_1a_2a_3b_1b_2b_3} &= \delta_{a_1b_1}\delta_{a_2b_2}\delta_{a_3b_3} \\ &+ \frac{\lambda}{N^{3/2}}(\phi_{c_1a_2a_3}\phi_{c_1b_2b_3}\delta_{a_1b_1} + \phi_{a_1c_2a_3}\phi_{b_1c_2b_3}\delta_{a_2b_2} + \phi_{a_1a_2c_3}\phi_{b_1b_2c_3}\delta_{a_3b_3}) \ ,\end{aligned} \tag{3.4.2}$$

and with $\mathbf{\Gamma}_2[\phi, G]$ constructed from 2PI graphs with propagator $G_{a_1a_2a_3b_1b_2b_3}$ and interaction

$$\mathbf{S}_{\text{int}}[\phi, \varphi] = \frac{\lambda}{N^{3/2}}\phi_{a_1a_2a_3}\varphi_{a_1b_2b_3}\varphi_{b_1a_2b_3}\varphi_{b_1b_2a_3} + \frac{\lambda}{4N^{3/2}}\varphi_{a_1a_2a_3}\varphi_{a_1b_2b_3}\varphi_{b_1a_2b_3}\varphi_{b_1b_2a_3} \ . \tag{3.4.3}$$

As in the vector model, $\mathbf{\Gamma}_2[\phi, G]$, and hence $\mathbf{\Gamma}[\phi, G]$, will only contain even powers of ϕ, and as a consequence, the equation of motion $\delta\mathbf{\Gamma}/\delta\phi = 0$ admits the solution $\phi = 0$, which is the only solution giving an invariant 1-point function. Here we will only consider the symmetric phase, and thus study the large-N expansion of $\mathbf{\Gamma}_2[0, G]$. Possible symmetry-breaking solutions (possible in $d > 2$ even at finite N) have been considered in [134].

In order to do a large-N expansion as in the vector case we need to identify quantities that scale like N. In the vector case we saw that $\text{Tr}[G^m] \sim N$ for any m. The easiest way to see such scaling is to assume that $G_{ab} \propto \delta_{ab}$ which we know to be true for the on-shell 2-point function. The analogue for the tensor case is to treat any "trace" over a given color as being of order N. Again the easiest way to see why it is so is to take $G_{a_1a_2a_3b_1b_2b_3} \propto \delta_{a_1b_1}\delta_{a_2b_2}\delta_{a_3b_3}$, which we know is going to be true on shell, due to the invariance of the theory. The identification of the scaling with N of the graphs contributing to the 2PI effective action is thus reduced to the well-studied problem of identifying the scaling with N of tensor model graphs. We can then borrow the results from [38] and claim that :

- $\mathbf{\Gamma}_2[0, G]$ can be expanded as:

$$\mathbf{\Gamma}_2[0, G] = \sum_{\omega\in\mathbb{N}/2} \mathbf{\Gamma}_2^{(3-\omega)}[G] \ , \qquad \text{with } \mathbf{\Gamma}_2^{(p)}[G] \sim N^p \ . \tag{3.4.4}$$

- In the large-N limit $\mathbf{\Gamma}_2[0, G]$ is given by a single diagram, i.e. the fundamental vacuum melon (whose Feynman diagram was depicted in Fig. 2.4, and whose edge-colored graph representation is given in Fig. 3.8), with propagators given by G: indeed, since the interaction is the known one, we know that melons dominate the large-N limit, and the fundamental melon is the only 2PI melon.

Since the fundamental melon diagram comes with a combinatorial factor of 4, we obtain:

$$\mathbf{\Gamma}_2^{(3)}[G] = -\frac{\lambda^2}{8N^3}G_{a_1a_2a_3b_1b_2b_3}G_{a_1a'_2a'_3b_1b'_2b'_3}G_{a'_1a_2a'_3b'_1b_2b'_3}G_{a'_1a'_2a_3b'_1b'_2b_3} \ . \tag{3.4.5}$$

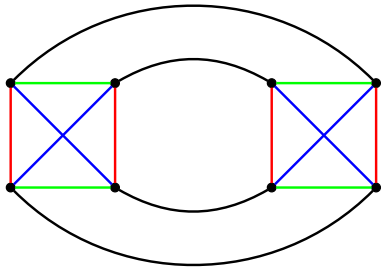

Figure 3.8: The fundamental melon for the CTKT model in the tetrahedron representation. Black edges represent propagators $G_{a_1a_2a_3b_1b_2b_3}$, and the tetrahedra provide the contraction pattern for their indices, as in (3.4.5).

In the symmetric phase, the two point function is diagonal in the tensor indices,

$$G_{a_1a_2a_3b_1b_2b_3} = G\,\delta_{a_1b_1}\delta_{a_2b_2}\delta_{a_3b_3}\ , \tag{3.4.6}$$

hence find

$$\mathbf{\Gamma}_2^{(3)}[G] = -\frac{1}{8}\lambda^2 N^3 G^4\ , \tag{3.4.7}$$

and for the full effective action at leading order in $1/N$ we obtain:

$$\frac{1}{N^3}\mathbf{\Gamma}[0,G] = \frac{1}{2}\ln G^{-1} + \frac{1}{2}G - \frac{1}{8}\lambda^2 G^4\ . \tag{3.4.8}$$

The LO equations of motion are simply

$$G^{-1} = 1 - \lambda^2 G^3\ , \tag{3.4.9}$$

which we recognize as the SD equations at leading order in the $1/N$ expansion [38].

Following [38], one finds that at next-to-leading order the dominant graphs are generated by inserting melonic 2-point functions in the propagators of the three core graphs obtained form the one depicted in Fig. 3.9 by permutation of the colors. Since any insertion of a melonic 2-point function makes the graph 2-particle reducible, we conclude that at NLO there is only a finite number of 2PI graphs, i.e. the three core graphs themselves They correspond to three contractions like:

$$\frac{\lambda}{4N^{3/2}} G_{a_1a_2a_3a_1b_2b_3} G_{a_1'a_2a_3a_1'b_2b_3}\ . \tag{3.4.10}$$

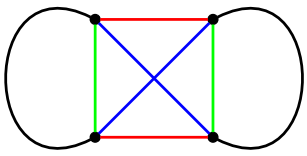

Figure 3.9: The NLO core graph for the CTKT model.

With the diagonal ansatz for the two point function, we obtain:

$$\frac{1}{N^3}\mathbf{\Gamma}[0,G] = \frac{1}{2}\ln G^{-1} + \frac{1}{2}G - \frac{1}{8}\lambda^2 G^4 + \frac{3\lambda}{4N^{1/2}}G^2 \,. \tag{3.4.11}$$

The equations of motion are now:

$$G^{-1} = 1 - \lambda^2 G^3 + \frac{3\lambda}{N^{1/2}}G \,. \tag{3.4.12}$$

Writing $G = G^{(0)} + N^{-1/2}G^{(-1/2)}$ and expanding to order $N^{-1/2}$ we recover the SD equations at NLO of [38].[9]

At NNLO the combinatorics of the $O(N)^3$ model with only the tetrahedron interaction has been carefully studied in [88]. Restricting to 2PI diagrams, it turns out that there is an infinite family of ladder-like diagrams, closed in a planar way as shown in Fig. 3.10, plus one special diagram, shown in Fig. 3.11. The ladders are similar to those found in the SYK model (see Fig. 3.7), although the non-planar ones in this case are more suppressed in $1/N$, and thus lead to a similar trace-log term. The extra diagram in Fig. 3.11 gives instead a term of a different form, which in particular implies that the NNLO effective action cannot be interpreted as the result of a Gaussian integral.

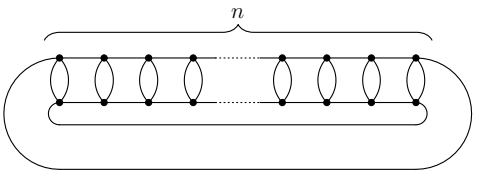

Figure 3.10: A generic NNLO vacuum 2PI diagram having the form of a closed ladder with $n \geq 2$ rungs, and vertices corresponding to the tetrahedron interaction. Similar diagrams but with a twist in the rails (similar to the second diagram in Fig. 3.7) appear only at higher order in $1/N$.

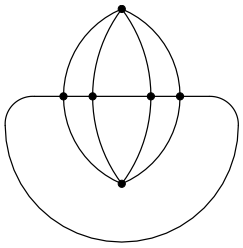

Figure 3.11: The unique NNLO vacuum 2PI diagram besides the ladders. All six vertices are tetrahedral.

3.4.2 The fermionic CTKT model in $d = 1$

Let us consider the $d = 1$ fermionic CTKT model, which is in some ways the simplest SYK-like tensor model [56]. Its classical action is:

$$\mathbf{S}_{\text{CTKT}}[\psi] = \int_t \left(\frac{1}{2}\psi_{abc}(t)\partial_t \psi_{abc}(t) + \frac{\lambda}{4N^{3/2}}\psi_{a_1a_2a_3}(t)\psi_{a_1b_2b_3}(t)\psi_{b_1a_2b_3}(t)\psi_{b_1b_2a_3}(t) \right) \,. \tag{3.4.13}$$

[9] Up to a factor of 3 which was forgotten in [38].

The selection of dominant graphs in the large-N limit is not affected by the dimension of spacetime, hence the analysis of $d = 0$ applies here without change. The Grassmann nature of the fields leads instead to some extra minus signs, just as in the SYK case.

We concentrate again on the symmetric phase $\underline{\Psi} = 0$, which is the only possible one in $d = 1$. At LO in the $1/N$ expansion, $\mathbf{\Gamma}_2[0, G]$ is given again by a single diagram, the fundamental vacuum melon; with respect to (3.4.5) we only need to add the time dependence:

$$\begin{aligned}\mathbf{\Gamma}_2^{(3)}[G] &= \frac{-\lambda^2}{8N^3}\int_{t,t'} G_{a_1a_2a_3b_1b_2b_3}(t,t')G_{a_1a'_2a'_3b_1b'_2b'_3}(t,t')G_{a'_1a_2a'_3b'_1b_2b'_3}(t,t')G_{a'_1a'_2a_3b'_1b'_2b_3}(t,t') \\ &= -\frac{1}{8}\lambda^2 N^3\int_{t,t'} G(t,t')^4 \ ,\end{aligned} \tag{3.4.14}$$

where in the last equality we used a diagonal ansatz:

$$G_{a_1a_2a_3b_1b_2b_3}(t,t') = G(t,t')\delta_{a_1b_1}\delta_{a_2b_2}\delta_{a_3b_3} \ , \tag{3.4.15}$$

which is valid on shell. By comparison with (3.3.8) it is obvious that we obtain the same behavior as in SYK, in particular the bilocal nature of the interaction. In fact, including also the one-loop contribution:

$$\frac{1}{N^3}\mathbf{\Gamma}[0,G] = -\frac{1}{2}\operatorname{Tr}[\ln G^{-1}] - \frac{1}{2}\operatorname{Tr}[\partial_t G(t,t')] - \frac{1}{8}\lambda^2\int_{t,t'} G(t,t')^4 \ , \tag{3.4.16}$$

which has the same form as (3.3.10). If one were to not use a diagonal ansatz one would get:

$$\mathbf{\Gamma}[0,G] = -\frac{1}{2}\operatorname{Tr}[\ln G^{-1}_{a_1a_2a_3b_1b_2b_3}] - \frac{1}{2}\operatorname{Tr}[\partial_t G_{a_1a_2a_3b_1b_2b_3}(t,t')] + \mathbf{\Gamma}_2^{(3)}[G] \ . \tag{3.4.17}$$

with $\mathbf{\Gamma}_2^{(3)}[G]$ written as in the first line of (3.4.14).

As pointed out in [62], if in the infrared we discard the time-derivative term, the global $O(N)^3$ symmetry of (3.4.17) is promoted to a local symmetry.[10] The would-be gauge degrees of freedom associated to such local transformations are however proper degrees of freedom due to the explicit breaking provided by the time-derivative term, which we expect to endow them with an effective action controlling their dynamics. The idea is very similar to what happens with conformal symmetry: the action (3.4.16) has precisely the same form as (3.3.10), and as such it is also conformally invariant (i.e. invariant under time reparametrizations) in the infrared/strong-coupling limit, i.e. when discarding the time-derivative term. The time derivative can then be viewed as a conformal breaking operator that generates an effective action for the conformal mode, which takes the form of a Schwarzian action [47, 49] (see [124, 125] for a derivation with an action with a single bilocal field, as in our (3.3.10), or [126] for more details on how to regularize the conformal breaking operator). Choudhury et al. [62] have followed a similar route to obtain an effective action for the would-be gauge degrees of freedom, arriving at a non-linear sigma model type action, as one would expect on general grounds. However, they postulated the action (3.4.17) as an effective classical action without any derivation, while we derived it here as a 2PI effective action. It is not clear at the moment whether a formulation analogous to the one in Sec. 3.2.1 exists for the KTCT model, but we can see two limitations to it: first, we expect such a formulation to be necessarily more complicated in the tensor case, because there are many more invariants, and the large-N expansion cannot be interpreted as a loop expansion; second, as we saw in $d = 0$, the NLO and NNLO corrections to the 2PI effective action of the KTCT model do not have the form of the result of a one-loop integral (compare (3.4.11) with (3.2.9) or (3.3.18)),

[10] Notice that this does not happen in the SYK model: in Eq. (3.3.8) the trace $G_{aa}(t,t')$ identifies indices at different times, while in (3.4.14) indices are identified at equal times.

thus an hypothetical effective bilocal action would necessarily not factor the N-dependence as simply as in the vector case. However, we can bypass such open question, and apply the same reasoning directly to the 2PI effective action. In order to see why, it is useful to recall that in Sec. 3.3 we found that $\mathbf{\Gamma}_{GG}$ gives the inverse 4-point function. The latter is then singular if $\mathbf{\Gamma}_{GG}$ has zero eigenvalues, as it is the case if there is a gauge invariance which has not been gauge-fixed. In the present case we do not need a gauge fixing because there is an explicit breaking of the gauge invariance. The would-be gauge modes give a non-zero contribution to the quadratic part of the action which can be obtained by evaluating the quadratic part of the breaking term in the gauge transformations around the stationary point.

In order to translate in formulas what we just said, we write:

$$\mathbf{\Gamma}_{\rm inv}[G] = -\frac{1}{2}\,\mathrm{Tr}[\ln G^{-1}_{a_1a_2a_3b_1b_2b_3}] + \mathbf{\Gamma}^{(3)}_2[G]\;, \tag{3.4.18}$$

$$\mathbf{\Gamma}_{\rm pert}[G] = -\frac{1}{2}\,\mathrm{Tr}[\partial_t G_{a_1a_2a_3b_1b_2b_3}(t,t')]\;. \tag{3.4.19}$$

The stationary point of the total action splits as (using boldface for a collective index only for the tensor indices, e.g. $\mathbf{a} = a_1a_2a_3$):

$$\underline{G}_{\mathbf{ab}} = \underline{G}_0(t-t')\delta_{\mathbf{ab}} + \underline{G}_1(t-t')\delta_{\mathbf{ab}}\;, \tag{3.4.20}$$

where:

$$\frac{\delta\mathbf{\Gamma}_{\rm inv}}{\delta G_{\mathbf{ab}}}[\underline{G}_0] = 0\;, \tag{3.4.21}$$

$$\frac{\delta^2\mathbf{\Gamma}_{\rm inv}}{\delta G_{\mathbf{ab}}\delta G_{\mathbf{cc}}}[\underline{G}_0]\underline{G}_1 + \frac{\delta\mathbf{\Gamma}_{\rm pert}}{\delta G_{\mathbf{ab}}}[\underline{G}_0] = 0\;. \tag{3.4.22}$$

We emphasize that $\underline{G}_{\mathbf{ab}}$ is leading order in $1/N$: $\underline{G}_1$ is a perturbation in the strong coupling expansion, i.e. it arises by treating (3.4.19) as a perturbation to (3.4.18), but it is still leading order in the large N limit. Next, consider the transformation:

$$G_{\mathbf{ab}}(t,t') \to G_{\mathbf{a'b'}}(t,t')\mathbb{V}_{\mathbf{aa'}}(t)\mathbb{V}_{\mathbf{bb'}}(t')\;, \tag{3.4.23}$$

where:

$$\mathbb{V}_{\mathbf{ac}}(t) \equiv V^{(1)}_{a_1b_1}(t)V^{(2)}_{a_2b_2}(t)V^{(3)}_{a_3b_3}(t) \simeq \delta_{\mathbf{ab}} + \mathbb{H}_{\mathbf{ab}}(t) + \frac{1}{2}\mathbb{H}_{\mathbf{ac}}(t)\mathbb{H}_{\mathbf{cb}}(t) + \dots\;, \tag{3.4.24}$$

$$\mathbb{H}_{\mathbf{ab}}(t) = H^{(1)}_{a_1b_1}(t)\delta_{a_2b_2}\delta_{a_3b_3} + \delta_{a_1b_1}H^{(2)}_{a_2b_2}(t)\delta_{a_3b_3} + \delta_{a_1b_1}\delta_{a_2b_2}H^{(3)}_{a_3b_3}(t)\;, \tag{3.4.25}$$

for $V^{(i)}_{ab} \in O(N)$ and $H^{(i)}_{ab}$ an antisymmetric matrix, for $i = 1\dots3$. Such transformation leaves $\mathbf{\Gamma}_{\rm inv}[G]$ invariant, but not $\mathbf{\Gamma}_{\rm pert}[G]$. Using the invariance of the former, and the linearity in G of the latter, it can be easily shown (expanding at first order in $\underline{G}_1$ the left-hand-side and using (3.4.22)) that:

$$\frac{\delta^2(\mathbf{\Gamma}_{\rm inv}+\mathbf{\Gamma}_{\rm pert})}{\delta G_{\mathbf{ab}}\delta G_{\mathbf{cd}}}[\underline{G}]g_{\mathbf{ab}}g_{\mathbf{cd}} = \frac{\delta^2\mathbf{\Gamma}_{\rm pert}[\underline{G}_0\mathbb{V}_{\mathbf{ac}}\mathbb{V}_{\mathbf{bc}}]}{\delta\mathbb{H}_{\mathbf{ab}}\delta\mathbb{H}_{\mathbf{cd}}}\Big|_{\mathbb{H}=0}\mathbb{H}_{\mathbf{ab}}\mathbb{H}_{\mathbf{cd}}\;, \tag{3.4.26}$$

where:

$$g_{\mathbf{ab}} = \underline{G}(t,t')(\mathbb{H}_{\mathbf{ab}}(t) - \mathbb{H}_{\mathbf{ab}}(t'))\;. \tag{3.4.27}$$

Rewriting the quadratic part of $\underline{G}(t-t')\mathbb{V}_{\mathbf{ab}}(t)\mathbb{V}_{\mathbf{ab}}(t')$ as:

$$\begin{aligned}&\frac{1}{2}\underline{G}(t-t')(\mathbb{H}_{\mathbf{ac}}(t)\mathbb{H}_{\mathbf{ca}}(t) + \mathbb{H}_{\mathbf{ac}}(t')\mathbb{H}_{\mathbf{ca}}(t') - 2\mathbb{H}_{\mathbf{ab}}(t)\mathbb{H}_{\mathbf{ba}}(t'))\\ &\quad\simeq \frac{1}{2}\underline{G}(t-t')\left(\partial_t\mathbb{H}_{\mathbf{ac}}(t)\partial_t\mathbb{H}_{\mathbf{ca}}(t)(t-t')^2 + O((t-t')^3)\right)\;,\end{aligned} \tag{3.4.28}$$

we obtain:

$$\frac{\delta^2 \mathbf{\Gamma}_{\text{pert}}[\underline{G}_0 \mathbb{V}_{\mathbf{ac}} \mathbb{V}_{\mathbf{bc}}]}{\delta \mathbb{H}_{\mathbf{ab}} \delta \mathbb{H}_{\mathbf{cd}}}\Big|_{\mathbb{H}=0} \mathbb{H}_{\mathbf{ab}} \mathbb{H}_{\mathbf{cd}} = -\frac{\alpha}{2} \int_t \partial_t \mathbb{H}_{\mathbf{ac}}(t) \partial_t \mathbb{H}_{\mathbf{ca}}(t) \,, \tag{3.4.29}$$

where

$$\alpha = \int_\tau \underline{G}_0(\tau) \tau^2 \sigma(\tau) \,, \tag{3.4.30}$$

with $\sigma(\tau)$ a suitable regularization of $\delta'(\tau)$. This is precisely the same coefficient that appears in front of the Schwarzian action, as derived in [126], and the action coincides with the one derived in [62].

Chapter 4

Melonic CFTs

The dominance of melonic diagrams in the large-N limit of tensor models provides an interesting tractable limit in QFTs. Like cactus diagrams, melonic diagrams are built by recursive insertions of a fundamental two-point diagram on propagator lines. However, unlike tadpoles in cacti, which are ultralocal insertions created by adding only one vertex, the fundamental melonic two-point diagrams are bilocal insertions based on two vertices (see Fig. 4.1). In momentun space, this means that, unlike in a tadpole, in a melonic two-point diagram the external momentum flows also in loops, resulting in a nontrivial momentum dependence of the loop corrections to the two-point function. The two-point structure is also manifest in the four-point function. In vector models, opening vacuum cactus diagrams on two edges to obtain leading-order four-point diagrams leads to chains of bubbles (with propagators resumming the tadpole insertions like those of Fig. 1.1), which are easily resummed, as the corresponding amplitudes give a geometric series. In tensor models, opening melonic diagrams on two edges leads instead to ladder diagrams (with propagators resumming the melonic insertions), which in general are more difficult to resum (see Fig. 4.2).

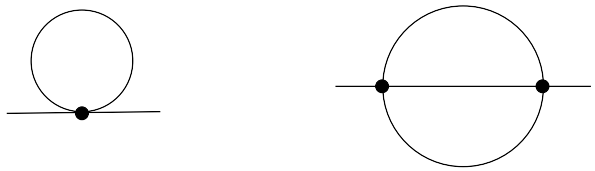

Figure 4.1: A tadpole two-point diagram (left) and a melonic two-point diagram (right), for models with quartic interactions.

Crucially, the melonic two-point function typically becomes conformal in the infrared limit, and so does also the four-point function. In such limit there exists a basis of conformal partial waves that diagonalize the four-point kernel associated to the ladders, and thus allows their resummation. One can also write renormalization group beta functions in the large-N limit, and show that they admit nontrivial fixed points corresponding to such conformal limit. This chapter is dedicated to reviewing these and related results, concentrating on the quartic $O(N)^3$ model: in Sec. 4.1 we will make the distinction between short-range and long-range models; in Sec. 4.2 we will show how the melonic limit simplifies the Schwinger-Dyson equations for two-point and four-point functions; in Sec. 4.3 we will discuss the beta functions and fixed points; and in Sec. 4.4 we will review the methods and results based on the conformal partial waves expansion. Lastly in Sec. 4.5 we will review an instability

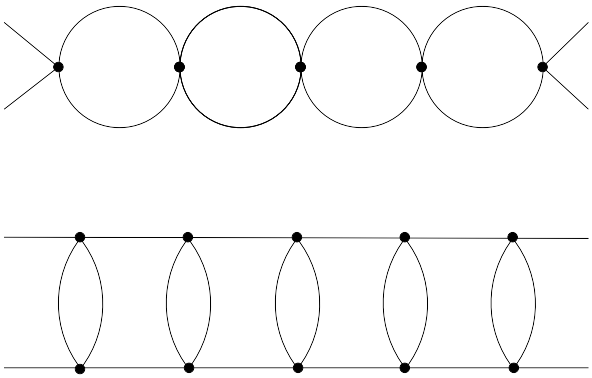

Figure 4.2: Two four-point diagrams contributing at the leading order in $1/N$ for vectors and tensors, respectively: a chain of bubbles (up) and a ladder (bottom).

theorem that is relevant for some melonic CFTs, but also for other large-N models, such as fishnet models.

4.1 Short-range and long-range models

Our case study for the application of the melonic large-N limit will be the $O(N)^3$ model with quartic interactions, introduced in Sec. 2.1, in dimensions $1 < d < 4$. For reasons that will become clear, we are interested in allowing a more general kinetic term than usual. The usual choice would be to take (2.1.3) with $C^{-1}(x,y) = -\partial_x^2\delta(x-y)$, leading to the short-range $O(N)^3$ model studied in [56, 71]. Our generalization consists in replacing the Laplacian operator with a fractional Laplacian $(-\partial^2)^\zeta$, with $0 < \zeta < 1$. The fractional power of the Laplacian can be defined in many equivalent ways [135]. The easiest definition is of course in Fourier space, where it is simply defined as the multiplication operator $p^{2\zeta}$. Going to position space one finds instead a representation as a hypersingular integral operator:[1]

$$(-\partial^2)^\zeta\phi(x) = \lim_{r\to 0} c(d/2+\zeta)\int_{|x-y|>r} \mathrm{d}^d y\, \frac{\phi(y)-\phi(x)}{|x-y|^{d+2\zeta}}\,, \tag{4.1.1}$$

with

$$c(\Delta) = \frac{\Gamma(\Delta)}{2^{d-2\Delta}\pi^{d/2}\Gamma(\frac{d}{2}-\Delta)}\,. \tag{4.1.2}$$

The subtraction term is often omitted, which can be justified by defining the integral by analytic continuation from $\zeta < 0$. For simplicity we will stick to this point of view, and therefore define the free part of the action as in (2.1.3), with convolution kernel

$$C^{-1}(x,y) = \frac{c(d/2+\zeta)}{|x-y|^{d+2\zeta}}\,. \tag{4.1.3}$$

[1] This can be derived by first writing

$$p^{2\zeta} = \frac{1}{\Gamma(-\zeta)}\int_0^{+\infty} \mathrm{d}t \frac{e^{-tp^2}-1}{t^{1+\zeta}}\,,$$

whose validity is trivially checked by rescaling $t \to t/p^2$ and recognizing that the integral reduces to $p^{2\zeta}$ times the Cauchy-Saalschütz representation of $\Gamma(-\zeta)$ for $0 < \zeta < 1$. The singular integral representation is then found by going back to position space and exchanging the order of integration [136].

Inverting (4.1.3) in momentum space, and then going back to position space, we find that the free covariance is[2]

$$C(x,y) = \frac{c(d/2-\zeta)}{|x-y|^{d-2\zeta}}\,, \tag{4.1.4}$$

from which one recognizes a conformal two-point function of a field with scaling dimension $\Delta_\phi = \frac{d-2\zeta}{2}$. We can also use the following formula in momentum space, valid for $0 < \zeta < 1$:

$$\tilde{C}(p) \equiv (p^2)^{-\zeta} = \frac{\sin(\pi\zeta)}{\pi}\int_0^{+\infty} ds\, \frac{s^{-\zeta}}{p^2+s}\,. \tag{4.1.5}$$

This provides a Källén-Lehmann spectral representation of the propagator, showing that the spectral density $\frac{\sin(\pi\zeta)}{\pi}s^{-\zeta}$ is positive for $0 < \zeta < 1$.

A Gaussian theory with a general covariance like (4.1.4) is often used as toy model in CFT, where it is known as generalized free field theory, or mean field theory (e.g. [137]). The choice of ζ distinguishes short-range models ($\zeta = 1$)[3] from long-range ones ($0 < \zeta < 1$).[4] The restriction to positive ζ guarantees standard thermodynamic properties, but some models with negative ζ are also of phenomenological interest. Models with positive and negative ζ are also known as "weak" and "strong" long-range models, respectively [138]. We will stick to positive ζ.

While short-range models are standard local QFTs, long-range models are nonlocal, and thus rather unusual from the point of view of high-energy physics. For example, the energy momentum tensor is not in their spectrum of local operators. However, long-range models are interesting models for statistical and mathematical physics (and more [139]), and they display several interesting features from a theoretical standpoint, justifying a long history of investigations. Most strikingly, such models admit phase transitions there where they are forbidden in their short-range analogs, for example in dimension $d = 1$, as proved for the long-range Ising model by Dyson [140]. Moreover, their critical exponents depend on ζ, thereby defining one-parameter families of universality classes [141]. Tuning this parameter, one can study, at fixed dimension, interesting phenomena such as the transition at some $\zeta^\star < 1$ from a long-range to a short-range universality class [142–149], or construct rigorous results [150–156]. For other applications and references we refer to recent works such as [157–162].

From a technical point of view, long-range models have advantages and disadvantages. On the challenging side, the computation of Feynman integrals is typically more complicated than in the short-range case, and indeed only recently we computed critical exponents for long-range quartic multiscalar models at three loops [163], while in the short-range case similar computations are available at seven loops [164]. One advantage of choosing a long-range model is instead that we can render the quartic interactions marginal (in the RG sense) in any dimension by choosing $\zeta = d/4$, so that $\Delta_\phi = d/4$. This can fact can be exploited for rigorous RG studies in integer dimension [152, 153, 156], and it is also our main reason for considering a long-range version of the $O(N)^3$ model.

Partially inspired by [165], where a long-range version of the SYK model was considered, a long-range version of the CTKT model was introduced in [75]. The model has the same potential (2.1.10), but in the free part of the action one chooses $\zeta = d/4$, a value that corresponds to the transition point between mean-field and non-trivial long-range behavior.[5]

[2] Notice that the covariance and its inverse are simply related by mapping ζ to $-\zeta$, which is an advantage of the chosen normalization. From a CFT perspective, this means that the inverse covariance has the interpretation of two-point function for the shadow operator (e.g. [137]), with a consistent normalization.

[3] The $\zeta \to 1$ limit of the right-hand side of (4.1.4) should be understood in the distributional sense, giving $C^{-1}(x,y) = -\partial_x^2\delta(x-y)$.

[4] Notice that in most of the literature a different notation is used for the power of the Laplacian, with $\zeta \equiv \sigma/2$.

[5] Mean field behavior for the long-range Ising model ($N = 1$) with $\zeta < d/4$ has been proved in [151].

4.2 Melonic Schwinger-Dyson equations

As we have seen in the previous chapter, the melonic limit allows us to write in closed form the 2PI effective action, and from it derive closed Schwinger-Dyson (SD) equations for the two- and four-point functions, that otherwise are usually known only perturbatively. We will review here such equations for $d > 1$.

Let us rewrite the general expression for the 2PI effective action (3.1.21) at $\phi = 0$, which will contain enough information in the symmetric phase of the model:

$$\Gamma[G] = \frac{1}{2}\,\mathrm{Tr}\left[C^{-1}G\right] + \frac{1}{2}\,\mathrm{Tr}[\ln G^{-1}] + \Gamma_2[G]\,. \tag{4.2.1}$$

In this chapter, we will slightly change notation with respect to Sec. 3.1, as we will use a boldface index $\mathbf{a}$ for an $O(N)^3$ triplet of indices abc, while writing separately the dependence on spacetime points. For example, for the first term in $\Gamma[G]$ we have

$$\mathrm{Tr}\left[C^{-1}G\right] \equiv \int_{x,y} (C^{-1})_{\mathbf{a},\mathbf{a}'}(x,y)G_{\mathbf{a}',\mathbf{a}}(y,x) = \int_{x,y} C^{-1}(x,y)G_{abc,abc}(y,x)\,, \tag{4.2.2}$$

where in the last step we used the fact that our free covariance is diagonal in the tensor indices. The two traces in (4.2.1) represent the classical and one-loop parts of the effective action, while $\Gamma_2[G]$ contains all the contributions from higher-loop 2PI diagrams, as explained before.

In the symmetric phase, the full two-point function is diagonal in the tensor indices:

$$G_{\mathbf{a},\mathbf{b}}(x,y) = G(x,y)\,\delta_{\mathbf{a},\mathbf{b}}\,, \tag{4.2.3}$$

hence $\mathrm{Tr}\left[C^{-1}G\right] = N^3 \int_{x,y}(C^{-1})(x,y)G(y,x)$. Similarly, the one-loop trace in (4.2.1) will also be of order N^3. Furthermore, as the propagator has the same index structure as in the free theory, the counting of factors of N is the same as in the original perturbative expansion, and thus the result (2.1.14) is still valid. Therefore, for any interacting part of the action as in (2.1.6), with ρ_b as in (2.1.9), we have the following expansion:

$$\Gamma_2[G] = \sum_{\omega\in\mathbb{N}/2} \Gamma_2^{(3-\omega)}[G]\,, \qquad \text{with } \Gamma_2^{(p)}[G] \sim N^p\,. \tag{4.2.4}$$

Our case study: the quartic model. For the particular choice of action (2.1.10), which will be our main focus, at leading order we have melon-tadpole diagrams. Imposing on such diagrams also the 2PI condition drastically reduces the number of leading order diagrams to just five: a melon with two tetrahedron bubbles (see Fig. 4.3), as in Sec. 3.4.1, and four figure-eight diagrams, three with one of the pillow bubbles and one with the double-trace (Fig. 4.4). In addition, if we do not include a mass term in the free part of the action, as we chose to do, we also need to add the one-loop diagram

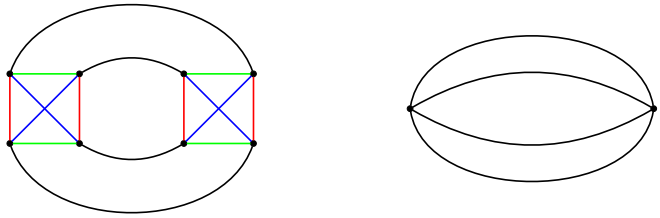

Figure 4.3: A vacuum 4-colored graph (left) built on two tetrahedron interactions, and the corresponding melonic Feynman diagram (right).

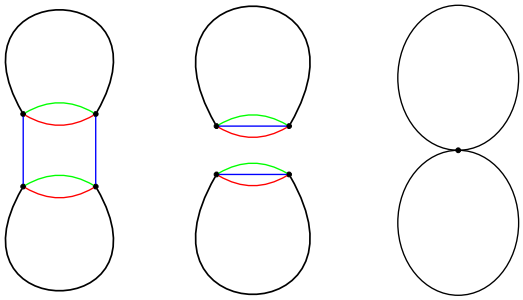

Figure 4.4: The two type of vacuum 4-colored graphs (left and center) corresponding to the figure-eight Feynam diagram (right), occurring at leading order in $1/N$.

with one two-valent vertex.[6] As a result, the 2PI effective action at leading order in $1/N$ is

$$\begin{aligned}\Gamma_2[G] =& \frac{m^{2\zeta}}{2}\int_x G_{a_1a_2a_3,a_1a_2a_3}(x,x) + \frac{\lambda_d}{4N^3}\int_x \left(G_{a_1a_2a_3,a_1a_2a_3}(x,x)\right)^2 \\ &+ \frac{\lambda_p}{12N^2}\sum_{i=1}^{3}\delta_{a_ia_i'}\delta_{b_ib_i'}\Big(\prod_{j\neq i}\delta_{a_jb_j}\delta_{a_j'b_j'}\Big)\int_x G_{a_1a_2a_3,b_1b_2b_3}(x,x)G_{a_1'a_2'a_3',b_1'b_2'b_3'}(x,x) \\ &- \frac{\lambda_t^2}{8N^3}\int_{x,y} G_{a_1a_2a_3,b_1b_2b_3}(x,y)G_{a_1a_2'a_3',b_1b_2'b_3'}(x,y)G_{a_1'a_2a_3',b_1'b_2b_3'}(x,y)G_{a_1'a_2'a_3,b_1'b_2'b_3}(x,y)\,.\end{aligned} \tag{4.2.5}$$

Notice that upon substitution of $G_{\mathbf{a},\mathbf{b}}$ by (4.2.3), we find that all the terms are indeed proportional to N^3:

$$\begin{aligned}\Gamma[G] = N^3\Big(&\frac{1}{2}\int_{x,y} C^{-1}(x,y)G(y,x) + \frac{1}{2}\int_{x,y}\ln(G^{-1})(x,y) + \frac{m^{2\zeta}}{2}\int_x G(x,x) \\ &+\frac{\lambda_p+\lambda_d}{4}\int_x G(x,x)^2 - \frac{\lambda_t^2}{8}\int_{x,y} G(x,y)^4\Big)\,.\end{aligned} \tag{4.2.6}$$

Strikingly, at leading order in $1/N$ we can write the full 2PI effective action in closed form. This is another manifestation of the fact that the melonic limit of tensor models lies somewhere in between

[6] This might seem to contradict what we said before about $\Gamma_2[G]$ containing only higher loops. More precisely, such statement holds if $S_{\text{int}}[\phi]$ includes only terms of order greater than two in ϕ, which in the present case is not true, as we chose to treat the mass term as a perturbation.

the planar limit of matrix models, for which a closed expression for the effective action is generally not possible, and the cactus limit of vector models, for which a closed expression is possible [122,123], but with a less interesting ultralocal structure at leading-order, identical to the first line of (4.2.5). As anticipated, the melon contribution in the last line of (4.2.5) is bilocal, thus leading to different physics than the vector model. This is an important feature of the melonic contributions, and it is also at the heart of the most interesting aspects of the SYK model.

4.2.1 Melonic two-point function

The melonic SD equations for the two-point function of the short- and long-range quartic $O(N)^3$ models have been studied in [56] and [75], respectively.

By plugging (4.2.5) into (3.1.23), and using (4.2.3), we find the melonic SD equation:

$$\begin{aligned} G^{-1}(x,y) &= C^{-1}(x,y) - \Sigma(x,y) \\ &= C^{-1}(x,y) + \delta(x-y)\left(m^{2\zeta} + (\lambda_d+\lambda_p)G(x,x)\right) - \lambda_t^2 G(x,y)^3 \,. \end{aligned} \tag{4.2.7}$$

The self energy $\Sigma(x,y)$ has the graphical interpretation in Fig. 4.5.

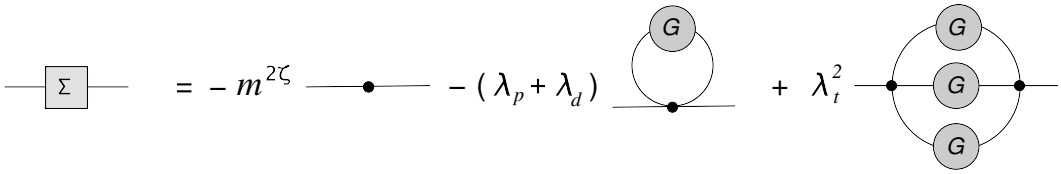

Figure 4.5: The self-energy $\Sigma(x,y)$ in Eq. (4.2.7). External legs are drawn for pictorial purposes, but they are actually amputated.

In momentum space this becomes:

$$G(p)^{-1} = C(p)^{-1} + m^{2\zeta} + (\lambda_p+\lambda_d)\int_q G(q) - \lambda_t^2 \int_{q_1,q_2} G(q_1)G(q_2)G(p+q_1+q_2)\,. \tag{4.2.8}$$

The bare mass can be tuned to cancel with the tadpoles and the melon contribution at $p=0$. Then, for $C(p)^{-1}=p^2$ (i.e. for $\zeta=1$), a simple power counting argument indicates that the solution admits two regimes [56]: a free scaling regime in the ultraviolet $G(p)^{-1}\sim p^2$ (with $C(p)^{-1}$ dominating over the self-energy), and an anomalous scaling regime in the infrared $G(p)^{-1}\sim p^{d/2}$ (with the self-energy dominating over $C(p)^{-1}$). Choosing instead, as in [75], $\zeta = d/4$ to match the infrared conformal behavior, one finds the same scaling behavior for all p. In fact, with $C(p)^{-1}=p^{d/2}$ and the bare mass tuned at criticality, the Schwinger-Dyson equation is formally solved by $G(p)=\mathcal{Z}p^{-d/2}$, as can be naively seen by plugging it into (4.2.8),

$$\frac{1}{\mathcal{Z}}p^{d/2} = p^{d/2} - \lambda_t^2\mathcal{Z}^3\int_{q_1,q_2}\frac{1}{q_1^{d/2}}\frac{1}{q_2^{d/2}}\left(\frac{1}{(p+q_1+q_2)^{d/2}} - \frac{1}{(q_1+q_2)^{d/2}}\right)\,, \tag{4.2.9}$$

and noticing that the double integral (which we call the melon integral) gives, after a rescaling of q_1 and q_2 by $|p|$, a global $|p|^{2d-3d/2}=|p|^{d/2}$. Differently from the $\zeta=1$ case of [56], here there is only one regime: $\Sigma(p)$ and $C(p)^{-1}$ are of the same order in p. However, the integrals in Eq. (4.2.8) are divergent, thus we need regularization and renormalization. The full procedure is detailed in [75], and we will not repeat it here. The final result of that analysis is that (4.2.9) is indeed satisfied in the

limit in which cutoffs are removed, with $\mathcal{Z}$ satisfying the algebraic equation:[7]

$$\mathcal{Z} = 1 - \lambda_t^2 \frac{1}{(4\pi)^d} \frac{\Gamma\left(1-\frac{d}{4}\right)}{\frac{d}{4}\Gamma\left(3\frac{d}{4}\right)} \mathcal{Z}^4 \,. \tag{4.2.10}$$

It should be stressed that $\mathcal{Z}$ is finite for $\zeta = d/4$ in $d < 4$, hence it is not a wave function renormalization, but rather a function that resums all the melonic insertions in the propagator. In fact, the quartic equation (4.2.10) is well known in combinatorics: it is the equation solved by the generating function of 4-Catalan (or order-4 Fuss-Catalan) numbers, which count rooted quaternary trees. That is, the series expansion of $\mathcal{Z}$ is

$$\mathcal{Z}(\lambda_t) = \sum_{n\geq 0} \frac{1}{4n+1}\binom{4n+1}{n}\kappa^n \,, \qquad \kappa = -\lambda_t^2 \frac{1}{(4\pi)^d} \frac{\Gamma\left(1-\frac{d}{4}\right)}{\frac{d}{4}\Gamma\left(3\frac{d}{4}\right)} \,. \tag{4.2.11}$$

The appearance of 4-Catalan numbers can be easily understood. In fact, since the subtracted melon integral with propagators $C(p) = p^{-d/2}$ is equal to $\kappa\, p^{d/2}$, any melonic insertion (i.e. insertion of a basic melon diagram in an edge) in a diagram γ has the simple effect of multiplying the amplitude of the original diagram by a factor κ. Therefore, the problem of summing all the perturbative melonic two-point diagrams reduces to a known combinatorial problem, whose solution is captured by the generating function of Fuss-Catalan numbers, because of the existing bijection between melonic two-point diagrams and rooted trees [35].

From the known properties of the Fuss-Catalan generating function, we know that the series (4.2.11) has a finite radius of convergence in κ, fixed by a singular point at $\kappa_c = 3^3/4^4 \simeq 0.105$, reached at a purely imaginary value of λ_t,

$$\lambda_{t,c}^2 = -\frac{3^3}{4^4} \frac{d(4\pi)^d \Gamma\left(3\frac{d}{4}\right)}{4\,\Gamma\left(1-\frac{d}{4}\right)} \,, \tag{4.2.12}$$

with the following singular behavior:

$$\mathcal{Z}(\lambda_t) \underset{\kappa\to\kappa_c^-}{\approx} \frac{1}{3}\Big(4 - \sqrt{\frac{8}{3}}\sqrt{1-\frac{\kappa}{\kappa_c}}\Big) \,. \tag{4.2.13}$$

It is also helpful to solve equation (4.2.10) in terms of the effective coupling

$$g_t = \lambda_t\, \mathcal{Z}(\lambda_t)^2 \,. \tag{4.2.14}$$

The rescaling by the square of the 4-Catalan function is an effective way of resumming the melonic two-point functions and absorbing their contribution in the coupling: once we switch to the coupling g_t, we only have to consider skeleton diagrams with no melonic insertions, and with $C(p) = p^{-d/2}$ as propagator. In terms of the effective coupling, the solution of (4.2.10) reads

$$\mathcal{Z} = 1 - g_t^2/g_{c,+}^2 \,, \qquad g_{c,+}^2 = \frac{d(4\pi)^d \Gamma\left(3\frac{d}{4}\right)}{4\,\Gamma\left(1-\frac{d}{4}\right)} = -\frac{\lambda_t^2}{\kappa} \,. \tag{4.2.15}$$

For real coupling, λ_t as a function of g_t blows up at $g_t = g_{c,+}$. For imaginary λ_t, and thus imaginary g_t, $\mathcal{Z}$ stays finite and positive, but becomes nonanalytic at the critical value $\lambda_t^2 = \lambda_{t,c}^2 = -\kappa_c g_{c,+}^2$. Since at such critical point we have $\mathcal{Z} = 4/3$, we find that the relation between g_t and λ_t ceases to be invertible at $g_t^2 = -g_{c,-}^2 = -\frac{1}{3}g_{c,+}^2$.

[7] Notice that because of the subtraction of the divergent term in (4.2.9), the melon integral, which naively would have seemed positive, gives a negative result for $d < 4$.

4.2.2 Melonic four-point kernel

The fact that, as anticipated, the melonic limit leads to a four-point function made of ladder diagrams has been first noticed and exploited in the context of the SYK model [49], and later used in higher dimensions in [56,70,71]. As we elaborated in a series of papers [75,116,166], this can be conveniently framed within the 2PI formalism.

The starting point is another important equation satisfied by the 2PI effective action, satisfied by its second derivative with respect to G:

$$\int_{u,v} \mathcal{F}_{(\mathbf{a},\mathbf{b});(\mathbf{c},\mathbf{d})}(x,y,u,v)\frac{\delta^2\Gamma}{\delta G_{\mathbf{cd}}(u,v)\delta G_{\mathbf{mn}}(w,z)} = \mathbb{I}_{\mathbf{ab};\mathbf{mn}}(x,y,w,z)\,, \tag{4.2.16}$$

where we have introduced the projector on symmetric bilocal matrices

$$\mathbb{I}_{\mathbf{ab};\mathbf{mn}}(x,y,w,z) = \frac{1}{2}(\delta_{\mathbf{am}}\delta_{\mathbf{bn}}\delta(x-w)\delta(y-z) + \delta_{\mathbf{an}}\delta_{\mathbf{bm}}\delta(x-z)\delta(y-w))\,, \tag{4.2.17}$$

and the *forward four-point function*, i.e. the four-point function connected and 1PI in the s-channel $(12\to 34)$:

$$\begin{aligned}\mathcal{F}_{(\mathbf{a},\mathbf{b});(\mathbf{c},\mathbf{d})}(x,y,w,z) = {}& \langle\phi_{\mathbf{a}}(x)\phi_{\mathbf{b}}(y)\phi_{\mathbf{c}}(w)\phi_{\mathbf{d}}(z)\rangle - \langle\phi_{\mathbf{a}}(x)\phi_{\mathbf{b}}(y)\rangle\,\langle\phi_{\mathbf{c}}(w)\phi_{\mathbf{d}}(z)\rangle \\ & - \int_{u,v}\langle\phi_{\mathbf{a}}(x)\phi_{\mathbf{b}}(y)\phi_{\mathbf{e}}(u)\rangle\, G^{-1}_{\mathbf{ef}}(u,v)\,\langle\phi_{\mathbf{f}}(v)\phi_{\mathbf{c}}(w)\phi_{\mathbf{d}}(z)\rangle\end{aligned} \tag{4.2.18}$$

Notice that if the expectation values here are evaluated without source term in the functional integral, then (4.2.16) holds for G on shell, i.e. for G that solves the SD equation.

We gave a proof of (4.2.16) in the case of vanishing one-point and three-point functions $\langle\phi\phi\phi\rangle$ in the previous chapter, see (3.1.18). The general case can be proved diagrammatically, or by the type of relations in footnote 11 of [12].

On the other hand, using (4.2.1), we find:

$$\frac{\delta^2\Gamma}{\delta G_{\mathbf{ab}}(x,y)\delta G_{\mathbf{mn}}(w,z)} = \frac{1}{2}\int_{u,v} G^{-1}_{\mathbf{ac}}(x,u)G^{-1}_{\mathbf{bd}}(y,v)\,(\mathbb{I}-K)_{\mathbf{cd};\mathbf{mn}}(u,v,w,z)\,, \tag{4.2.19}$$

where we introduced the four-point kernel K, also known as Bethe-Salpeter kernel,

$$K_{\mathbf{ab};\mathbf{mn}}(x,y,w,z) = \int_{u,v} G_{\mathbf{ac}}(x,u)G_{\mathbf{bd}}(y,v)\frac{\delta\Sigma_{\mathbf{m},\mathbf{n}}(w,z)}{\delta G_{\mathbf{cd}}(u,v)}\,. \tag{4.2.20}$$

Combining (4.2.16) and (4.2.19), we obtain:

$$\mathcal{F}_{(\mathbf{a},\mathbf{b});(\mathbf{m},\mathbf{n})}(x,y,w,z) = \int_{u,v}(\mathbb{I}-K)^{-1}_{\mathbf{ab};\mathbf{cd}}(x,y,u,v)\,(G_{\mathbf{cm}}(u,w)G_{\mathbf{dn}}(v,z) + G_{\mathbf{cn}}(u,z)G_{\mathbf{dm}}(v,w))\,. \tag{4.2.21}$$

This is a general equation, as we have not made any approximation so far, and it has a nice graphical interpretation, generalizing the type of expansion of Fig. 3.1 to the four-point function. Indeed, it is stating that since $\mathcal{F}_s$ is 1PI in the s-channel, it can be written as a sum of ladders whose rungs are 2PI in the s-channel, i.e. as a geometric series in the Bethe-Salpeter kernel, see Figure 4.6.

Going back to our quartic $O(N)^3$ model, in the large-N limit the 2PI effective action is given explicitly from (4.2.1) and (4.2.5), hence by taking derivatives we find an explicit expression for the four-point kernel. Going on shell, i.e. using the symmetric ansatz (4.2.3), the inversion of the tensor structure in $\mathbb{I}-K$ can also be performed explicitly, after recognizing that K can be decomposed in a

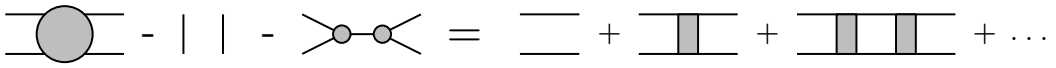

Figure 4.6: Graphical representation of $\mathcal{F}$, combining (4.2.18), on the left-hand side, with (4.2.21), on the right-hand side. The grey disks with four and three legs represent the full four-point and three-point functions, respectively, while a grey rectangle, together with the two edges to its left, represents the Bethe-Salpeter kernel K. For simplicity we have omitted the graphs with crossed edges on the right.

sum of orthogonal projectors:

$$\begin{aligned} K_{\mathbf{ab};\mathbf{cd}}(x_1,x_2,x_3,x_4) &= G(x_1,x_3)G(x_2,x_4)\Big(\lambda_t^2\, G(x_3,x_4)^2 - \lambda_1\delta(x_3-x_4)\Big)\hat{P}^{(1)}_{\mathbf{ab};\mathbf{cd}} \\ &\quad + G(x_1,x_3)G(x_2,x_4)\Big(3\lambda_t^2\, G(x_3,x_4)^2 - \lambda_2\delta(x_3-x_4)\Big)\hat{P}^{(2)}_{\mathbf{ab};\mathbf{cd}} \\ &\equiv K_1(x_1,x_2,x_3,x_4)\hat{P}^{(1)}_{\mathbf{ab};\mathbf{cd}} + K_2(x_1,x_2,x_3,x_4)\hat{P}^{(2)}_{\mathbf{ab};\mathbf{cd}}\,. \end{aligned} \tag{4.2.22}$$

where we have introduced the couplings $\lambda_1 = \lambda_p/3$ and $\lambda_2 = \lambda_d + \lambda_p$, and the orthogonal projectors[8]

$$\hat{P}^{(1)}_{\mathbf{ab};\mathbf{cd}} \;=\; 3(\hat{\delta}^{p}_{\mathbf{ab};\mathbf{cd}} - \hat{\delta}^{d}_{\mathbf{ab};\mathbf{cd}})\,, \qquad \hat{P}^{(2)}_{\mathbf{ab};\mathbf{cd}} \;=\; \hat{\delta}^{d}_{\mathbf{ab};\mathbf{cd}}\,. \tag{4.2.23}$$

in terms of the rescaled operators

$$\hat{\delta}^{p}_{\mathbf{ab};\mathbf{cd}} = \frac{1}{N^2}\,\delta^{p}_{\mathbf{ab};\mathbf{cd}}\,, \quad \hat{\delta}^{d}_{\mathbf{ab};\mathbf{cd}} = \frac{1}{N^3}\,\delta^{d}_{\mathbf{ab};\mathbf{cd}}\,, \tag{4.2.24}$$

with

$$\delta^{p}_{\mathbf{ab};\mathbf{cd}} = \frac{1}{3}\sum_{i=1}^{3}\delta_{a^i c^i}\delta_{b^i d^i}\prod_{j\neq i}\delta_{a^j b^j}\delta_{c^j d^j}\,, \qquad \delta^{d}_{\mathbf{ab};\mathbf{cd}} = \delta_{\mathbf{ab}}\delta_{\mathbf{cd}}\,. \tag{4.2.25}$$

As a consequence, we can resolve the index structure of (4.2.21):

$$\begin{aligned} \mathcal{F}_{(\mathbf{a},\mathbf{b});(\mathbf{c},\mathbf{d})}(x,y,w,z) &= \int_{u,v}\left(\mathbb{I}-K_1\right)^{-1}(x,y,u,v)\,\Big(G(u,w)G(v,z)\hat{P}^{(1)}_{\mathbf{ab};\mathbf{cd}} + G(u,z)G(v,w)\hat{P}^{(1)}_{\mathbf{ab};\mathbf{dc}}\Big) \\ &\quad + \hat{P}^{(2)}_{\mathbf{ab};\mathbf{cd}}\int_{u,v}\left(\mathbb{I}-K_2\right)^{-1}(x,y,u,v)\,\big(G(u,w)G(v,z)+G(u,z)G(v,w)\big)\,. \end{aligned} \tag{4.2.26}$$

Expanding $(\mathbb{I}-K_i)^{-1}$ as a geometric series in K_i, for $i=1,2$, one recognizes that (4.2.26) expresses the four-point function as a sum over a mixture of ladder and chain diagrams, built on the building blocks represented in Fig. 4.7. For $\lambda_t = 0$ we would have the typical chain diagrams of vector models, while for $\lambda_p = \lambda_d = 0$ we would have pure ladder diagrams (see Fig. 4.2). When all couplings are turned on, we have in general a ladder inside each bubble.

Clearly, the expansion of (4.2.26) in powers of K_i is a useful way to understand and generate the perturbative expansion of the four-point function, hence it is useful for the purpose of renormalization [75,167]. For example, we can write the all-order relation between the coupling λ_1 and its renormalized counterpart g_1, in the following way.

First, we define the renormalized coupling as

$$g_1 = \mathcal{Z}^2\Gamma^{(4;1)}(0,0,0,0)\,, \tag{4.2.27}$$

[8]This corresponds to the traceless-trace decomposition in the intermediate field representation of the pillow and double-trace interactions [84].

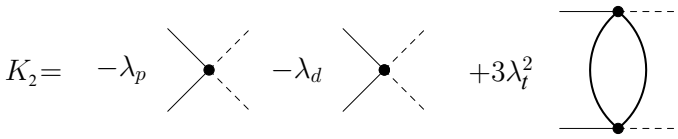

Figure 4.7: Graphical representation of the kernel K_2 in (4.2.22). Solid lines represent full two-point functions, while dashed lines represent amputated external legs. The first two terms are based respectively on pillow and double-trace vertices while the last one is based on a pair of tetrahedral vertices.

where we introduce the (traceless) pillow part of the proper (i.e. 1PI) vertex $\Gamma^{(4)}$ at vanishing external momenta.[9] In the present case, $\Gamma^{(4)}$ is simply minus the amputated connected four-point function, and in order to write the connected four-point function, we just have to subtract one more term from the forward four-point function $\mathcal{F}$, that is, the one represented by the first diagram on the right-hand side of Fig. 4.6. We thus schematically have

$$\Gamma^{(4;1)}\hat{P}_1 + \Gamma^{(4;2)}\hat{P}_2 = -G^{-1}G^{-1}\frac{K}{1-K}\ , \tag{4.2.28}$$

where the $G^{-1}G^{-1}$ prefactor amputates the external legs on the left (K is already amputated on the right), and the K in the numerator accounts for the subtraction of the disconnected term.

Next, we notice that the amplitude of any four-point diagram factors on the one-vertex irreducible (1VI) components : $A(\mathcal{G}) = A(\mathcal{G}_1)\dots A(\mathcal{G}_q)$. A diagram is called one-vertex reducible (1VR) if it disconnects into two nontrivial diagrams (i.e diagrams having internal vertices) by cutting a vertex (see Fig. 4.8), and 1VI if it has no such vertex. As there are no two-point subdiagrams (we are using the full propagator, which we implement by allowing no melonic insertions and using the effective tetrahedron coupling g_t, (4.2.14)), any 1VR four-point chain-ladder diagram disconnects into two four-point diagrams by cutting a pillow or double-trace vertex "vertically" and adding a pair of external edges on each resulting "half vertex". We write $\mathcal{G} = \mathcal{G}_1\mathcal{G}_2$. By this procedure, any four-point chain-ladder diagram can be decomposed as a chain $\mathcal{G} = \mathcal{G}_1\dots\mathcal{G}_q$ where $\mathcal{G}_i$ are 1VI.

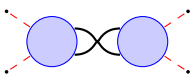

Figure 4.8: One vertex reducible graph. We represented in dashed red the amputated external edges.

We classify the 1VI diagrams into three families:

- The pure *ladders* depicted in Fig. 4.9 consisting in a nonempty sequence of vertical ladders with tetrahedral vertices g_t. We denote U_r the amplitude of the ladder diagram with r rungs. The sum over the ladders is:

$$U(g_t) = \sum_{r\geq 1} g_t^{2r} U_r\ . \tag{4.2.29}$$

[9] Notice that this is a non-minimal subtraction scheme, for a discussion of minimal subtraction for this model, see [167].

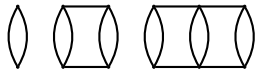

Figure 4.9: The pure ladders U_1, U_2 and U_3.

- The "v-ladders" or *caps*, that is ladders having a blue bare vertex at one end, depicted in Fig. 4.10. They consist in a blue bare vertex followed by a nonempty sequence of vertical ladder rungs with tetrahedral vertices. We denote S_r the amplitude of the cap with r rungs. The sum over the caps is:

$$S(g_t) = \sum_{r\geq 1} g_t^{2r} S_r \ . \tag{4.2.30}$$

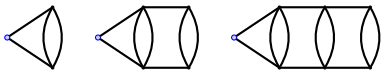

Figure 4.10: The caps S_1, S_2 and S_3.

- The "vv-ladders" or *double caps* having a blue bare vertex at each end, depicted in Fig. 4.11. They consist in a blue bare vertex followed by a *possibly empty* sequence of vertical ladder rungs with tetrahedral vertices, followed by a blue bare vertex. We denote T_r the amplitude of the double cap graph with r rungs (and the graph itself also T_r). The sum over the double caps is:

$$T(g_t) = \sum_{r\geq 0} g_t^{2r} T_r \ . \tag{4.2.31}$$

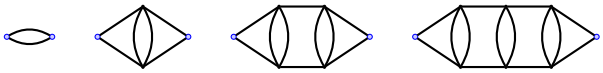

Figure 4.11: Some double caps.

Observing that in the generating functions $S(g)$ and $T(g)$ we have *not* included any coupling constants for the blue vertices, and by counting the number of reducibility vertices in a diagram, the bare series is simply:

$$\begin{aligned} g_1 &= -U(g_t) + \lambda_1 \mathcal{Z}^2 \big[1+S(g_t)\big] \Big[\sum_{q\geq 0} (-\lambda_1 \mathcal{Z}^2)^q \sum_{r_1,\dots r_q \geq 0} \prod_{i=1}^{q} g_t^{2r_i} T_{r_i} \Big] \big[1+S(g)\big] \\ &= -U(g_t) + \lambda_1 \mathcal{Z}^2 \frac{\big[1+S(g_t)\big]^2}{1+\lambda_1 \mathcal{Z}^2 T(g_t)} \ . \end{aligned} \tag{4.2.32}$$

A similar expression holds for g_2 as a function of λ_2, after replacing g_t^2 by $3g_t^2$. Notice that at $g_t = 0$ only T_0 is non-vanishing, and thus we recover the usual resummation of chain diagrams, as in the large-N limit of the vector $O(N)$ model.

Of course the amplitudes U_r, S_r and T_r need UV regularization, as well as IR regularization, due to the definition at vanishing external momentum. One can use a momentum cutoff [75] or an analytic regularization, deforming $\zeta = d/4 \to (d+\epsilon)/4$ [167]. We refer to the original papers for details and explicit computations.

Even more interestingly, if we were able to evaluate expression (4.2.33) without expanding it at small couplings, then we would have access to a nonperturbative result, that is, a resummation of all the four-point diagrams that are leading-order in $1/N$. As we will review in Sec. 4.4, it turns out that this is possible in the conformal limit, i.e. at the RG fixed points, and that this allows us to compute nonperturbatively the spectrum of operators appearing in the operator product expansion (OPE) of two fundamental fields. In this respect, we will mostly concentrate on the expression for the double trace of $\mathcal{F}$, which is useful in the determination of the spectrum of bilinear singlet operators. By taking a double trace on the forward four-point function, only the $\hat{P}^{(2)}$ projector contributes, and thus we find

$$\mathcal{F}_{(\mathbf{a},\mathbf{a});(\mathbf{c},\mathbf{c})}(x,y,w,z) = N^3 \int_{u,v} \left(\mathbb{I} - K_2\right)^{-1}(x,y,u,v)\left(G(u,w)G(v,z) + G(u,z)G(v,w)\right) . \quad (4.2.33)$$

4.3 Melonic fixed points

As we discussed, the SD equation (4.2.8) admits scaling solutions, either asymptotically in the UV or IR (for $\zeta = 1$), or at all scales (for $\zeta = d/4$). However, the additive mass renormalization that was used for the two point function (plus wave function renormalization in the short-range case) is not sufficient to cure the divergences appearing in the 4-point functions, hence we need also coupling renormalization. Scaling invariance (and likely conformal invariance) for the full theory will be achieved only at a fixed point of the renormalization group. This section is devoted to reviewing what we know so far about fixed points for the quartic $O(N)^3$ model (2.1.10).

4.3.1 Fixed points *à la* Wilson-Fisher

We first review the status of short-range models, that is, models with free covariance (4.1.4) with $\zeta = 1$. The tensor structure is irrelevant for the standard power counting, which is then the same as for ordinary scalar field theory. Therefore, we know that the critical dimension of quartic models is $d_c = 4$, while for sextic models is $d_c = 3$, and so on. In this case, fixed points will be found by dimensional continuation below the critical dimension, as in the classical Wilson-Fisher fixed point [6]. That is, fixed points are found at small ϵ in dimension $d = 4 - \epsilon$ for the quartic model, and so on.

The short-range model with interaction (2.1.10) was studied first in $d > 0$ (without pillow and double trace terms) by Klebanov and Tarnopolsky in [56], where the scaling solution for the two-point function was discussed. Soon after, Giombi, Klebanov and Tarnopolsky in [71] developed further such analysis and studied the system of beta functions for the full set of quartic interactions, using the results of [168] for a theory of scalar fields with a generic quartic potential. At leading order in $1/N$, and at cubic order in the couplings (i.e. at two loops) the beta functions have the following expression:

$$\beta_t = -\epsilon g_t + 2g_t^3 , \quad (4.3.1)$$

$$\beta_p = -\epsilon g_p + \left(6g_t^2 + \frac{2}{3}g_p^2\right) - 2g_t^2 g_p , \quad (4.3.2)$$

$$\beta_d = -\epsilon g_d + \left(\frac{4}{3}g_p^2 + 4g_p g_d + 2g_d^2\right) - 2g_t^2\left(4g_p + 5g_d\right) , \quad (4.3.3)$$

where we denote by g_i, with $i = t, p, d$, the renormalized couplings, rescaled by $(4\pi)^2$.

The beta function of g_t depends only on g_t itself, and it is entirely due to the wave function renormalization. That is, the tetrahedron coupling receives no vertex corrections at leading order in

$1/N$; this facts holds at all loop orders [75], as can be understood by analyzing the structure of the four-point function (4.2.26), which projects on the subspace spanned by the pillow and double-trace interactions.

Notice also that the double-trace coupling only enters in its own beta function. This can in part be understood as follows: setting $g_t = g_p = 0$ we obtain a vector model in disguise, with $O(N^3)$ invariance. Such enhanced symmetry prevents the generation of the pillow and tetrahedron interactions if they are initially absent, hence there cannot be pure g_d terms in their beta functions. That there are also no mixed terms involving g_d, at any loop order, can again be understoof from the structure of the four-point function (4.2.26), as the kernel K_1 contributing to the renormalization of the pillow interaction is independent of the double-trace coupling.

The beta functions (4.3.1) admit several fixed points: the trivial one, the $O(N^3)$ Wilson-Fisher fixed point, two Wilson-Fisher-like with $g_t = 0$ but non-zero pillow, and lastly eight non-trivial fixed points with $g_t \neq 0$, i.e.

$$g_t^* = \pm\sqrt{\epsilon/2}\,, \quad g_p^* = \pm 3\,\mathrm{i}\,\sqrt{\epsilon/2}\,, \quad g_d^* = \mp\,\mathrm{i}(3 \pm \sqrt{3})\sqrt{\epsilon/2}\,, \tag{4.3.4}$$

where for the global sign of g_d^* the choice is synchronized with that for g_p^*. It is the latter fixed points that we call *melonic*, as only for non-zero tetrahedron coupling we have melonic diagrams at large-N. The critical exponents (i.e. the eigenvalues of the stability matrix $\mathcal{B}_{ab} = \partial_{g_a}\beta_b|_{g=g^*}$) of the melonic fixed points are

$$\{\, 2\epsilon\,,\ \pm 2\,\mathrm{i}\,\sqrt{2\epsilon}\,,\ \pm 2\,\mathrm{i}\,\sqrt{6\epsilon}\,\}\,, \tag{4.3.5}$$

with corresponding right-eigenvectors in $\{g_t, g_p, g_d\}$ space (at leading order in ϵ)

$$\{\,(1,0,0)\,,\ (\pm\,\mathrm{i}\,3, 1, 0)\,,\ (\pm\,\mathrm{i}\,\sqrt{3}, 1, 1)\,\}\,. \tag{4.3.6}$$

The first exponent is real positive, that the fixed points are all IR-stable under perturbations of the tetrahedron coupling. However, the other two exponents are purely imaginary, meaning that in the (complex) space defined by the other two eigendirections the trajectories circle around the fixed point without ever reaching it.

Moreover, the complex critical exponents mean that the fixed-point theory has operators of complex dimension, hence it is non-unitary and, as we will discuss later, unstable.

The appearance of an instability is not unexpected, as the tetrahedron invariant is not positive definite. However, the unstable potential does not prevent the theory to be defined perturbatively, and in principle in the large-N limit the instability of the potential might be invisible (in $d = 0$ this is very familiar, as critical points of matrix models are usually found at the "wrong" sign of the coupling [112]). The above result shows that this is not the case for such type of melonic fixed point, as the imaginary part of the scaling dimensions is not suppressed at large N.

Notice that the melonic fixed points above are real, with real exponents, for $\epsilon < 0$, i.e. above the critical dimension. However, in such case the tetrahedron is always a relevant perturbation, that is, the fixed point is UV attractive. Moreover, complex dimensions reappear for $d > 4.155$ [71].

4.3.2 Lines of fixed points in long-range models

In the long range model, with $\zeta = d/4$ and $d < 4$, the kinetic term is nonlocal, and thus one finds that there is no wave function renormalization. As we explained above, at large N, the wave function renormalization is the only possible reason for a renormalization group flow of the tetrahedron coupling, as this receives no radiative correction at leading order; therefore, in the long-range case

one finds that the tetrahedron coupling is exactly marginal at large-N. As a consequence, we can consider d smaller and not close to 4, for example $d = 3$ or $d = 2$, while still having the luxury of a small parameter, which this time is the marginal coupling g_t. The combination of large-N and small g_t gives full control on the fixed points of the theory in any $d < 4$.

Surprisingly, it turns out that the fixed points and their critical exponents, as well as the scaling dimensions, and as we will see later also other CFT data, are all real at small g_t, if one chooses the latter to be purely imaginary [75, 167, 169]. Notice that since the tetrahedron invariant is not positive definite, the choice of imaginary coupling is almost[10] mandatory from the point of view of a non-perturbative finite-N functional integral, and it is also reminiscent of the Lee-Yang model with an $\mathrm{i}\,\lambda\phi^3$ interaction [170, 171]. It has been argued (see for example [172] and references therein) that in the case of a model with just a cubic interaction the instability and its related problems can be avoided by taking an imaginary coupling [173], or by taking special limits, such as the $n \to 0$ limit of the $(n+1)$-state Potts model [174], as in the percolation problem [175]. The large-N limit, can have a similar effect, at least near the upper critical dimension and for small imaginary coupling, as we will see below.

Defining the couplings $\lambda_1 = \lambda_p/3$, $\lambda_2 = \lambda_p + \lambda_d$ as in (4.2.22), and $\lambda = -\mathrm{i}\,\lambda_t$, the beta functions of the respective renormalized couplings g_1 and g_2 decouple, and as a consequence of the bare expansion (4.2.32), they can be written as

$$\begin{aligned}\beta_{g_1} &= \beta_0^g - 2\beta_1^g\, g_1 + \beta_2^g\, g_1^2\,,\\ \beta_{g_2} &= \beta_0^{\sqrt{3}g} - 2\beta_1^{\sqrt{3}g}\, g_2 + \beta_2^{\sqrt{3}g}\, g_2^2\,,\end{aligned} \tag{4.3.7}$$

where β_0^g, β_1^g and β_2^g are power series in g^2, with $g = -\mathrm{i}\, g_t = -\mathrm{i}\,\lambda_t \mathcal{Z}(\lambda_t)^2$ and $\mathcal{Z}(\lambda_t)$ given in (4.2.11). Notice that the fact that the beta functions are quadratic polynomials in g_i is not due to an approximation, it is instead the full result at large N, with the contribution of diagrams with arbitrarily large number of loops being contained in the g-dependent coefficients.

At lowest order in g, the coefficients are

$$\begin{aligned}\beta_0^g &= -\frac{2}{(4\pi)^{d/2}\Gamma(d/2)} g^2 + \mathcal{O}(g^4)\,,\\ \beta_1^g &= -\frac{2}{(4\pi)^{d}\Gamma(d/2)^2}\Big[\psi(1) + \psi(d/2) - 2\psi(d/4)\Big] g^2 + \mathcal{O}(g^4)\,,\\ \beta_2^g &= \frac{2}{(4\pi)^{d/2}\Gamma(d/2)} + \mathcal{O}(g^2)\,,\end{aligned} \tag{4.3.8}$$

where $\psi(z)$ denotes the digamma function.

The beta function β_{g_1} admits two fixed points:

$$g_{1\pm} = \frac{\beta_1^g \pm \sqrt{(\beta_1^g)^2 - \beta_0^g \beta_2^g}}{\beta_2^g} = \pm\sqrt{g^2} + \mathcal{O}(g^2)\,, \tag{4.3.9}$$

and the beta function β_{g_2} admits two fixed points of the same form, with $g^2 \to 3g^2$. The corresponding critical exponents are

$$\beta'_{g_1}(g_{1\pm}) = \pm 2\sqrt{(\beta_1^g)^2 - \beta_0^g\beta_2^g} = \pm\sqrt{g^2}\,\frac{4}{(4\pi)^{d/2}\Gamma(d/2)} + \mathcal{O}(g^3)\,, \tag{4.3.10}$$

[10] As argued in [92], one could in principle choose the pillow and double-trace (full) couplings sufficiently larger than the tetraehedron one, such that the whole potential is bounded from below. However, in the large-N limit the positivity constraint of [92] is violated, because at fixed 't Hooft couplings the tetrahedron term is enhanced by a factor $N^{1/2}$ and $N^{3/2}$ with respect to pillow and double-trace, respectively.

$$\beta'_{g_2}(g_{2\pm}) = \pm 2\sqrt{(\beta_1^{\sqrt{3}g})^2 - \beta_0^{\sqrt{3}g}\beta_2^{\sqrt{3}g}} = \pm\sqrt{3g^2}\frac{4}{(4\pi)^{d/2}\Gamma(d/2)} + \mathcal{O}(g^3)\,, \tag{4.3.11}$$

which are real for $g \in \mathbb{R}$, i.e. λ_t purely imaginary. Hence, the model has four fixed points in total, each of them actually defining a line parameterized by g in the $\{g_1, g_2\}$ plane. One of them, namely $\{g_{1+}, g_{2+}\}$, is IR stable, one is UV stable, and two are saddles (see Fig. 4.12). For $g \to 0$, they all merge into the trivial fixed point: for $g = 0$, non-trivial fixed points can only be obtained by moving away from marginality (i.e. by taking $4\zeta - d = \epsilon > 0$).

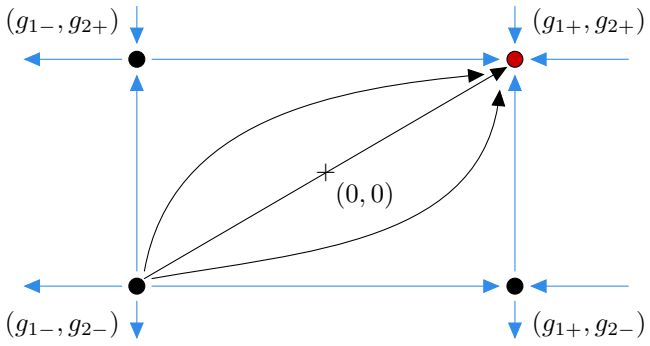

Figure 4.12: Trajectory between the fixed points in the space (g_1, g_2). The red dot is the IR stable fixed point.

4.3.3 Subleading orders in $1/N$

While the large-N limit provides on its own an interesting toy CFT to play with, in order to use the $1/N$ expansion as an approximation scheme, it is essential to understand how subleading corrections in $1/N$ affect the leading-order results. From both general experience, and simple inspection of diagrams that can provide radiative corrections to the tetrahedron interaction, we expect that the lines of fixed points will collapse to (potentially empty) set of isolated fixed points. This expectation has been verified and studied in [176].

It turns out that in the long-range quartic $O(N)^3$ model, sticking to $\zeta = d/4$, all the lines of fixed points collapse to the trivial fixed point. In order to find a precursor of the leading order melonic fixed points, one thus has to let $\zeta = (d+\epsilon)/4$ and allow $\epsilon > 0$. Actually, naively turning on ϵ does not help, as it contributes to the tetrahedron beta function with a term $-\epsilon\tilde{g}$, that being the only term of order N^0, leads to a trivial fixed point $\tilde{g}^\star = 0$ already at leading order. In order to get some guidance, it is instructive to consider a fictitious single-coupling beta function; the situation we have in the long-range model, at $\epsilon > 0$ and at next-to-leading order in $1/N$, is captured by a beta function of the form $-\epsilon g + g^2/N$. Its fixed points are the trivial one, and $g^\star = N\epsilon$, which goes to infinity if we take $N \to \infty$ at fixed ϵ. The problem is resolved by specifying how small should ϵ be in comparison to $1/N$. In particular, it is clear that we now need $N\epsilon \ll 1$. In other words, we should move the $-\epsilon\tilde{g}$ term to the first non-trivial order in $1/N$, by setting

$$\epsilon = \frac{\tilde{\epsilon}}{N}\,, \tag{4.3.12}$$

and expanding in $1/N$ first, and then in $\tilde{\epsilon}$.

While at leading order an imaginary tetrahedron coupling leads to four stable fixed lines of real pillow and double-trace couplings, going up to next-to-leading non-trivial order for all the beta functions fixes all the couplings to eight isolated fixed points, having the same reality properties as before

at leading order, but the opposite one at subleading order (i.e. real tetrahedron and purely imaginary pillow and double-trace corrections). As with the fixed point values, we have that also for the critical exponents what was real at leading order gets an imaginary part at subleading order. More precisely, we have

$$\begin{aligned}\beta_1'(\tilde{g}^\star) &= \frac{1}{3}\left(\tilde{\epsilon} - \frac{\alpha}{6}\tilde{\epsilon}^2\right) \pm \frac{2i}{3N^{1/2}}\left(\tilde{\epsilon} - \frac{\alpha}{2}\tilde{\epsilon}^2\right) + \mathcal{O}(\tilde{\epsilon}^3, N^{-1})\,,\\ \beta_2'(\tilde{g}^\star) &= \frac{1}{\sqrt{3}}\left(\tilde{\epsilon} - \frac{\alpha}{6}\tilde{\epsilon}^2\right) \pm \frac{2i}{\sqrt{3}N^{1/2}}\left(\tilde{\epsilon} - \frac{\alpha}{2}\tilde{\epsilon}^2\right) + \mathcal{O}(\tilde{\epsilon}^3, N^{-1})\,,\end{aligned} \tag{4.3.13}$$

where α is a constant resulting from a two-loop integral, and the combination $(\tilde{\epsilon} - \frac{\alpha}{6}\tilde{\epsilon}^2)$ is essentially the value of the tetrahedron coupling $\tilde{g}$ at the fixed point.

A similar analysis can be done also for the short-range model [176]. In this case, we need to assume $\epsilon N^2 \gg 1$. To this end, we set:

$$N = \tilde{N}/\sqrt{\epsilon}\,, \tag{4.3.14}$$

and we expand beta functions, fixed points and critical exponents in $1/\tilde{N}$ first, and only afterwards in ϵ. It turns out that the complex fixed points found in [71] persists at subleading orders in $1/N$. Importantly, the order $\tilde{N}^{-1/2}$ corrections to the critical exponents are zero, but the order $\tilde{N}^{-1}$ endow them with a real part, meaning that the fixed point is infrared stable. The situation is thus similar to the long-range model, but in this case it is the real part of the critical exponents which is suppressed in $1/N$, rather than the imaginary part; therefore, while the two models have probably qualitatively similar behavior at finite N, it is only in the long-range case that a real and unitary CFT arises in the strict large-N limit.

4.4 Conformal methods and results

As argued in [167], following the footsteps of [157], the fixed-point of the long-range $O(N)^3$ model is not only scale invariant, as any fixed-point theory should be, but also conformally invariant. Although this symmetry enhancement is rather common, there is no general proof, except in two dimensions [3] (see also the review [4]), and under assumptions which include unitarity and locality. As the long-range $O(N)^3$ model is clearly non-local, and (likely) unitary only at large N, the statement of conformal invariance is not obvious.

In [167], in order to tackle such question, we adapted to our model the methods of [157], where a proof of conformal invariance was given to all orders in perturbation theory for the infrared fixed-point of the long-range Ising model with propagator $C(p) = 1/p^{(d+\epsilon)/2}$. Most of that proof is built on standard ideas (e.g. from [177]), except that the non-local propagator of the long-range model implies the absence of a local energy-momentum tensor. To overcome this obstacle, the main idea is to use the Caffarelli-Silvestre trick [178] of localizing the kinetic term by means of an embedding of the theory in $d+p$ dimensions, with $p = 2-(d+\epsilon)/2$. The argument goes through also in our case, with some small modifications: we are interested in $\epsilon = 0$, and we must deal with multiple quartic interactions which mix under renormalization. At the end we conclude that, at the fixed-point of our $O(N)^3$ model, the n-point functions of fundamental fields are conformal invariant. The next step would be to generalize the above result to correlators of composite operators. A possible strategy, starting from correlators of fundamental fields and using an operator-product expansion to generate the composite fields, is sketched in [157], but has not been pursued further in our case. However, explicit computations of

some correlators of quadratic and quartic composite operators corroborate the statement that the theory is indeed conformal invariant [167].

Having conformal invariance at the fixed point allows us to borrow some powerful machinery from conformal field theory, and in particular from the representation theory of the conformal group, as we will review in the following subsections.

4.4.1 Basics of conformal partial wave expansion

We provide here some important formulas and background on the conformal partial wave expansion used to give nonperturbative meaning to the right-hand side of (4.2.26). The main results on conformal partial waves have been derived by Dobrev et al. in [179–181], and largely revived in recent years [137, 182–184].[11] Here we mostly follow the notation of [166], where a more general and detailed review can be found.

The main point is that, in the conformal limit, the Bethe-Salpeter kernel $K(x_1, x_2, x_3, x_4)$ of scalar fields of dimension Δ admits eigenfunctions with the structure of a conformal three-point function of the type:

$$\langle \phi_\Delta(x_3)\phi_\Delta(x_4)\mathcal{O}_h^{\mu_1\cdots\mu_J}(x_0)\rangle_{\rm cs} = \frac{\mathcal{S}_{\nu_1\cdots\nu_J}^{\mu_1\cdots\mu_J} Z^{\nu_1}\cdots Z^{\nu_J}}{|x_{34}|^{2\Delta-h}|x_{30}|^h|x_{40}|^h}\,, \tag{4.4.1}$$

where $\mathcal{S}_{\nu_1\cdots\nu_J}^{\mu_1\cdots\mu_J}$ is the projector on the symmetric-traceless part of rank-J tensors, $x_{ij} = x_i - x_j$ and

$$Z^\mu = \frac{|x_{30}||x_{40}|}{|x_{34}|}\left(\frac{x_{30}^\mu}{|x_{30}|^2} - \frac{x_{40}^\mu}{|x_{40}|^2}\right). \tag{4.4.2}$$

The eigenvalue equation reads

$$\int_{x_3x_4} K(x_1, x_2, x_3, x_4)\,\langle \phi_\Delta(x_3)\phi_\Delta(x_4)\mathcal{O}_h^{\mu_1\cdots\mu_J}(x_0)\rangle_{\rm cs} = k(h, J)\,\langle \phi_\Delta(x_1)\phi_\Delta(x_2)\mathcal{O}_h^{\mu_1\cdots\mu_J}(x_0)\rangle_{\rm cs}\,. \tag{4.4.3}$$

The subscript "cs" stands for conformal structure, meaning that the three-point function is just a notation for the structure on right-hand side of (4.4.1). In particular, there is no structure constant, and the operator $\mathcal{O}_h^{\mu_1\cdots\mu_J}(z)$, of conformal dimension h and in the spin-J symmetric-traceless representation of the spacetime rotation group $O(d)$, is in general not part of the spectrum of the CFT. We denote $\phi_\Delta(x)$ a generic scalar primary of dimension Δ, without introducing any flavor/color index structure, which we assume to be already diagonalized, as for example in (4.2.22).

Multiplied by the following normalization factor ($\tilde{h} = d - h$ is the dimension of the shadow operator [193])

$$\mathcal{N}_{h,J}^\Delta = \frac{2^{(2\Delta+h+J)/2}}{(2\pi)^{d/2}}\left(\frac{\Gamma(\frac{\tilde{h}+J+2\Delta-d}{2})\Gamma(\frac{h+J+2\Delta-d}{2})}{\Gamma(\frac{\tilde{h}+J-2\Delta+d}{2})\Gamma(\frac{h+J-2\Delta+d}{2})}\right)^{1/2}\frac{\Gamma(\frac{h+J}{2})}{\Gamma(\frac{\tilde{h}+J}{2})}\,, \tag{4.4.4}$$

the three-point functions (4.4.1) with fixed $\mathrm{Re}(\Delta) \in (d/4, 3d/4)$ form a complete and orthonormal basis in an appropriate space of bilocal functions [179, 181], the basis elements being labeled by the spin $J \in \mathbb{N}_0$, the position $x_0 \in \mathbb{R}^d$, and the scaling dimension $h \in \mathcal{P}_+$, where

$$\mathcal{P}_+ = \left\{ h \,\middle|\, h = \frac{d}{2} + \mathrm{i}\, r,\, r \in \mathbb{R}_+ \right\}, \tag{4.4.5}$$

[11] These methods have been at the heart of a very active field in recent years, see for example their use with Mellin amplitudes [185, 186], their application to the Sachdev-Ye-Kitaev (SYK) model [49, 70], to the bootstrap crossing equations [187–190], and to the construction of an AdS/CFT map [191, 192].

labels the principal series representations of the Euclidean conformal group $SO(d+1,1)$. More precisely, the space of bilocal functions $\mathcal{V}_\Delta$ can be defined as the space of smooth functions $f(x_1,x_2)$ that are square integrable with respect to the scalar product

$$(f_1,f_2)=\int_{x_1\dots x_4}\overline{f_1(x_1,x_2)}G^{-1}(x_1,x_3)G^{-1}(x_2,x_4)f_2(x_3,x_4)\,, \tag{4.4.6}$$

i.e. $(f,f)<\infty$, and satisfy the asymptotic boundary condition $f(x_1,x_2)\sim|x_1|^{-2\Delta}$ for $|x_1|\to\infty$ and similar for $|x_2|\to\infty$. Here, we have assumed that the bilocal functions have no symmetry under permutation of their two arguments, and we denoted $G(x,y)=c(\Delta)/|x-y|^{2\Delta}$ the full two-point function $\langle\phi_\Delta(x)\phi_\Delta(y)\rangle$ (conveniently normalized as in (4.1.4)). Similarly, we can introduce the shadow space $\mathcal{V}_{\widetilde{\Delta}}$ with its basis of three-point functions defined as above but with Δ replaced by its shadow $\widetilde{\Delta}=d-\Delta$. Since the two-point function of ϕ_Δ and that of $\phi_{\widetilde{\Delta}}$ are the inverse of each other (see (4.1.3)), we can write the analogue of the scalar product (4.4.6) for $\mathcal{V}_{\widetilde{\Delta}}$ by replacing G^{-1} with G, the two-point function of ϕ_Δ.

The relation between $\mathcal{V}_\Delta$ and $\mathcal{V}_{\widetilde{\Delta}}$ can better be understood in terms of raising and lowering of indices by the metric associated to the scalar product on them. Let us denote $f^{x_1x_2}$, with contravariant indices x_1,x_2, the elements of $\mathcal{V}_\Delta$, signaling that f has dimension Δ on each of its arguments. The factor $g_{x_1x_2;x_3x_4}=G^{-1}(x_1,x_3)G^{-1}(x_2,x_4)$ in the scalar product in (4.4.6) is a metric on $\mathcal{V}_\Delta$ with covariant indices, that is with dimension $\tilde{\Delta}=d-\Delta$ on each of its arguments. The inverse metric is $g^{x_1x_2;x_3x_4}=G(x_1,x_3)G(x_2,x_4)$ and the contraction on an index (integral over the position) has dimension $-d$. The metric and its inverse allow one to lower respectively raise indices, i.e. map $\mathcal{V}_\Delta$ to its dual $\mathcal{V}_{\widetilde{\Delta}}$. The mapping holds also for the basis elements:[12]

$$\begin{aligned}&\int\mathrm{d}^dx_3\mathrm{d}^dx_4\,C^{-1}(x_1,x_3)C^{-1}(x_2,x_4)\,\langle\phi_\Delta(x_3)\phi_\Delta(x_4)\mathcal{O}_h^{\mu_1\cdots\mu_J}(x_0)\rangle_{\mathrm{cs}}\,\mathcal{N}^\Delta_{h,J}\\&\quad=\langle\phi_{\widetilde{\Delta}}(x_1)\phi_{\widetilde{\Delta}}(x_2)\mathcal{O}_h^{\mu_1\cdots\mu_J}(x_0)\rangle_{\mathrm{cs}}\,\mathcal{N}^{\widetilde{\Delta}}_{h,J}\,.\end{aligned} \tag{4.4.7}$$

The completeness relation, or resolution of the identity, reads

$$\begin{aligned}\mathbb{I}(x_1,x_2,x_3,x_4)&\equiv\delta(x_1-x_3)\delta(x_2-x_4)\\&=\sum_{J\in\mathbb{N}_0}\int_{\frac{d}{2}}^{\frac{d}{2}+\mathrm{i}\,\infty}\frac{\mathrm{d}h}{2\pi\,\mathrm{i}}\rho(h,J)\,\mathcal{N}^\Delta_{h,J}\mathcal{N}^{\widetilde{\Delta}}_{\tilde{h},J}\,\Psi^{\Delta,\Delta,\widetilde{\Delta},\widetilde{\Delta}}_{h,J}(x_1,x_2,x_3,x_4)\,,\end{aligned} \tag{4.4.8}$$

where the equality holds in a distributional sense when acting from the left (integration over x_3 and x_4) on $\mathcal{V}_\Delta$, or from the right (integration over x_1 and x_2) on $\mathcal{V}_{\widetilde{\Delta}}$. We have introduced the Plancherel weight

$$\rho(h,J)=\frac{\Gamma(\frac{d}{2}+J)}{2(2\pi)^{d/2}J!}\frac{\Gamma(\tilde{h}-1)\Gamma(h-1)}{\Gamma(\frac{d}{2}-h)\Gamma(\frac{d}{2}-\tilde{h})}(h+J-1)(\tilde{h}+J-1)\,, \tag{4.4.9}$$

and the conformal partial wave, defined as[13]

$$\Psi^{\Delta,\Delta,\widetilde{\Delta},\widetilde{\Delta}}_{h,J}(x_1,x_2,x_3,x_4)=\int\mathrm{d}^dz\,\langle\phi_\Delta(x_1)\phi_\Delta(x_2)\mathcal{O}_h^{\mu_1\cdots\mu_J}(z)\rangle_{\mathrm{cs}}\langle\phi_{\widetilde{\Delta}}(x_3)\phi_{\widetilde{\Delta}}(x_4)\mathcal{O}^{\mu_1\cdots\mu_J}_{\tilde{h}}(z)\rangle_{\mathrm{cs}}\,. \tag{4.4.10}$$

[12] The three-point functions are not in $\mathcal{V}$, as they are not integrable, but they form a basis in the continuous sense, just like the Fourier basis does for $\mathrm{L}^2(\mathbb{R}^d)$.

[13] In the literature the same name has been often attributed to different objects appearing in this formalism, in particular to what we call $\mathcal{G}^{\Delta_i}_{h,J}(x_i)$ below (e.g. [5,194–196]), or to the $(n-1)$-point function appearing in the expansion of an n-point function in [180] (i.e. the eigenfunctions themselves for $n=4$). We follow [137, 183, 184] in the choice of naming.

We notice that the product of normalization factors of the basis simplifies to

$$\mathcal{N}^{\Delta}_{h,J}\mathcal{N}^{\widetilde{\Delta}}_{\tilde{h},J} = \frac{2^{3d/2+J}}{(2\pi)^d}\,. \tag{4.4.11}$$

Any endomorphism $\mathcal{E}:\mathcal{V}_\Delta\to\mathcal{V}_\Delta$ associated to a conformal kernel can be diagonalized by convoluting the kernel with the appropriate resolution of the identity, e.g.

$$\begin{aligned}\mathcal{E}(x_1,x_2,x_3,x_4) &= \int \mathrm{d}^d y_1 \mathrm{d}^d y_2\, \mathcal{E}(x_1,x_2,y_1,y_2)\,\mathbb{I}(y_1,y_2,x_3,x_4)\\ &= \sum_{J\in\mathbb{N}_0}\int_{\frac{d}{2}}^{\frac{d}{2}+\mathrm{i}\,\infty}\frac{\mathrm{d}h}{2\pi\,\mathrm{i}}\rho(h,J)\,\Lambda_{\mathcal{E}}(h,J)\,\mathcal{N}^{\Delta}_{h,J}\mathcal{N}^{\widetilde{\Delta}}_{\tilde{h},J}\,\Psi^{\Delta,\Delta,\widetilde{\Delta},\widetilde{\Delta}}_{h,J}(x_1,x_2,x_3,x_4)\,,\end{aligned} \tag{4.4.12}$$

where $\Lambda_{\mathcal{E}}(h,J)$ is the eigenvalue of $\mathcal{E}$, satisfying an equation similar to (4.4.3). Using the following relation between the conformal partial waves and the conformal blocks $\mathcal{G}_{h,J}$ [183, 195],

$$\begin{aligned}\Psi^{\Delta,\Delta,\widetilde{\Delta},\widetilde{\Delta}}_{h,J}(x_1,x_2,x_3,x_4) = \left(-\tfrac{1}{2}\right)^J\Big(&S_{\tilde{h},J}\,\mathcal{G}^{\Delta,\Delta,\widetilde{\Delta},\widetilde{\Delta}}_{h,J}(x_1,x_2,x_3,x_4)\\ &+ S_{h,J}\,\mathcal{G}^{\Delta,\Delta,\widetilde{\Delta},\widetilde{\Delta}}_{\tilde{h},J}(x_1,x_2,x_3,x_4)\Big)\,,\end{aligned} \tag{4.4.13}$$

with

$$S_{h,J} = \frac{\pi^{d/2}\Gamma(h-\frac{d}{2})\Gamma(h+J-1)\Gamma(\frac{\tilde{h}+J}{2})^2}{\Gamma(h-1)\Gamma(d-h+J)\Gamma(\frac{h+J}{2})^2}\,, \tag{4.4.14}$$

one can then write

$$\begin{aligned}&\mathcal{E}(x_1,x_2,x_3,x_4) =\\ &\sum_{J\in\mathbb{N}_0}\left(-\tfrac{1}{2}\right)^J\int_{\frac{d}{2}-\mathrm{i}\,\infty}^{\frac{d}{2}+\mathrm{i}\,\infty}\frac{\mathrm{d}h}{2\pi\,\mathrm{i}}\rho(h,J)\,\Lambda_{\mathcal{E}}(h,J)\,\mathcal{N}^{\Delta}_{h,J}\mathcal{N}^{\widetilde{\Delta}}_{\tilde{h},J}\,S_{\tilde{h},J}\,\mathcal{G}^{\Delta,\Delta,\widetilde{\Delta},\widetilde{\Delta}}_{h,J}(x_1,x_2,x_3,x_4)\,,\end{aligned} \tag{4.4.15}$$

where we used the symmetry of the measure factor $\rho(h,J)\,\mathcal{N}^{\Delta}_{h,J}\mathcal{N}^{\widetilde{\Delta}}_{\tilde{h},J}$ under shadow reflection $h\to\tilde{h}$ to extend the integration to negative imaginary parts and keep only one conformal block term.

Acting by convolution on the last two arguments of $\mathcal{E}(x_1,x_2,x_3,x_4)$ with the inverse metric, we obtain an operator mapping $\mathcal{V}_{\widetilde{\Delta}}$ to $\mathcal{V}_\Delta$, with a similar conformal partial wave expansion, except that the $\widetilde{\Delta}$ arguments are replaced by Δ:

$$\begin{aligned}&\int \mathrm{d}^d y_3 \mathrm{d}^d y_4\,\mathcal{E}(x_1,x_2,y_3,y_4)G(y_3,x_3)G(y_4,x_4)\\ &\quad= \sum_{J\in\mathbb{N}_0}\int_{\frac{d}{2}}^{\frac{d}{2}+\mathrm{i}\,\infty}\frac{\mathrm{d}h}{2\pi\,\mathrm{i}}\rho(h,J)\,\Lambda_{\mathcal{E}}(h,J)\,\mathcal{N}^{\Delta}_{h,J}\mathcal{N}^{\Delta}_{\tilde{h},J}\,\Psi^{\Delta,\Delta,\Delta,\Delta}_{h,J}(x_1,x_2,x_3,x_4)\\ &\quad= \sum_{J\in\mathbb{N}_0}\left(-\tfrac{1}{2}\right)^J\int_{\frac{d}{2}-\mathrm{i}\,\infty}^{\frac{d}{2}+\mathrm{i}\,\infty}\frac{\mathrm{d}h}{2\pi\,\mathrm{i}}\rho(h,J)\,\Lambda_{\mathcal{E}}(h,J)\,\mathcal{N}^{\Delta}_{h,J}\mathcal{N}^{\Delta}_{\tilde{h},J}\,S_{\tilde{h},J}\,\mathcal{G}^{\Delta,\Delta,\Delta,\Delta}_{h,J}(x_1,x_2,x_3,x_4)\,.\end{aligned} \tag{4.4.16}$$

In this case, the product of normalization factors has a ratio of gamma functions, with its own poles:[14]

$$\mathcal{N}^{\Delta}_{h,J}\mathcal{N}^{\Delta}_{\tilde{h},J} = \frac{2^{(2\Delta+d/2+J)}}{(2\pi)^d}\frac{\Gamma(\frac{\tilde{h}+J+2\Delta-d}{2})\Gamma(\frac{h+J+2\Delta-d}{2})}{\Gamma(\frac{\tilde{h}+J-2\Delta+d}{2})\Gamma(\frac{h+J-2\Delta+d}{2})}\,. \tag{4.4.17}$$

For $\mathcal{E}=\mathbb{I}$, (4.4.16), with $\Lambda_{\mathbb{I}}(h,J)=1$, gives a conformal partial wave expansion of the inverse metric. A similar expansion is obtained for the metric itself, replacing G with G^{-1} in the first line, and Δ with $\widetilde{\Delta}$ in the expansion.

[14] These poles do not cross the principal series as long as $\Delta > d/4$. Similarly, the poles of $\mathcal{N}^{\widetilde{\Delta}}_{h,J}\mathcal{N}^{\widetilde{\Delta}}_{\tilde{h},J}$ stay away from $h=d/2$ for $\Delta<3d/4$. Together, these two conditions explain the condition on Δ mentioned below (4.4.4).

In the case of symmetric bilocal functions,[15] the completeness relation is of the same type, but with contribution only from even spin:

$$\begin{aligned}\mathbb{I}_{\text{symm}}(x_1,x_2,x_3,x_4) &\equiv \frac{1}{2}\left(\delta(x_1-x_3)\delta(x_2-x_4)+\delta(x_1-x_4)\delta(x_2-x_3)\right)\\ &= \sum_{J\in\mathbb{N}_0^{\text{even}}}\int_{\frac{d}{2}}^{\frac{d}{2}+\mathrm{i}\,\infty}\frac{\mathrm{d}h}{2\pi\,\mathrm{i}}\rho(h,J)\,\mathcal{N}^{\Delta}_{h,J}\mathcal{N}^{\widetilde{\Delta}}_{h,J}\,\Psi^{\Delta,\Delta,\widetilde{\Delta},\widetilde{\Delta}}_{h,J}(x_1,x_2,x_3,x_4)\,.\end{aligned} \tag{4.4.18}$$

Non-normalizable contributions and OPE. In practical applications, such as those we encounter in the bulk in our long-range $O(N)^3$ model, some of the hypotheses behind what we just reviewed can be violated. Typically, we have two possible situations:

1. A four-point kernel $\mathcal{E}(x_1,x_2,x_3,x_4)$ with the correct conformal transformation might nevertheless not be an endomorphism on $\mathcal{V}_\Delta$ (or a map $\mathcal{V}_{\widetilde{\Delta}}\to\mathcal{V}_\Delta$) because its action on an element $f\in\mathcal{V}_\Delta$ (or $\tilde{f}\in\mathcal{V}_{\widetilde{\Delta}}$) leads to a function not satisfying the integrability condition associated to the scalar product (4.4.6).

2. The scalar field dimension might lie outside the range $(d/4,3d/4)$. This is in particular the case of the standard free theory (or the critical $O(N)$ model at large N) with $\Delta=d/2-1<d/4$, for $d<4$.

In both cases, we can still use the conformal partial wave machinery, as long as we take care of deforming the contour of integration over h, or isolating the non-normalizable contributions from the four-point kernel [183]. We discuss here only the first case, for the second see [197].

The typical example of a four-point kernel which is not an endomorphism is a physical four-point function of one scalar field ϕ whose s-channel OPE contains operators of dimension smaller than $d/2$. The identity operator is one such operator and it is always present, hence we always need to subtract the contribution that is disconnected in the s-channel, $C(x_1,x_2)C(x_3,x_4)$, before applying the expansion (4.4.16).[16] Similarly, if the field ϕ has $\Delta<d/2$ and the three-point function with itself is non-vanishing, then we need to subtract the contribution that is one-particle reducible in the s-channel (the s-channel skeleton tree diagram). Interestingly, these are the same terms that we had to subtract for the definition of the forward four-point function (4.2.18), appearing naturally in the 2PI formalism. From the expression (4.2.21), and remembering that since the Bethe-Salpeter kernel is right amputated in the conformal limit it is an endomorphism on $\mathcal{V}_\Delta$ (or $\mathcal{V}^{\text{symm}}_\Delta$), we recognize an expression of the type (4.4.16). Therefore, we can apply to $\mathcal{F}$ the expansion in the last line of (4.4.16), and pushing the integration contour to the right, the integral is reduced to a sum over the residues at the poles of the integrand (the poles of $\Lambda_{(\mathbb{I}-K)^{-1}}(h,J)$ being now the solutions of $k(h,J)=1$):

$$\begin{aligned}\mathcal{F}(x_1,x_2,x_3,x_4) &= \sum_{J\in\mathbb{N}_0}\int_{\frac{d}{2}-\mathrm{i}\,\infty}^{\frac{d}{2}+\mathrm{i}\,\infty}\frac{\mathrm{d}h}{2\pi\,\mathrm{i}}\frac{\mu_\Delta(h,J)}{1-k(h,J)}\,\mathcal{G}^{\Delta,\Delta,\Delta,\Delta}_{h,J}(x_1,x_2,x_3,x_4)\\ &= \sum_{m,J}c^2_{m,J}\,\mathcal{G}^{\Delta,\Delta,\Delta,\Delta}_{h_{m,J},J}(x_i)\,,\end{aligned} \tag{4.4.19}$$

[15] The corresponding space $\mathcal{V}^{\text{symm}}_\Delta$ is defined as before, except that the metric needs also symmetrization: $g^{\text{symm}}_{x_1x_2;x_3x_4}=\frac{1}{2}(G^{-1}(x_1,x_3)G^{-1}(x_2,x_4)+G^{-1}(x_1,x_4)G^{-1}(x_2,x_3))$.

[16] Convoluting $G(x_1,x_2)G(x_3,x_4)$ with $f(x_3,x_4)\in\mathcal{V}_\Delta$, we obtain a new function proportional to $G(x_1,x_2)$. Regardless of whether the proportionality constant is finite or not, $G(x_1,x_2)$ is not square integrable with respect to the scalar product in (4.4.6), and therefore it is not in $\mathcal{V}_\Delta$.

where we defined[17]

$$\mu_\Delta(h,J) = \left(-\tfrac{1}{2}\right)^J \rho(h,J)\mathcal{N}^\Delta_{h,J}\mathcal{N}^\Delta_{\tilde{h},J}\, S_{\tilde{h},J}\,, \tag{4.4.20}$$

and 'where in the second line the dimensions of spin-J operators, $h_{m,J}$, are the poles of $(1-k(h,J))^{-1}$, and the squares of the OPE coefficients $c_{m,J}$ are the residues at the poles:

$$c^2_{m,J} = -\mathrm{Res}\left[\frac{\mu_\Delta(h,J)}{1-k(h,J)}\right]_{h=h_{m,J}} = \frac{\mu_\Delta(h_{m,J},J)}{k'(h_{m,J},J)}\,, \tag{4.4.21}$$

This reproduces the operator product expansion of the four-point function in the s channel, if no other physical operators have dimension smaller than $d/2$. If instead other primaries have dimension smaller than $d/2$, then on the right of the principal series we pick their shadow pole; this must be corrected by deforming the contour in the conformal block representation to keep only the physical poles on the right, or equivalently (because of (4.4.13)), by adding to the expansion the appropriate Ψ contributions:

$$\begin{aligned}\mathcal{F}(x_1,x_2,x_3,x_4) = &\sum_{J\in\mathbb{N}_0}\int_{\frac{d}{2}}^{\frac{d}{2}+\mathrm{i}\,\infty}\frac{\mathrm{d}h}{2\pi\,\mathrm{i}}\frac{\rho(h,J)}{1-k(h,J)}\mathcal{N}^\Delta_{h,J}\mathcal{N}^\Delta_{\tilde{h},J}\,\Psi^{\Delta,\Delta,\Delta,\Delta}_{h,J}(x_1,x_2,x_3,x_4)\\ &-\sum_{i,J}\mathrm{Res}\left[\frac{\rho(h,J)}{1-k(h,J)}\mathcal{N}^\Delta_{h,J}\mathcal{N}^\Delta_{\tilde{h},J}\,\Psi^{\Delta,\Delta,\Delta,\Delta}_{h,J}(x_1,x_2,x_3,x_4)\right]_{h=h_i(J)<d/2}\,,\end{aligned} \tag{4.4.22}$$

where $h_i(J)$ are the physical solutions of $k(h,J)=1$ on the left of the principal series. These isolated contributions are exactly analogue to the contributions we subtracted from the four-point function to define $\mathcal{F}$. If such operators are present, we first subtract them from $\mathcal{F}$, then we use the resolution of the identity to decompose the subtracted $\mathcal{F}$, and finally we add them back as in (4.4.22) to give the expansion of $\mathcal{F}_s$ itself.

4.4.2 CFT data

We now return to our case study, the long-range $O(N)^3$ model with quartic interactions. Its spectrum of dimensions of bilinear operators of arbitrary spin, as well as their OPE coefficients, and some OPE coefficients of quartic operators, have been computed in [75,167,169], by applying the conformal partial wave method outlined above in combination with the knowledge of the Bethe-Salpeter kernel defined in (4.2.22).

The eigenvalues of K_2 and K_1 are [71,199]:

$$k_2(h,J) = 3k_1(h,J) = -\frac{3g^2}{(4\pi)^d}\frac{\Gamma(-\frac{d}{4}+\frac{h+J}{2})\Gamma(\frac{d}{4}-\frac{h-J}{2})}{\Gamma(\frac{3d}{4}-\frac{h-J}{2})\Gamma(\frac{d}{4}+\frac{h+J}{2})}\,, \tag{4.4.23}$$

with obvious notations. Notice that we have expressed the eigenvalues in terms of the effective tetrahedron coupling $g = -\,\mathrm{i}\,\lambda_t\,\mathcal{Z}(\lambda_t)^2$, which resums all the two-point melonic insertions. The latter are absent by construction in the 2PI effective action, but reappear when going on shell, i.e. when replacing the generic G by the solution of the SD equations $G_\star(x,y) = \mathcal{Z}(\lambda_t)C(x,y)$. By writing all quantities in terms of g we can keep ignoring the melonic insertions and use the free propagator, but we should restrict its range to $g^2 < g^2_{c,-}$, because of the square root singularity at the critical coupling (4.2.12).

A striking feature of the kernel eigenvalues is that they are only sensitive to the ladder part of the kernel.This fact can be puzzling, as the diagrams having λ_1 or λ_2 vertices are necessary at the

[17] This differs from the $\mu_\Delta(h,J)$ defined in [169] or [198] because of a differ normalization of two-point functions and conformal blocks.

perturbative level: expressing λ_1 as a series in the renormalized coupling g_1 and in g, they have to cancel the UV divergences of the ladder diagrams [75, 167]. Nevertheless, the result of the resummed series of diagrams, evaluated at the fixed point, where g_1 takes a specific g-dependent value, turns out to be expressible in terms of only ladder diagrams. This is a familiar situation in the four-point function of these models [71, 75, 169],[18] and it is due to the fact that in the conformal limit, the local kernel has zero eigenvalues.[19] The resummed series captures the contribution of the chain diagrams in a subtle manner. When evaluating the forward four-point function $\mathcal{F}$ by the conformal partial waves expansion, only the ladder kernel contributes, and thus one needs to integrate over the principal series an analytic function of g^2. However, the result of the integration (for $J = 0$) is a non-analytic function with a $\sqrt{g^2}$ branch cut. In the perturbative expansion such a branch cut can only come from the λ_1 diagrams, due to the branch cut in the $g_{1\pm}$ fixed points (4.3.9). Therefore, the non-perturbative resummation of the ladder diagrams automatically includes the contribution of the chain diagrams as well, which is a very non-trivial fact. A cross check of this statement is provided in [166].

As explained above, we can obtain the OPE spectrum and coefficients for the product of two fields from the representation (4.4.19) by computing the poles and residues of the integrand. Notice that in the application to (4.2.26), due to symmetry, only even spins contribute.

We concentrate on the part of $\mathcal{F}$ in (4.2.26) that is proportional to $\hat{P}^{(2)}$, i.e. the part part that has the index structure of the double-trace invariant, and that allows studying the OPE of $\phi_{abc}(x)\phi_{abc}(y)$, which involves only singlet operators. The part proportional to $\hat{P}^{(1)}$ is instead relevant for the OPE of $\hat{P}^{(1)}_{\mathbf{ab};\mathbf{a'b'}}\phi_{\mathbf{a'}}(x)\phi_{\mathbf{b'}}(y)$, which contains instead operators that are in a symmetric-traceless matrix representation of one of the $O(N)$'s, and the singlet one of the other two.[20] As K_1 and K_2 are simply related by the mapping $g^2 \to 3g^2$, we will consider only the spectrum of singlet operators.

One finds [169] two types of solutions of the equation $k_2(h, J) = 1$ at small renormalized tetrahedron coupling g. The first type,

$$h_\pm = \frac{d}{2} \pm \frac{2}{(4\pi)^{d/2}\Gamma(d/2)}\sqrt{3g^2} + \mathcal{O}(g^3)\,, \tag{4.4.24}$$

only exists for the scalar (spin $J = 0$) case. It is real (at all orders in g) only for real g, i.e. for purely imaginary tetrahedron coupling λ_t. Moreover we recognize that $h_\pm = \frac{d}{2} + \frac{1}{2}\beta'_{g_2}(g_{2\pm})$, as the expected dimension of the composite operator $\phi_{abc}\phi_{abc}$ in the large-N limit (that is, half the dimension of $(\phi_{abc}\phi_{abc})^2$). Notice that $h_- < d/2$, hence at the (UV) fixed points with $g_2 = g_{2-}$ we need to deform the contour of the conformal partial waves representation in order to take h_- and not its shadow h_+. At $g_2 = g_{2+}$ (IR fixed point) instead the contour needs no deformation. The fact that the conformal dimensions at the UV and IR fixed points are related by $h_- = d - h_+$ is expected on general grounds for large-N flows between fixed points triggered by double-trace deformations [202].

The second type of solution,

$$h_{m,J} = \frac{d}{2} + J + 2m - \frac{\Gamma(m+J)\Gamma(m+1-\frac{d}{2})\sin\left(\frac{\pi d}{2}\right)}{\Gamma(\frac{d}{2}+J+m)\Gamma(m+1)\,(4\pi)^d\pi}6g^2 + \mathcal{O}(g^4)\,, \tag{4.4.25}$$

with $m, J \in \mathbb{N}_0$, but not simultaneously zero, exists for both $J = 0$ and $J > 0$. It is real (at all orders in g) for both real and purely imaginary tetrahedron coupling. In the free limit $g = 0$, we recover the

[18] As well as in the fishnet model [200, 201].

[19] This is straightforward for $\mathrm{Re}(h) > d/2$, as (4.4.1) is proportional to $|x_{34}|^{h-d/2}$ and thus it vanishes when we apply $\delta(x_{34})$ on it. The results is then extended by analytic continuation to the principal series and beyond.

[20] These types of operators have been considered for the one-dimensional CTKT model in [61].

classical dimensions $\frac{d}{2}+J+2m$ of the primary bilinear operators with arbitrary spin J, schematically of the form

$$O_{h,J} \sim \phi_{abc}\partial_{\mu_1}\dots\partial_{\mu_J}(\partial^2)^m\phi_{abc}\,. \tag{4.4.26}$$

The same scaling dimensions of the free theory are obtained also in the large J or large m limits, consistently with general results [203].

The solutions (4.4.24) and (4.4.25) are all real for real g, and above unitarity bounds (e.g. [5]) for g small enough:

$$h_\pm, h_{m,0} \geq \frac{d}{2}-1\,, \qquad h_{m,J} \geq d+J-2\,. \tag{4.4.27}$$

The associated OPE coefficients are also real [169]. These facts indicate that, despite the imaginary coupling and unbounded potential, for which we expect the full model to be non-unitary, at large N and small g it is actually unitary. As we have seen in Sec. 4.3.3, the large-N mechanism for such outcome is that the non-unitarity manifests itself in the form of complex operator dimensions, but with imaginary part suppressed in the large-N limit, $h \simeq \alpha_0 + \mathrm{i}\,\alpha_1/\sqrt{N} + \mathrm{O}(1/N^2)$. As we will see below, nonunitarity can also manifest itself by violations of the bounds (4.4.27), which can happen at large values of g, as we will now see.

One powerful aspect of having an exact expression of the Bethe-Salpeter kernel at large N is the fact that we do not have to limit ourselves to infinitesimal tetrahedron coupling g: we can find numerical solutions also at finite coupling. We can visualize the solutions by plotting the function $k_2(h,J)-1$ at various values of d and J, and looking at its intersections with the horizontal axis, as in Fig. 4.13. Notice that, as expected, there is no solution that would correspond to a local energy momentum tensor, which would have $J=2$ and $h=d$.

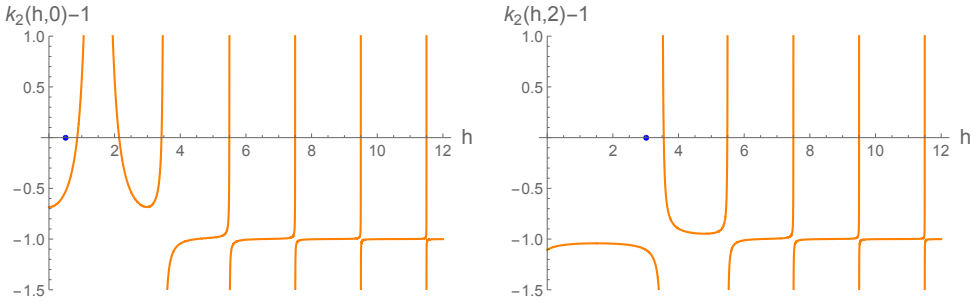

Figure 4.13: Plots of $k_2(h,0)-1$ (left) and $k_2(h,2)-1$ (right) for $d=3$ (left) and $g=7$. The zeros on the left panel correspond (from left to right) to h_-, h_+, and $h_{1,0}$ to $h_{5,0}$, while on the right panel they correspond to $h_{0,2}$ to $h_{4,2}$. The blue dot marks the lower bound from unitarity.

It turns out that if we crank up the coupling beyond some threshold $g_\star$, some scaling dimensions merge and then become complex. More specifically, at $J=0$ we find that h_+ merges with $h_{1,0}$ at $g=g_\star$, and similarly do their shadows. Threshold coupling for $J>0$ exist as well, but are larger than for spin zero. However, we should remember to keep $g^2 < g^2_{c,-}$, as otherwise we loose the mapping to the original coupling λ_t. It turns out that in this quartic model we always have $g^2_\star > g^2_{c,-}$, except at $d \simeq 2.9728 \equiv d_\star$, at which the reality threshold and the critical coupling coincide. Therefore, as long as melonic insertions are summable, the spectrum remains always real.

Surprisingly, at $g^2 = g^2_{c,-}$ we find two exact solutions of the equation $k_2(h,0)=1$, namely at $h=0$ and $h=d$, for any d. From a numerical check, we find that for $d \lesssim d_\star$ these correspond to $h_\pm$, while for $d \gtrsim d_\star$ the solution $h=0$ comes from the continuation of a negative solution, and $h=d$

corresponds to h_1.[21] This is depicted in Fig. 4.14 for $d = 2.7$ and $d = 3.3$. Notice that in both cases h_- violates the unitarity bound, hence the UV fixed point gives a nonunitary CFT for g^2 larger than some value $g^2_{\text{n.u.}} < g^2_{c,-}$. By numerical inspection, this only happens for $d \lesssim 3.5236$, while for larger dimensions h_- stays above the unitary bound.

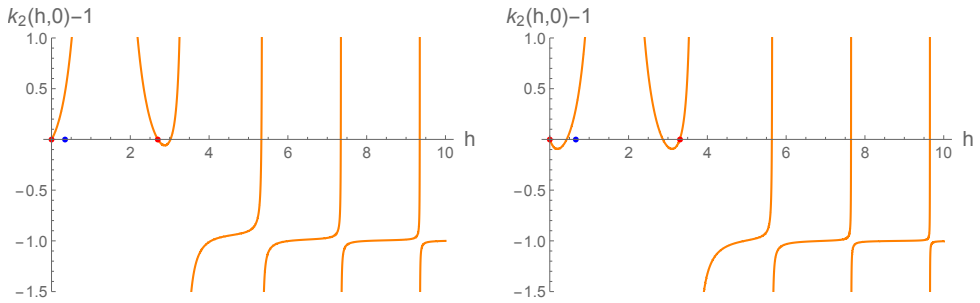

Figure 4.14: Plots of $k_2(h, 0) - 1$ for $d = 2.7$ (left) and $d = 3.3$ (right) at $g = g_{c,-}$ (roughly equal to 8.76 and 16.97, respectively). The zeros on the left panel correspond (from left to right) to h_-, h_+, and $h_{1,0}$ to $h_{4,0}$, while on the right panel the same solutions correspond to the zeros at $h > 0$, and a new solution appear at $h = 0$ as continuation of a negative one. The zeros at $h = 0$ and $h = d$ are marked by a red dot. The blue dot marks instead the lower bound from unitarity, i.e. $h \geq d/2 - 1$.

The main conclusion is that the infrared-stable fixed point of Fig. 4.12 is always compatible with a unitary CFT for any value of $d < 4$ and $g^2 < g^2_{c,-}$, while for the other fixed points unitarity is possible only up to some smaller value of g^2, or for $d \gtrsim 3.5236$.

4.4.3 F-theorem

We have seen in Sec. 4.2 that at large N the first and second functional derivatives of the 2PI effective action give us the exact structure of two-point and four-point functions, and in this section we have applied conformal methods to the latter in order to give nonperturbative meaning to such expression and extract CFT data. We are now going to briefly review how the 2PI formalism and the conformal partial wave expansion can also be jointly applied to the evaluation of the 2PI effective action itself, i.e. without taking any derivatives, on the solution of the SD equations, at the fixed point [197]. Formally this gives us the free energy of the CFT, which is a central quantity in statistical physics. However, the free energy is ill-defined in a CFT, because the vacuum diagrams on which it is built suffer from both UV and IR divergences. In order to cure the infrared divergences, without destroying the symmetries of the CFT, we can exploit the fact that any CFT can be placed on S^d, a d-sphere of radius a, by means of a Weyl mapping. On the other hand, ultraviolet divergences are still present on the sphere, and thus they require a regularization and subtraction. In $d = 3$, the remaining finite part of the sphere free energy is universal and independent of the sphere radius, and it is the quantity called F in the F-theorem.

[21] The solution $h_1 = d$ means that the kinetic operator of the short-range model, $\phi_{abc}\partial^2\phi_{abc}$, becomes marginal. Interestingly, this is the expected mechanism by which the crossover between long-range and short-range should occur [142], and it has been analyzed in a melonic approximation in [143]. However, this observation does not seem to be useful in the $O(N)^3$ model, as we do not know how to make sense of the model at $g^2 > g^2_{c,-}$, and in any case we do not expect a crossover to short-range behavior, as for example the scaling dimension of the tetrahedron operator would be discontinuous.

The F-theorem states that, if two unitary three-dimensional CFTs are connected by an RG flow, then $F_{UV} > F_{IR}$, i.e. the finite part of the sphere free energy is smaller for the CFT in the IR than for the one in the UV. It was first conjectured in [204, 205], where various checks were performed on supersymmetric theories, then extended to non-supersymmetric ones in [206] (see also [207] for a review and more references). Shortly after, the F-theorem was proven in [208], using the relation between the free energy and the entanglement entropy across a circle [209].

Since unitarity plays a crucial role in the entanglement-based proof of the F-theorem (like in other similar results, such as the c-theorem [210] and the a-theorem [211, 212]), testing if $F_{UV} > F_{IR}$ holds in our fixed points in Fig. 4.12 is non-trivial. As we reviewed above, all the evidence so far suggests that all such fixed points are unitary CFTs (at least at small g), but of course this evidence is far from being a proof, as we cannot exclude that non-unitarity might manifest itself in some operators of large dimension, and certainly we know that it fails at subleading orders in $1/N$. Therefore, this model does not fall straightforwardly in the domain of applicability of the F-theorem, as proved so far, and testing it is non-trivial.

In [197], we studied the long-range $O(N)^3$ model on the sphere, computed the free energy at next-to-next-to-leading order (NNLO), and tested the F-theorem. We briefly review this here, to highlight the results, and also to show another application of the methods reviewed above.

Mapping a CFT to the sphere in practice amounts to replacing the flat-space distances $|x-y|$ appearing in the conformal correlators with the chordal distance

$$s(x,y) = 2a\frac{|x-y|}{(1+x^2)^{1/2}(1+y^2)^{1/2}} = |x-y|\Omega(x)^{1/2}\Omega(y)^{1/2}\,, \tag{4.4.28}$$

where we used stereographic coordinates, in which the metric is explicitly conformally flat, i.e.

$$g_{\mu\nu}(x) = \Omega(x)^2\delta_{\mu\nu}\,, \qquad \Omega(x) = \frac{2a}{(1+x^2)}\,. \tag{4.4.29}$$

The square root of the determinant of the metric is then given $\sqrt{g} = \Omega(x)^d$, and for our purposes its appearance in the integration measure is the other main difference with respect to the flat case.

In order to evaluate the on-shell 2PI effective action, i.e. the free energy, at leading order, we start from (4.2.6), and replace G by the solution $G_\star(x,y) = \mathcal{Z}C(x,y)$ (and remembering that we defined $\lambda_2 = \lambda_p + \lambda_d$ and $\lambda = -\,\mathrm{i}\,\lambda_t$):

$$\begin{aligned}\Gamma[G] =& N^3\left(\frac{1}{2}\mathcal{Z}\,\mathrm{Tr}[C^{-1}C] + \frac{1}{2}\,\mathrm{Tr}[\ln(\mathcal{Z}^{-1}C^{-1})] + \frac{m^{2\zeta}}{2}\mathcal{Z}\int_x C(x,x)\right.\\ &\left. + \frac{\lambda_2\mathcal{Z}^2}{4}\int_x C(x,x)^2 + \frac{\lambda^2\mathcal{Z}^4}{8}\int_{x,y} C(x,y)^4\right)\,,\end{aligned} \tag{4.4.30}$$

where now the integrals and the covariance are the ones for the d-sphere (and ultimately we will be interested in $d=3$). We have five terms to evaluate, all of which are UV divergent. By analytic regularization, it turns out that they are all zero (i.e. they have no finite part), except for $\frac{1}{2}\,\mathrm{Tr}[\ln(C^{-1})]$, which reproduces the free energy of a generalized free field theory, and has been computed in [206,213]. As this is independent of the interacting terms, it is the same at all the fixed points, and thus we need to move to subleading orders if we want to make a non-trivial test of the F-theorem.[22]

As we recalled in Sections 2.1 and 3.4, the free energy of the $O(N)^3$ model has a series expansion in $1/\sqrt{N}$ [38]. At NLO the only 2PI diagram is a figure eight with one tetrahedron vertex, as in Fig. 3.9, and hence its contribution vanishes like the similar LO contributions from the λ_2 coupling.

[22] The same happens in the $O(N)$ model [206].

The NNLO 2PI diagrams of the $O(N)^3$ model with only the tetrahedron interaction have been reviewed in Sec. 3.4.1: they are given by an infinite family of ladder-like diagrams, closed in a planar way as shown in Fig. 3.10, plus one special diagram, shown in Fig. 3.11. It is straightforward to complement that analysis by adding the effect of the pillow and double-trace interactions. It turns out that we only need to add diagrams obtained from the ladder diagrams by replacing one or more rungs (each made by two λ vertices) with one or more local λ_1 vertices, as in the expansion of the four-point function.[23]

It turns out that the graph of Fig. 3.11 gives a finite contribution to the sphere free energy. However, since it only depends on the tetrahedron coupling, it takes the same value at all the fixed points, and thus it does not play a role in checking the F-theorem for this model.

As for the ladder-chain diagrams, they can be resummed in terms of the K_1 kernel defined in (4.2.22):[24]

$$\Gamma_{\text{NNLO}}[G] = \frac{N^2}{2}\left(\text{Tr}[\ln(\mathbb{I} - K_1)] + \text{Tr}[K_1]\right) . \tag{4.4.31}$$

In order to evaluate the NNLO free energy we substitute again G by the solution of the SD equations at LO; this is justified by the fact that the NLO correction to the SD equations is just a tadpole term, that is absorbed in the bare mass in order to tune to criticality. Any RG running of the couplings at NLO is also irrelevant because the coupling-dependent part of F_{LO} vanishes.

Next, we use the conformal partial wave formalism reviewed before. Inserting the resolution of the identity (4.4.8) inside the trace in (4.4.31), we find the following formal expression:

$$F_{\text{NNLO}} = \frac{N^2}{2}\sum_{J\in\mathbb{N}_0}\int_{\frac{d}{2}}^{\frac{d}{2}+\mathrm{i}\,\infty}\frac{\mathrm{d}h}{2\pi\,\mathrm{i}}\rho(h,J)\left(\ln(1-k_1(h,J)) + k_1(h,J)\right)\mathcal{N}^{\Delta}_{h,J}\mathcal{N}^{\widetilde{\Delta}}_{\tilde{h},J}\ \text{Tr}[\Psi^{\Delta,\Delta,\widetilde{\Delta},\widetilde{\Delta}}_{h,J}] , \tag{4.4.32}$$

where now the sum includes also odd J, because there is no symmetrization on the final part of the rails of the ladder before closing it. And it is actually convenient to consider the derivative of the free energy in order to get rid of the logarithm:

$$-\,g\frac{\partial}{\partial g}F_{\text{NNLO}} = N^2\sum_{J\in\mathbb{N}_0}\int_{\frac{d}{2}}^{\frac{d}{2}+\mathrm{i}\,\infty}\frac{\mathrm{d}h}{2\pi\,\mathrm{i}}\rho(h,J)\,\frac{k_1(h,J)^2}{1-k_1(h,J)}\,\mathcal{N}^{\Delta}_{h,J}\mathcal{N}^{\widetilde{\Delta}}_{\tilde{h},J}\ \text{Tr}[\Psi^{\Delta,\Delta,\widetilde{\Delta},\widetilde{\Delta}}_{h,J}] . \tag{4.4.33}$$

The problem with this expression is that the trace of the conformal partial wave is divergent. From (4.4.10) we have:

$$\text{Tr}[\Psi^{\Delta,\Delta,\widetilde{\Delta},\widetilde{\Delta}}_{h,J}] = \int_{x_1,x_2,z}\langle\phi_{\Delta}(x_1)\phi_{\Delta}(x_2)\mathcal{O}^{\mu_1\cdots\mu_J}_{h}(z)\rangle_{\text{cs}}\langle\phi_{\widetilde{\Delta}}(x_1)\phi_{\widetilde{\Delta}}(x_2)\mathcal{O}^{\mu_1\cdots\mu_J}_{\tilde{h}}(z)\rangle_{\text{cs}} . \tag{4.4.34}$$

Formally this integral is conformally invariant, but as a consequence it is also divergent because of the infinite volume of the conformal group. Notice that the same type of integral appears as a natural pairing (or inner product) of n-point functions [137]; however, in that case one divides by the volume of $SO(d+1,1)$ (or in other words, one considers a gauge-fixed version of the integral) in order to define a finite pairing. In our case, we do not have the freedom to divide the free energy by a diverging quantity: the idea of the F-theorem is that instead we should look at the finite part of the free energy. This might be hiding behind some divergence, which we have to regulate and subtract. To that end,

[23] Similar diagrams with λ_2 instead of λ_1, appear only at order N^0.

[24] We have subtracted a $\text{Tr}[K_1]$ from the expansion of the logarithm because its ladder contribution does not correspond to a 2PI diagram. As for its contribution from the local part of the kernel, it is another figure eight diagram, which evaluates to zero, and hence we can add or subtract it at will.

we employ an analytic regularization, that is, we shift the dimensions of the shadow operators, and define:

$$\mathcal{I}_\epsilon(J) = \int_{x_1,x_2,z} \langle \phi_\Delta(x_1)\phi_\Delta(x_2)\mathcal{O}_h^{\mu_1\cdots\mu_J}(z)\rangle_{\rm cs}\langle \phi_{\widetilde{\Delta}-\epsilon}(x_1)\phi_{\widetilde{\Delta}-\epsilon}(x_2)\mathcal{O}_{\tilde{h}-\epsilon}^{\mu_1\cdots\mu_J}(z)\rangle_{\rm cs}\,. \tag{4.4.35}$$

This analytic regularization breaks the conformal invariance of the integral, but not its translation invariance. Therefore, on flat space there is still a space-time volume divergence, which is instead regularized on the sphere. UV divergences (at coincident points) are still there, but will be cured in an appropriate range of ϵ, and then we will use analytic continuation to take the limit $\epsilon \to 0$.

After some manipulations we find:

$$\mathcal{I}_\epsilon(J) = (2a)^{3\epsilon}\frac{\pi^{3d/2}\Gamma(\frac{\epsilon}{2})^3\Gamma(\frac{3\epsilon}{2}-\frac{d}{2})\Gamma(d-2+J)\Gamma(\frac{d-2}{2})}{2^J\Gamma(\epsilon)^3\Gamma(d-2)\Gamma(\frac{d-2}{2}+J)\Gamma(d)}\,. \tag{4.4.36}$$

and removing the regulator ϵ we get:

$$\mathcal{I}_0(J) = \frac{8\pi^{3d/2}\Gamma(-\frac{d}{2})\Gamma(d-2+J)\Gamma(\frac{d-2}{2})}{2^J\Gamma(d-2)\Gamma(\frac{d-2}{2}+J)\Gamma(d)}\,. \tag{4.4.37}$$

The ϵ regularization thus provides a finite result for the trace of the conformal partial wave, as long as d is not an even integer. However, it turns out that it is important to consistently shift by ϵ also the normalization factor of the three-point function of shadow operators, as otherwise the resulting series in J would diverge. The product of normalization factors (4.4.11) is then replaced, at large J, by:

$$\mathcal{N}^{\Delta}_{h,J}\mathcal{N}^{\widetilde{\Delta}-\epsilon}_{\tilde{h}-\epsilon,J} \sim \frac{2^{3(d+\epsilon)/2+J}}{(2\pi)^d}\,J^{-3\epsilon}\,(1+\mathcal{O}(1/J))\,. \tag{4.4.38}$$

This $J^{-3\epsilon}$ factor regularizes the series over J, which would otherwise diverge because its coefficients behave asymptotically as $1/J$.

We can now perform the integral on h and sum over J in (4.4.33). At large J, the integral behaves as $\frac{f(\epsilon)}{J^{1+3\epsilon}}$ with $f(\epsilon)$ an analytic function at $\epsilon = 0$. We then write:

$$\begin{aligned}-g\frac{\partial}{\partial g}F^{\epsilon}_{\rm NNLO} =& N^2\int_{\frac{d}{2}}^{\frac{d}{2}+{\rm i}\,\infty}\frac{{\rm d}h}{2\pi\,{\rm i}}\rho(h,0)\,\frac{k(h,0)^2}{1-k(h,0)}\,\mathcal{N}^{\Delta}_{h,0}\mathcal{N}^{\widetilde{\Delta}-\epsilon}_{\tilde{h}-\epsilon,0}\,\mathcal{I}_\epsilon(0)\\ &+N^2\Bigg[\sum_{J\in\mathbb{N}_+}\left(\int_{\frac{d}{2}}^{\frac{d}{2}+{\rm i}\,\infty}\frac{{\rm d}h}{2\pi\,{\rm i}}\rho(h,J)\,\frac{k(h,J)^2}{1-k(h,J)}\,\mathcal{N}^{\Delta}_{h,J}\mathcal{N}^{\widetilde{\Delta}-\epsilon}_{\tilde{h}-\epsilon,J}\,\mathcal{I}_\epsilon(J)-\frac{f(\epsilon)}{J^{1+3\epsilon}}\right)\\ &+\sum_{J\in\mathbb{N}_+}\frac{f(\epsilon)}{J^{1+3\epsilon}}\Bigg]\,.\end{aligned} \tag{4.4.39}$$

The first sum is now convergent for $\epsilon = 0$, and thus can be computed numerically, while the second sum gives and explicit pole in ϵ. We thus define the finite part of the NNLO sphere free energy, or rather its derivative, as:

$$-g\frac{\partial}{\partial g}F_{\rm NNLO} = \lim_{\epsilon\to 0}\left(-g\frac{\partial}{\partial g}F^{\epsilon}_{\rm NNLO}-\frac{N^2 f(0)}{3\epsilon}\right)\,, \tag{4.4.40}$$

which numerically can be computed nonperturbatively, for example giving, at $d = 3$, $g = 1$ and $a = 1$:

$$-g\frac{\partial}{\partial g}F_{\rm NNLO} = 7.57\times 10^{-4}\,N^2\,. \tag{4.4.41}$$

We have thus succeeded in resumming an infinite series of vacuum diagrams!

In the context of the F-theorem we are interested in the difference between the free energy at the UV fixed point and at the IR fixed point. The value of g being the same at the two fixed points, and the above result being seemingly independent of g_1 or g_2, it would naively seem that the free energy is the same at all the fixed points of Fig. 4.12.

Things are however more subtle than this. As explained in Sec. 4.4.1, the resolution of the identity (4.4.8) is valid in a functional space with appropriate integrability conditions, and the latter are violated by four-point functions whose s-channel OPE contains operators of dimension smaller than $d/2$. It turns out that this is precisely what happens in the ultraviolet CFT, due to a primary operator in the OPE of $\hat{P}^{(1)}_{\mathbf{ab};\mathbf{cd}}(\phi_{\mathbf{c}} \times \phi_{\mathbf{d}})$ whose dimension descends below $d/2$. In fact, at $J = 0$, the equation $k_1(h, 0)$ has two solutions $h_\pm$ lying respectively on the right and on the left of the integration contour $\mathcal{P}_+$, obtained from (4.4.24) by the mapping $g^2 \to g^2/3$:

$$h_\pm = \frac{d}{2} \pm \frac{2}{\Gamma(d/2)(4\pi)^{d/2}} \sqrt{g^2} + \mathcal{O}(|g|^3)\,, \tag{4.4.42}$$

and in the UV, the physical dimension is actually the one on the left of the contour. Therefore, in evaluating the free energy of the UV theory by the CPW method we need to subtract these contributions from the operator being traced before applying it on the resolution of identity (4.4.8), and then add them back. This amounts to including, besides the principal series integral, an isolated non-normalizable contribution, as in (4.4.22). That is, in the UV version of (4.4.33) we have to add minus the residue of the integrand at $h = h_-$.

With this in mind, it is clear that the difference between the free energy of the UV theory and the one of the IR theory is given precisely by the isolated non-normalizable contribution of the former. Going again through the same regularization procedure as in the IR case, we thus find:

$$\begin{aligned} g\frac{\partial}{\partial g}\left(F^{UV}_{\text{NNLO}} - F^{IR}_{\text{NNLO}}\right) &= N^2\, \text{Res}\left[\rho(h,0)\, \frac{k(h,0)^2}{1-k(h,0)}\, \mathcal{N}^{\Delta}_{h,0}\mathcal{N}^{\tilde{\Delta}}_{\tilde{h},0}\, \mathcal{I}_0(0)\right]_{h=h_-} \\ &= N^2\, \frac{16\,\Gamma(-d/2)}{2^{3d}\pi^{3d/2}\Gamma(d)}\, |g|^3 + \mathcal{O}(|g|^5)\,, \end{aligned} \tag{4.4.43}$$

which is positive for $2 < d < 4$. By numerical evaluation at finite g, it can be checked that the positivity remains valid also at all values of g, within the radius of convergence of the melonic series (see Fig. 4.15).

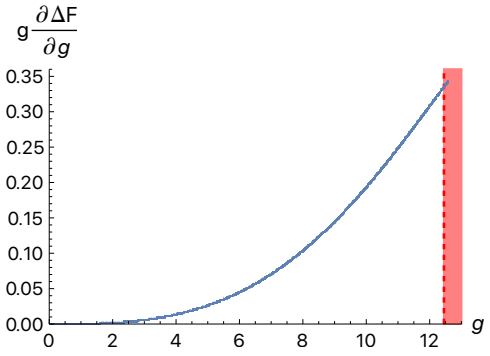

Figure 4.15: Difference between the free energy in the UV and the free energy in the IR at $d = 3$. The red area corresponds to $g > g_c$, where nothing seems to happen, but in fact there is no λ giving such values of g.

This result can also be checked perturbatively. When flowing from the UV to the IR, the fixed point value of the pillow coupling goes from $g_{1-} \simeq -\sqrt{g^2}$ to $g_{1+} \simeq \sqrt{g^2}$ (except for the vertical

trajectories in Fig. 4.12, which we will discuss below): therefore, at leading order in g, graphs with an even number of vertices have the same amplitude in the UV as in the IR, while graphs with an odd number of vertices have opposite signs. The difference between the free energy in the UV and the free energy in the IR is thus expanded in odd powers of $|g|$. Up to order $|g|^3$, only the graph of Fig. 4.16 contributes, where the vertices are either two tetrahedron and one g_1 or three g_1. Using again dimensional regularization with $\Delta = \frac{d-\epsilon}{4}$, we recover (4.4.43).

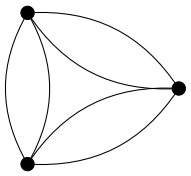

Figure 4.16: Feynman graph contributing to the free energy at order 3 in the coupling constant. The vertices are either two tetrahedron couplings (e.g. the two on the left could form the rung of a ladder) and one g_1 or three g_1.

In conclusion, the difference between the sphere free energy at the fixed points (g_{1-}, g_{2-}) or (g_{1-}, g_{2+}) and the one at the fixed points (g_{1+}, g_{2-}) or (g_{1+}, g_{2+}) (see Fig. 4.12)[25] grows with growing $|g|$. Since the difference vanishes at $g = 0$, we conclude that for the fixed points at fixed $g \neq 0$ the sphere free energy satisfies $F^{UV}_{\text{NNLO}} > F^{IR}_{\text{NNLO}}$, in accordance with the F-theorem.

Trajectories at fixed g_1. The reader will note in Fig. 4.12 the presence of two vertical lines: these are two trajectories at fixed g_1 connecting two different pairs of fixed points. As neither the tetrahedral coupling nor g_1 change along these trajectories, the above computation implies that at NNLO the free energy at the two ends of such trajectories is the same. We expect that in order to see a change of the free energy along these trajectories one would need to push the evaluation to higher orders in $1/N$.

The first non-trivial contribution involving the double trace coupling g_2, which does vary along the vertical trajectories, comes from ladder graphs generated by the double trace part $K_2\hat{P}^{(2)}$ of the Bethe-Salpeter kernel (4.2.22). They essentially behave the same as the ladders generated by $K_1\hat{P}^{(1)}$, up to replacing g^2 by $3g^2$, but the isolated contribution to the conformal partial wave expansion in the UV would in this case depend on the fixed-point value of g_2.

However, it should be noted that, as such ladders appear only at order N^0, one should include the effect of the $1/N$ corrections of the on-shell two-point function and of the fixed-point values of the couplings to our F_{NNLO}. We know from [176] that such corrections have a drastic effect on the fixed-point theory, as we reviewed briefly in Sec. 4.3.3. The whole analysis becomes much more involved, and since in this case the theory is manifestly non-unitary we do not expect the F-theorem to necessarily hold.

[25] Notice that (g_{1+}, g_{2-}) can be reached only through one trajectory emanating from (g_{1-}, g_{2-}), while (g_{1-}, g_{2+}) has only one trajectory to flow to an IR fixed point, i.e. (g_{1+}, g_{2+}). Between (g_{1-}, g_{2-}) and (g_{1+}, g_{2+}) there is instead an infinite set of trajectories.

4.5 An instability theorem

CFTs with complex scaling dimensions can arise as renormalization group fixed points at complex values of the couplings, for example when real fixed points merge and move to the complex plane as some parameter of theory is varied. Many examples of such merging of fixed points are known, see for example the list of references in [214]. In some instances, a special case of complex scaling dimension is found, one whose real part is equal to $d/2$, d being the space(-time) dimension; examples include non-supersymmetric orbifolds of $\mathcal{N} = 4$ super Yang-Mills [215–217], gauge theories with matter in the Veneziano limit [218, 219], and large-N theories dominated by fishnet diagrams [200, 201, 220–222], or, as we have seen in the previous sections, by melonic diagrams [66, 68, 70–72, 74, 75, 93, 198]. The typical large-N mechanism leading to complex dimensions of such type is the following [217]: due to the large-N simplifications, the beta function for the coupling of a double-trace operator $\mathcal{O}^2$ turns out to be governed by a quadratic beta function, and hence the reality of the fixed points depends on its discriminant D; in the case $D < 0$, the fixed points are complex, and the scaling dimension of $\mathcal{O}^2$ is $h_{\mathcal{O}^2} = d + 2\,\mathrm{i}\,\sqrt{|D|}$; lastly, the large-$N$ limit implies that the scaling dimension of $\mathcal{O}$ is half that of $\mathcal{O}^2$, and thus it is of the claimed form. Here we will be concerned with such particular case of scaling dimensions, although not necessarily in the large-N limit.

Operators with a scaling dimension equal to $d/2 + \mathrm{i}\,r$ (with $r \in \mathbb{R}$) are commonly seen as a sign of instability, the reason being that in the AdS/CFT correspondence they are dual to tachyonic fields. By the standard AdS/CFT dictionary [223, 224] the conformal dimension h of a scalar operator in the d-dimensional CFT is related to the mass m of a scalar field in $(d+1)$-dimensional anti-de Sitter space (AdS_{d+1}) by the equation $m^2 = h(h-d)$, or

$$h_\pm = \frac{d}{2} \pm \sqrt{\frac{d^2}{4} + m^2}\,. \tag{4.5.1}$$

In AdS_{d+1}, thanks to the constant curvature of spacetime, the squared mass can be negative without generating a tachyonic instability, as long as $m^2 \geq -d^2/4$. The latter is the well-known Breitenlohner-Freedman bound [225, 226], below which a tachyonic instability develops. The square root in(4.5.1) becomes imaginary precisely for $m^2 < -d^2/4$, hence the expectation that CFTs with such complex scaling dimensions are unstable, in the sense that the conformal vacuum is not the true vacuum of the theory.[26] However, elevating this argument to a proof does not seem feasible, in particular because the AdS/CFT correspondence is mostly based on matching calculations on both sides of the conjecture, something that requires having at least a guess for the bulk dual of a given CFT, while in some of the models displaying a scaling dimensions equal to $d/2 + \mathrm{i}\,r$ this is currently missing. Moreover, most of such matching calculations rely importantly on the large-N limit, while one might suspect that if a complex scaling dimension of this type is a synonym of instability, this might be a more general result. The reason is that $d/2 + \mathrm{i}\,r$ also happens to be the conformal dimension labelling the principal series representations of the Euclidean conformal group $SO(d+1,1)$, and therefore it seems plausible that we might not need the large-N limit in order to single out such scaling dimensions. And although we only know of examples involving a large-N limit, this might be just because for either fundamental or practical (i.e. computational) reasons the limit is essential for the appearance of such type of scaling dimensions in a CFT (in interacting theories we do not usually find such neat numbers as $d/2$), and not because it is needed in order to prove the instability.

[26] Within the large-N setting discussed above, Pomoni and Rastelli in [217] have shown that the theory with real coupling is in a broken phase; however, they have not directly argued for the instability of the fixed point theory itself, which is at complex coupling, instead referring for that to the AdS/CFT picture.

In [166] we have given a proof of such instability directly for generic d-dimensional CFTs that can be obtained as limits of multiscalar quantum field theories, without invoking the large-N limit, and under a set of more technical assumptions. The main result of that paper is informally summarized by the following statement:

Proposition 1. *Consider a Euclidean quantum field theory whose Schwinger-Dyson equations admit a conformal solution. If the OPE of two fundmental scalar fields includes a contribution from one primary operator $\mathcal{O}_{h_\star}$ of dimension $h_\star = \frac{d}{2} + \mathrm{i}\, r_\star$, with non-vanishing $r_\star \in \mathbb{R}$, then the conformal solution is unstable.*

By fundamental fields we here mean the fields which enter the definition of the quantum field theory, through the functional integral. We assume that the CFT can be obtained as a fixed point of the renormalization group, and that at least in some limit the conformal two-point functions of the fundamental scalar fields can be identified as solutions of the Schwinger-Dyson (SD) equations. As should be clear from our review, these are assumptions that are satisfied explicitly by theories with a melonic large-N limit. However, the proof is rather generic, and does not rely on any large-N limit.

The main claim is that a conformal solution leading to a primary operator of scaling dimension $h_\star = \frac{d}{2} + \mathrm{i}\, r_\star$ is necessarily unstable. By unstable here we mean that the free energy is not minimized (not even locally) by the conformal solution of the SD equations, as there exist fluctuations that lower the free energy. In order to further clarify the meaning of instability in this context, it might be useful to compare the type of instability we are discussing here with a more familiar one. Consider a single-scalar field theory in $d \geq 2$ with quartic interaction and $\mathbb{Z}_2$ invariance. By tuning the renormalized mass, the model can go through a phase transition. One way to see that is by constructing the effective potential $V(\phi)$ (i.e. the one-particle irreducible (1PI) effective action at constant field configuration, divided by the volume), whose stationary point $V'(\phi_\star) = 0$ gives the one-point function, $\phi_\star = \langle \varphi \rangle$, while $V(\phi_\star)$ is the free energy per unit volume in the absence of external sources. At negative squared mass, we find that the symmetric solution $\phi_\star = 0$ has become a local maximum of the potential, and that non-trivial minima have appeared, with a lower free energy. In this case, we say that the symmetric solution is unstable. Similarly, in the case of Proposition 1, the conformal solution of the SD equations is not a (local) minimum of the free energy.[27]

We outline here a sketch of the proof from [166]:

1. We use the 2PI formalism reviewed in Ch. 3, in which field equations for the 2PI effective action are the Schwinger-Dyson equations for the two-point function $G(x, y)$ of the fundamental fields $\phi(x)$; this is the two-point function analogue of the usual effective potential for the one-point function. The first main hypothesis consists in assuming that such equations admit a conformal solution, $G_\star(x, y) \sim 1/|x - y|^{2\Delta}$.

2. The 2PI effective action $\Gamma[G]$ evaluated on shell is the free energy in the absence of external sources, and we denote it F.[28] In order to test the stability of the conformal solution, we need to consider the effective action at quadratic order in the fluctuations $\delta G = G - G_\star$. The expansion at quadratic order can be written schematically as

$$\Gamma[G] \simeq F + \frac{1}{2} \delta G_{12} \cdot {G_\star^{-1}}_{11'} {G_\star^{-1}}_{22'} (1 - K[G_\star])_{1'2'34} \cdot \delta G_{34} \,, \tag{4.5.2}$$

[27] A very explicit example of instability of this kind is provided by the Bardeen-Moshe-Bander phenomenon [227] (see also [228–231] and references therein), which however is not associated to complex scaling dimensions.

[28] This could be regularized as in Sec. 4.4.3, but it is not essential for the rest of the argument.

where $K[G_\star]$ is the Bethe-Salpeter kernel and the subscripts stand for the points x_1, x_2, etc, which are integrated in $\mathbb{R}^d$.

3. The fluctuations $\delta G(x,y)$ belong to the Hilbert space of bilocal functions $\mathcal{V}_\Delta$, defined in Sec. 4.4.1, for which the set of three-point functions (4.4.1) forms a complete and orthonormal basis, with the conformal dimension of the (at this stage unphysical) operator $\mathcal{O}_h$ in the principal series: $h = \frac{d}{2} + \mathrm{i}\, r$. As we saw, such functions form also an eigenbasis of the Bethe-Salpeter kernel, with eigenvalues $k(h,J)$, parametrized by the conformal dimension h and the spin J. With the aid of such basis, we can therefore write

$$\Gamma[G] - F \simeq \frac{1}{8} \sum_{J \in \mathbb{N}_0} \int_{\frac{d}{2} - \mathrm{i}\,\infty}^{\frac{d}{2} + \mathrm{i}\,\infty} \frac{\mathrm{d}h}{2\pi\,\mathrm{i}}\, \rho(h,J)\,(1 - k(h,J)) \int \mathrm{d}^d z\, \overline{F}_h^{\mu_1 \cdots \mu_J}(z) F_h^{\mu_1 \cdots \mu_J}(z)\,, \qquad (4.5.3)$$

where $F_h^{\mu_1 \cdots \mu_J}(z)$ are the expansion coefficients of δG on the basis of three-point functions.

4. As we saw in (4.4.19), the equation $k(h,J) = 1$ defines the poles that lead to the s-channel OPE of the four-point function. The second main hypothesis of Proposition 1 is then stated as the fact that the equation $k(h,J) = 1$, at some fixed J, admits a simple root $h_\star$ on the principal series. Therefore, if $r_\star \neq 0$, the integrand in (4.5.3) is negative for $\mathrm{Im}(h)$ either just above or just below $r_\star$, and thus there is an instability (see Fig. 4.17). For example, if $1 - k(h,J) < 0$ for $\mathrm{Im}(h) < r_\star$, choosing $F_h^{\mu_1 \cdots \mu_J}(z)$ such that the integral of its squared modulus over z is peaked around $h_\star - \mathrm{i}\,\epsilon$, for some $\epsilon > 0$, leads to a negative quadratic fluctuation of the effective action, that is, an instability.

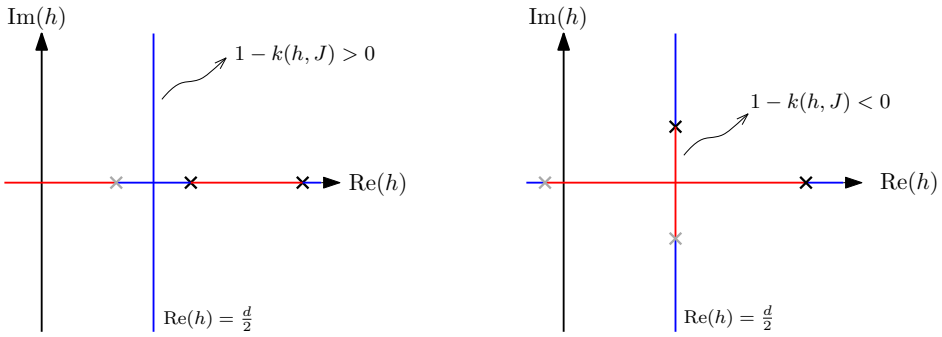

Figure 4.17: Illustration in the complex h plane of some hypothetical solutions of $k(h,J) = 1$. Physical solutions are represented by black crosses, while their shadow by gray crosses. On the principal series (vertical line) and the real line we have marked in blue the intervals with $1 - k(h,J) > 0$ and in red those with $1 - k(h,J) < 0$. On the left panel all solutions are real, while on the right panel the smallest physical one has merged with its shadow to form a complex pair, thus leading to a negative interval on the principal series. Sign changes can occur also at poles of $k(h,J)$, which we have ignored here for simplicity.

The detailed proof in [166] is written for a generic multiscalar theory; therefore, with respect to what sketched above the formulas result to be complicated by field indices, which however are useful for understanding some of the available examples.

In the long-range quartic $O(N)^3$ model with real tetrahedron coupling, the complex solutions $h_\pm$ in (4.4.24) (with $g^2 = -g_t^2 < 0$) are precisely of the form assumed in Proposition 1. Figure 4.18 shows

how such complex solutions imply the existence of a region with $1 - k(h, 0) < 0$ along the principal series, thus providing an example of mechanism underlying Proposition 1.

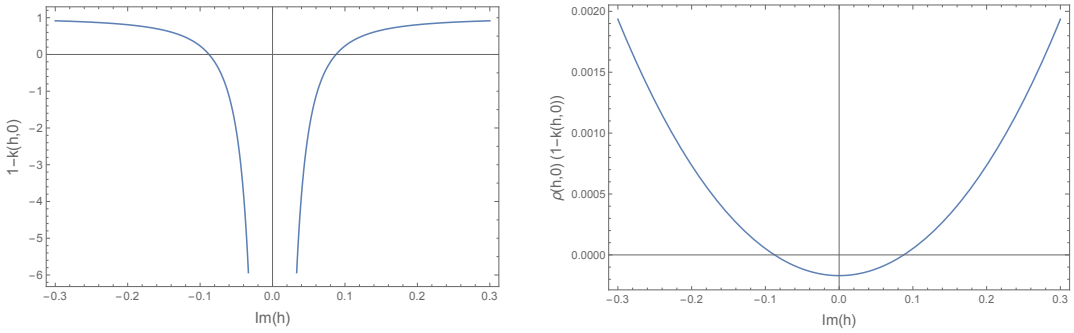

Figure 4.18: Plot of $1-k(h,0)$ (left) and $\rho(h,0)(1-k(h,0))$ (right) at $d = 3$ along the principal series, for the long-range quartic $O(N)^3$ model, with real tetrahedron coupling.

Chapter 5

Conclusions and outlook

We have tried to convey some essential information on the status of QFTs in the melonic limit. Our presentation has concentrated mostly on one case study, provided by the long-range $O(N)^3$ multiscalar model with quartic interactions [75, 167, 169, 176, 197], but we have used this model to highlight some rather general methods and features of the melonic limit, which apply also to other models. In particular, we have discussed:

- the general structure of the invariants, their graphical representation, and the combinatorics of the large-N limit in tensor models;
- the usefulness of the 2PI formalism, due to the fact that melonic diagrams are built by insertions of two-point diagrams, and therefore are two-particle reducible;
- the role of the large-N melonic dominance in the simplification of the Schwinger-Dyson equations for the two-point function, which can be fully solved in the critical long-range models, with an exact resummation of the infinite series of melonic two-point diagrams;
- the ladder structure of the large-N four-point function, with an exact Bethe-Salpeter kernel;
- the two main mechanisms by which fixed points can appear, namely: the usual Wilson-Fisher dimensional continuation below the upper critical dimension in the short-range models, or the exact marginality of the maximally-single-trace interaction in the long-range models;
- the usefulness of the conformal partial wave expansion, which at the fixed points allows us to compute nonperturbatively the OPE spectrum from the ladder four-point function, as well as to calculate nonperturbatively the sphere free energy at next-to-next-to-leading order, by resumming an infinite series of vacuum ladder diagrams;
- the fact that complex scaling dimensions often show up, and can be proven to lead to an instability of the conformal solution of the SD equations (again by 2PI formalism and conformal partial wave expansion), but for some models there exist ranges of parameters (the dimension or the exactly marginal coupling) for which all the scaling dimensions and OPE coefficients computed so far are real and above unitarity bounds.

The long-range models are of particular interest, as they allow us to define real melonic CFTs in some integer dimensions (such as $d = 2$ or $d = 3$) for a small-enough exactly marginal coupling. However, the exact marginality is lost at higher orders in the $1/N$ expansion, and complex scaling

dimensions reappear. Supersymmetric tensor models [57,65,76,77], might be better behaved from this point of view, but their subleading corrections have not been studied so far. Another well behaved model in this sense seems to be the "prismatic" model [74], with a positive-definite sextic interaction. It would be interesting to study in some detail the $1/N$ expansion of these models.

Other examples of tensor models have been omitted from this review for the sake of preventing the manuscript from becoming too long. In particular, we did not discuss further the sextic model of equation (2.1.11), which shares most of the main features of the quartic model, but with some interesting differences, see [93, 232]. And we did not review the status of (short-range) fermionic models in $d > 1$ [72, 73, 84]: in such models, $d = 2$ is the upper critical dimension, therefore melonic fixed points are only found in $d = 2 - \epsilon$, which might possibly be the continuation from $d = 1$ of SYK-like tensor models; nevertheless, interesting new patterns of symmetry breaking can be studied in $d = 3$.

We also omitted commenting on the Amit-Roginsky model [233], which is a multiscalar model with a $SO(3)$-invariant cubic interaction, made possible by contractions with a Wigner $3jm$ symbol, and that is a so far unique case of quantum field theory with melonic limit having a cubic interaction, as tensor models admitting a melonic limit have always interactions with an even number of fields. We revisited the model in [198] with the hindsight of recent developments in tensor models, correcting some small mistakes in the original analysis, and providing some further results and generalizations of the model. Interestingly, the $SO(3)$-invariant $3jm$ symbol also appears as a possible symmetry breaking solution of the $O(N)^3$ quartic tensor model [134].

It is also worth mentioning some similarities to a non-melonic model. As noticed in [167], the quartic long-range $O(N)^3$ model has several similarities with the long-range version [201] of fishnet theory [234]. This is due in particular to the structure of the four-point function, renormalizing the double-trace (and pillow, in the tensor case) interactions: the ladder structure indeed can originate both from opening two lines in melonic vacuum graphs, or from considering a fishnet graph with only four external legs. The double-trace (and pillow) couplings thus present in both models similar lines of fixed points, parametrized by an exactly marginal coupling. Moreover, in both models the latter is associated with a complex operator: i times the tetrahedron invariant in the tensor case, and a chiral vertex without hermitian conjugate in the fishnet case. Therefore, both models are expected to be non-unitary. However, while the non-unitarity shows up in the fishnet theory even at leading order (in the form of a logarithmic correlators), the large-N results in the long-range tensor models are so far compatible with a unitary CFT. Lastly, the fishnet model is usually considered at real coupling, where however it also has a complex scaling dimension of the type $d/2+\mathrm{i}\,r$, as clear from the similarity of its four-point function with that of the $O(N)^3$ model. As shown in [166], the instability theorem proved there, and reviewed here in Sec. 4.5, applies also to the fishnet model with real coupling, where it implies a spontaneous symmetry breaking of a $U(1) \times U(1)$ symmetry down to $\mathbb{Z}_2 \times \mathbb{Z}_2$. This is reminiscent of the coupled tensors of [68], where however the leftover invariance is the diagonal subgroup of $U(1) \times U(1)$.

5.1 Some open questions

We conclude with a non-exhaustive list of open questions and possible future research directions for tensor models and other QFTs with a melonic limit:

- For the $O(N)$ and SYK models in collective (or intermediate) variables the large-N limit is essentially a saddle-point approximation (see Sec. 3.2.1). To some extent, this is often also the

case for matrix models, when they can be reduced to eigenvalues or to a character expansion. For tensor models, a similar construction is hindered by the great proliferation of invariants. On the other hand, infinite families of diagrams appearing at subleading order in the $1/N$ expansion support a saddle point interpretation (e.g. Fig. 3.10), while there are also a finite number of special diagrams (e.g. Fig. 3.11) that do not seem to derive from a loop expansion of some effective action. It might be that such terms could be explained as subleading corrections to the saddle-point solution itself. In other words, perhaps a collective field effective action could be possible, although with a not completely factorized N-dependence. It would be interesting to understand this point.

- One of the main motivations for the SYK model, and for SYK-like tensor models ($d = 1$ fermionic models), was the AdS_2/CFT_1 correspondence. It would be interesting to understand if the AdS/CFT duality could hold for higher dimensional bosonic or fermionic models. In particular, given the point of view on the tensor models as symmetry-breaking perturbations of the vector models (e.g. $O(N^3)$ broken down to $O(N)^3$), it is natural to wonder whether melonic CFTs could correspond to deformations of the duality between the vector $O(N)$ model in three dimensions and Vasiliev's higher-spin theory in AdS_4 [19] (see [20] for a review). Few years ago, Vasiliev proposed a new type of higher-spin theory that has extra structure suggesting that it might be a candidate dual to tensor theories [235]. However, the theory is rather complicated and, as far as we know, still poorly understood.

- One approach to holography is based on the idea of collective field theory [10,11]. As we reviewed in Sec. 3.2.1, the collective field theory for the $O(N)$ model rewrites the functional integral in terms of a bilocal field, and that provides a way to reconstruct the dual higher-spin theory in AdS space [191, 192, 236]. Lacking an analogue for tensor models, we have argued that the 2PI effective action is the only way we have to obtain a bilocal field theory, although one in which the functional integral has already been performed. Perhaps this could still serve for the purpose of the holographic reconstruction: the rough idea could be to map the bilocal scalar field in d dimensions to a tower of spin fields in $d+1$ dimensions as in [11,191,192] and attempt to identify the resulting effective action as the 1PI effective action for an higher-spin theory. It would be interesting to put this idea to test.

- As we reviewed in Sec. 4.2.1, in the long-range $O(N)^3$ model the Schwinger-Dyson equation for the two-point function reduces, after additive mass renormalization, to the algebraic equation (4.2.10), whose solution amounts to analytically resumming all the melonic two-point diagrams. The short range case is instead complicated by the wave function renormalization, or in other words by the fact that the insertion of a fundamental two-point diagram (see Fig. 2.4) on a propagator line alters the momentum dependence of the propagator, and it does so with a divergent coefficient that needs renormalization. The corresponding SD equation can still be solved in the limit of vanishing momentum, but so far the full momentum dependence of the propagator remains out of reach, except in one dimensional SYK-like models, where it can be obtained numerically [49, 66, 68]. It would be interesting to explore further this task in the case of the short-range Amit-Roginsky model at $d = 6 - \epsilon$, where, the vertices being cubic, the melonic insertions are one-loop rather than two-loops, and thus easier to handle. Perhaps the Hopf algebraic approach used in other cubic models [237] might be useful to this end.

- The study of nontrivial (symmetry-breaking) solutions of the quartic $O(N)^3$ tensor model [134] has highlighted the fact that probably this model has a rich landscape of solutions in the large-

N limit. This suggests that it might make sense to introduce for tensor models the notion of complexity in the spin glass sense, i.e. as the logarithm of the number of solutions with given energy [238]. Indeed there are interesting connection between tensor models and glasses, signaled of course by the relation to the SYK model, but also to the p-spin model [239] in the bosonic case. It would be interesting to explore the possibility that tensor models provide examples of systems with glassy behavior, without quenched disorder (see [240] for another example).

- Concerning the instability proved in [166], and reviewed here in Sec. 4.5, it would be interesting to understand what happens in the case that the real part of the complex scaling dimension is not exactly equal to $d/2$, but close to it. In fact, at finite N we do not expect such a simple value for a critical exponent, but we also do not expect that the theory would suddenly become stable for infinitesimal deviations from the $d/2$ value.

- Another interesting open question related to the instability of Sec. 4.5 is raised by the conjecture made in [66], that can be stated as following:

  Conjecture 1. *Under the same assumptions as in Proposition 1, in the true vacuum of the theory, the operator $\mathcal{O}_{h_\star}$ acquires a non-trivial vacuum expectation value: $\langle \mathcal{O}_{h_\star} \rangle \neq 0$.*

  In other words, the conjecture, tested with success on some coupled SYK and SYK-like tensor models in [66, 68], claims the existence of a stable solution of the SD equations, with spontaneous breaking of conformal invariance. The instability of the conformal solution was implicitly assumed in [66], based on the AdS/CFT picture. With the results of [166] we have completed the picture by presenting a proof that does not rely on the duality. We have instead failed so far to use the same methods in order to prove remaining part of Conjecture 1. Ideally one would try to find a stable solution $G_1(x_1, x_2) \neq G_\star(x_1, x_2)$ and show that it leads to $\langle \mathcal{O}_h \rangle \neq 0$. However, identifying a stable solution in full generality is out of reach, as it requires going beyond the linear perturbations, hence some new idea would probably be needed. Proving that a stable vacuum should exist at all seems also non-trivial. For tensor models, showing that for $d > 1$, in the regime in which complex scaling dimensions appear (e.g. short-range quartic $O(N)^3$ model or long-range one with real tetrahedron coupling), there exists a different (and energy-favourable) solution of the SD equations has so far proved to be an elusive task. Therefore, it cannot even be excluded that in such case those models might have no stable vacuum at all, and that the stable solution found in [66, 68] is peculiar to $d = 1$, or to the fermionic nature of the fields. Looking at the 2PI effective action (4.2.6) of the $O(N)^3$ model, it might be tempting to infer that the term proportional to G^4 has the good sign only for $\lambda_t^2 < 0$, and that if $\lambda_t^2 > 0$ the effective action is unbounded from below (even at large-N) and hence no truly stable vacuum exists. However, the bilocal nature of the effective action makes such a statement nontrivial, as replacing $G(x, y)$ by some explicit ansatz will typically lead to divergences that need to be subtracted, and the sign of the subtracted melon integral is not obvious a priori. It would be desirable to better understand the global stability properties of such bilocal effective actions, and possibly find the true vacuum (if it exists) of some $d > 1$ model.

- Many other applications of the melonic limit can be envisaged, such as applications to defect CFTs (a first promising example has been studied in [241]) or to finite-temperature CFTs (for example to construct examples of persistent symmetry breaking [161]). There are of course many questions in QFT or CFT that might benefit from a new controllable limit.

- The strict large-N limit provides interesting toy models, but often also leads to somewhat pathological or non-standard features, such as lines of fixed points, logarithmic CFTs (e.g. in fishnet model, or in the short-range sextic $U(N)^3$ model [93]), apparent violations of the Coleman-Mermin-Wagner theorem [73,129], and unitarization of nonunitary theories. Therefore, in order to approach more realistic situations, it is important to understand and be able to incorporate the subleading corrections in $1/N$. We took a step in this direction in [176] (see Sec. 4.3.3), starting from a loop expansion of the beta functions at finite N, but it would also be nice to push further nonperturbative computations even at subleading orders. The F-theorem computation of [197] (see Sec. 4.4.3) shows that this is possible for vacuum diagrams, but correlators have not yet been computed at subleading order by nonperturbative means.

- Another setting in which subleading corrections should definitely be studied is that of the large-D limit introduced by Ferrari in [96]. While the strict large-N and large-D limit is again a melonic limit, the subleading corrections have an extra layer of organization, and it would be interesting to apply to QFT the double-scaling limit (2.3.14), that is, a genus expansion as in matrix field theories, but with only vanishing grade diagrams contributing at each genus order.

The list could go on, but perhaps, as often is the case, the most interesting questions will be the ones we have not thought about yet.

Bibliography

[1] K.G. Wilson and J.B. Kogut, *The Renormalization group and the epsilon expansion*, *Phys. Rept.* **12** (1974) 75.

[2] J. Zinn-Justin, *Phase transitions and renormalization group*, Oxford Univ. Pr., Oxford (2007), 10.1093/acprof:oso/9780199227198.001.0001.

[3] J. Polchinski, *Scale and Conformal Invariance in Quantum Field Theory*, *Nucl. Phys. B* **303** (1988) 226.

[4] Y. Nakayama, *Scale invariance vs conformal invariance*, *Phys. Rept.* **569** (2015) 1 [1302.0884].

[5] D. Poland, S. Rychkov and A. Vichi, *The conformal bootstrap: Theory, numerical techniques, and applications*, *Rev.Mod.Phys.* **91** (2019) 015002 [1805.04405].

[6] K.G. Wilson and M.E. Fisher, *Critical exponents in 3.99 dimensions*, *Phys. Rev. Lett.* **28** (1972) 240.

[7] K.G. Wilson, *Quantum field theory models in less than four-dimensions*, *Phys.Rev.D* **7** (1973) 2911.

[8] M. Moshe and J. Zinn-Justin, *Quantum field theory in the large N limit: A review*, *Phys. Rept.* **385** (2003) 69 [hep-th/0306133].

[9] S. Coleman, *Aspects of symmetry: selected Erice lectures*, Cambridge University Press, Cambridge, U.K. (1985), 10.1017/CBO9780511565045.

[10] A. Jevicki and B. Sakita, *Collective Field Approach to the Large N Limit: Euclidean Field Theories*, *Nucl. Phys. B* **185** (1981) 89.

[11] S.R. Das and A. Jevicki, *Large N collective fields and holography*, *Phys. Rev. D* **68** (2003) 044011 [hep-th/0304093].

[12] J.M. Cornwall, R. Jackiw and E. Tomboulis, *Effective action for composite operators*, *Phys. Rev.* **D10** (1974) 2428.

[13] A.N. Vasiliev, Y.M. Pismak and Y.R. Khonkonen, *Simple Method of Calculating the Critical Indices in the 1/N Expansion*, *Theor. Math. Phys.* **46** (1981) 104.

[14] A.N. Vasiliev, Y.M. Pismak and Y.R. Khonkonen, *1/N Expansion: Calculation of the Exponents η and Nu in the Order $1/N^2$ for Arbitrary Number of Dimensions*, *Theor. Math. Phys.* **47** (1981) 465.

[15] S.R. Coleman, R. Jackiw and H. Politzer, *Spontaneous symmetry breaking in the O(N) model for large N*, *Phys. Rev. D* **10** (1974) 2491.

[16] D.J. Gross and A. Neveu, *Dynamical symmetry breaking in asymptotically free field theories*, *Phys. Rev.* **D10** (1974) 3235.

[17] G. Parisi, *The Theory of Nonrenormalizable Interactions. 1. The Large N Expansion*, *Nucl. Phys. B* **100** (1975) 368.

[18] C. de Calan, P.A. Faria da Veiga, J. Magnen and R. Seneor, *Constructing the three-dimensional Gross-Neveu model with a large number of flavor components*, *Phys. Rev. Lett.* **66** (1991) 3233.

[19] I.R. Klebanov and A.M. Polyakov, *AdS dual of the critical O(N) vector model*, *Phys. Lett. B* **550** (2002) 213 [hep-th/0210114].

[20] S. Giombi, *Higher Spin — CFT Duality*, in *Theoretical Advanced Study Institute in Elementary Particle Physics: New Frontiers in Fields and Strings*, pp. 137–214, 2017, DOI [1607.02967].

[21] G. 't Hooft, *A planar diagram theory for strong interactions*, *Nucl. Phys.* **B72** (1974) 461.

[22] E. Brezin and S. Wadia, eds., *The Large N expansion in quantum field theory and statistical physics: From spin systems to two-dimensional gravity*, World Scientific, Singapore (1994).

[23] O. Aharony, S.S. Gubser, J.M. Maldacena, H. Ooguri and Y. Oz, *Large N field theories, string theory and gravity*, *Phys.Rept.* **323** (2000) 183 [hep-th/9905111].

[24] P. Di Francesco, P.H. Ginsparg and J. Zinn-Justin, $2 - D$ *Gravity and random matrices*, *Phys. Rept.* **254** (1995) 1 [hep-th/9306153].

[25] V.A. Kazakov, *Solvable matrix models*, hep-th/0003064.

[26] N. Beisert et al., *Review of AdS/CFT Integrability: An Overview*, *Lett. Math. Phys.* **99** (2012) 3 [1012.3982].

[27] J. Ambjorn, B. Durhuus and T. Jonsson, *Three-dimensional simplicial quantum gravity and generalized matrix models*, *Mod. Phys. Lett.* **A6** (1991) 1133.

[28] N. Sasakura, *Tensor model for gravity and orientability of manifold*, *Mod. Phys. Lett.* **A6** (1991) 2613.

[29] J. Ambjorn and J. Jurkiewicz, *Scaling in four-dimensional quantum gravity*, *Nucl. Phys. B* **451** (1995) 643 [hep-th/9503006].

[30] B.V. de Bakker, *Further evidence that the transition of 4-D dynamical triangulation is first order*, *Phys. Lett. B* **389** (1996) 238 [hep-lat/9603024].

[31] P. Bialas, Z. Burda, A. Krzywicki and B. Petersson, *Focusing on the fixed point of 4-D simplicial gravity*, *Nucl. Phys. B* **472** (1996) 293 [hep-lat/9601024].

[32] R. Gurau, *Colored Group Field Theory*, *Commun. Math. Phys.* **304** (2011) 69 [0907.2582].

[33] R. Gurau, *The 1/N expansion of colored tensor models*, *Annales Henri Poincare* **12** (2011) 829 [1011.2726].

[34] R. Gurau and V. Rivasseau, *The 1/N expansion of colored tensor models in arbitrary dimension*, *Europhys. Lett.* **95** (2011) 50004 [1101.4182].

[35] V. Bonzom, R. Gurau, A. Riello and V. Rivasseau, *Critical behavior of colored tensor models in the large N limit*, *Nucl. Phys. B* **853** (2011) 174 [1105.3122].

[36] V. Bonzom, R. Gurau and V. Rivasseau, *Random tensor models in the large N limit: Uncoloring the colored tensor models*, *Phys. Rev. D* **85** (2012) 084037 [1202.3637].

[37] S. Dartois, V. Rivasseau and A. Tanasa, *The $1/N$ expansion of multi-orientable random tensor models*, *Annales Henri Poincare* **15** (2014) 965 [1301.1535].

[38] S. Carrozza and A. Tanasa, *$O(N)$ random tensor models*, *Lett. Math. Phys.* **106** (2016) 1531 [1512.06718].

[39] F. Ferrari, V. Rivasseau and G. Valette, *A new large N expansion for general matrix-tensor models*, 1709.07366.

[40] I.R. Klebanov and G. Tarnopolsky, *On Large N Limit of Symmetric Traceless Tensor Models*, *JHEP* **10** (2017) 037 [1706.00839].

[41] D. Benedetti, S. Carrozza, R. Gurau and M. Kolanowski, *The $1/N$ expansion of the symmetric traceless and the antisymmetric tensor models in rank three*, *Commun. Math. Phys.* **371** (2019) 55 [1712.00249].

[42] S. Carrozza, *Large N limit of irreducible tensor models: $O(N)$ rank-3 tensors with mixed permutation symmetry*, *JHEP* **06** (2018) 039 [1803.02496].

[43] S. Carrozza and S. Harribey, *Melonic Large N Limit of 5-Index Irreducible Random Tensors*, *Commun. Math. Phys.* **390** (2022) 1219 [2104.03665].

[44] D. Benedetti and R. Gurau, *Phase Transition in Dually Weighted Colored Tensor Models*, *Nucl. Phys. B* **855** (2012) 420 [1108.5389].

[45] R. Gurau and J.P. Ryan, *Melons are branched polymers*, *Annales Henri Poincare* **15** (2014) 2085 [1302.4386].

[46] S. Sachdev and J. Ye, *Gapless spin fluid ground state in a random, quantum Heisenberg magnet*, *Phys. Rev. Lett.* **70** (1993) 3339 [cond-mat/9212030].

[47] A. Kitaev, *A simple model of quantum holography*, *KITP strings seminar and Entanglement 2015* (Feb. 12, April 7, and May 27, 2015) .

[48] J. Polchinski and V. Rosenhaus, *The Spectrum in the Sachdev-Ye-Kitaev Model*, *JHEP* **04** (2016) 001 [1601.06768].

[49] J. Maldacena and D. Stanford, *Remarks on the Sachdev-Ye-Kitaev model*, *Phys. Rev.* **D94** (2016) 106002 [1604.07818].

[50] G. Sárosi, *AdS_2 holography and the SYK model*, *PoS* **Modave2017** (2018) 001 [1711.08482].

[51] N. Delporte and V. Rivasseau, *The tensor track V: Holographic tensors*, in *Proceedings, 17th Hellenic School and Workshops on Elementary Particle Physics and Gravity (CORFU2017): Corfu, Greece, September 2-28, 2017*, 4, 2018 [1804.11101].

[52] V. Rosenhaus, *An introduction to the SYK model*, *J. Phys. A* **52** (2019) 323001 [1807.03334].

[53] V. Bonzom, L. Lionni and A. Tanasa, *Diagrammatics of a colored SYK model and of an SYK-like tensor model, leading and next-to-leading orders*, *J. Math. Phys.* **58** (2017) 052301 [1702.06944].

[54] V. Bonzom, V. Nador and A. Tanasa, *Diagrammatic proof of the large N melonic dominance in the SYK model*, *Lett. Math. Phys.* **109** (2019) 2611 [1808.10314].

[55] E. Witten, *An SYK-like model without disorder*, *J. Phys.* **A52** (2019) 474002 [1610.09758].

[56] I.R. Klebanov and G. Tarnopolsky, *Uncolored random tensors, melon diagrams, and the SYK models*, *Phys. Rev.* **D95** (2017) 046004 [1611.08915].

[57] C. Peng, M. Spradlin and A. Volovich, *A Supersymmetric SYK-like Tensor Model*, *JHEP* **05** (2017) 062 [1612.03851].

[58] C. Krishnan, S. Sanyal and P.N. Bala Subramanian, *Quantum chaos and holographic tensor models*, *JHEP* **03** (2017) 056 [1612.06330].

[59] M. Beccaria and A.A. Tseytlin, *Partition function of free conformal fields in 3-plet representation*, *JHEP* **05** (2017) 053 [1703.04460].

[60] S.S. Gubser, M. Heydeman, C. Jepsen, S. Parikh, I. Saberi, B. Stoica et al., *Melonic theories over diverse number systems*, *Phys. Rev. D* **98** (2018) 126007 [1707.01087].

[61] K. Bulycheva, I.R. Klebanov, A. Milekhin and G. Tarnopolsky, *Spectra of operators in large N tensor models*, *Phys. Rev. D* **97** (2018) 026016 [1707.09347].

[62] S. Choudhury, A. Dey, I. Halder, L. Janagal, S. Minwalla and R. Poojary, *Notes on melonic $O(N)^{q-1}$ tensor models*, *JHEP* **06** (2018) 094 [1707.09352].

[63] J. Yoon, *SYK models and SYK-like tensor models with global symmetry*, *JHEP* **10** (2017) 183 [1707.01740].

[64] C. Krishnan, K.V. Pavan Kumar and D. Rosa, *Contrasting SYK-like Models*, *JHEP* **01** (2018) 064 [1709.06498].

[65] C.-M. Chang, S. Colin-Ellerin and M. Rangamani, *On Melonic Supertensor Models*, *JHEP* **10** (2018) 157 [1806.09903].

[66] J. Kim, I.R. Klebanov, G. Tarnopolsky and W. Zhao, *Symmetry breaking in coupled SYK or tensor models*, *Phys. Rev. X* **9** (2019) 021043 [1902.02287].

[67] I.R. Klebanov, P.N. Pallegar and F.K. Popov, *Majorana Fermion Quantum Mechanics for Higher Rank Tensors*, *Phys. Rev. D* **100** (2019) 086003 [1905.06264].

[68] I.R. Klebanov, A. Milekhin, G. Tarnopolsky and W. Zhao, *Spontaneous Breaking of $U(1)$ Symmetry in Coupled Complex SYK Models*, *JHEP* **11** (2020) 162 [2006.07317].

[69] M. Berkooz, P. Narayan, M. Rozali and J. Simón, *Comments on the Random Thirring Model*, *JHEP* **09** (2017) 057 [1702.05105].

[70] J. Murugan, D. Stanford and E. Witten, *More on Supersymmetric and 2d Analogs of the SYK Model*, *JHEP* **08** (2017) 146 [1706.05362].

[71] S. Giombi, I.R. Klebanov and G. Tarnopolsky, *Bosonic tensor models at large N and small ϵ*, *Phys. Rev.* **D96** (2017) 106014 [1707.03866].

[72] S. Prakash and R. Sinha, *A complex fermionic tensor model in d dimensions*, *JHEP* **02** (2018) 086 [1710.09357].

[73] D. Benedetti, S. Carrozza, R. Gurau and A. Sfondrini, *Tensorial Gross-Neveu models*, *JHEP* **01** (2018) 003 [1710.10253].

[74] S. Giombi, I.R. Klebanov, F. Popov, S. Prakash and G. Tarnopolsky, *Prismatic large N models for bosonic tensors*, *Phys. Rev.* **D98** (2018) 105005 [1808.04344].

[75] D. Benedetti, R. Gurau and S. Harribey, *Line of fixed points in a bosonic tensor model*, *JHEP* **06** (2019) 053 [1903.03578].

[76] F.K. Popov, *Supersymmetric tensor model at large N and small ϵ*, *Phys. Rev. D* **101** (2020) 026020 [1907.02440].

[77] D. Lettera and A. Vichi, *A large-N tensor model with four supercharges*, *JHEP* **08** (2022) 192 [2012.11600].

[78] I.R. Klebanov, F. Popov and G. Tarnopolsky, *TASI lectures on large N tensor models*, *PoS* **TASI2017** (2018) 004 [1808.09434].

[79] R. Gurau, *Random Tensors*, Oxford University Press, Oxford (2016).

[80] R. de Mello Koch, D. Gossman and L. Tribelhorn, *Gauge Invariants, Correlators and Holography in Bosonic and Fermionic Tensor Models*, *JHEP* **09** (2017) 011 [1707.01455].

[81] R. de Mello Koch, D. Gossman, N. Hasina Tahiridimbisoa and A.L. Mahu, *Holography for Tensor models*, *Phys. Rev. D* **101** (2020) 046004 [1910.13982].

[82] R. Gurau, V. Rivasseau and A. Sfondrini, *Renormalization: an advanced overview*, 1401.5003.

[83] D. Kreimer, *Bananas: multi-edge graphs and their Feynman integrals*, 2202.05490.

[84] D. Benedetti and N. Delporte, *Phase diagram and fixed points of tensorial Gross-Neveu models in three dimensions*, *JHEP* **01** (2019) 218 [1810.04583].

[85] L. Lionni, *Colored discrete spaces: higher dimensional combinatorial maps and quantum gravity*, Ph.D. thesis, Saclay, 2017. 1710.03663. 10.1007/978-3-319-96023-4.

[86] S.S. Gubser, C. Jepsen, Z. Ji and B. Trundy, *Higher melonic theories*, *JHEP* **09** (2018) 049 [1806.04800].

[87] S. Prakash and R. Sinha, *Melonic Dominance in Subchromatic Sextic Tensor Models*, *Phys. Rev. D* **101** (2020) 126001 [1908.07178].

[88] V. Bonzom, V. Nador and A. Tanasa, *Diagrammatics of the quartic $O(N)^3$-invariant Sachdev-Ye-Kitaev-like tensor model*, *J. Math. Phys.* **60** (2019) 072302 [1903.01723].

[89] J. Ben Geloun and S. Ramgoolam, *Counting tensor model observables and branched covers of the 2-sphere*, *Ann. Inst. H. Poincare D Comb. Phys. Interact.* **1** (2014) 77 [1307.6490].

[90] J. Ben Geloun and S. Ramgoolam, *Tensor models, Kronecker coefficients and permutation centralizer algebras*, *JHEP* **11** (2017) 092 [1708.03524].

[91] R.C. Avohou, J. Ben Geloun and N. Dub, *On the counting of $O(N)$ tensor invariants*, *Adv. Theor. Math. Phys.* **24** (2020) 821 [1907.04668].

[92] L. Freidel and D. Louapre, *Nonperturbative summation over 3-D discrete topologies*, *Phys. Rev. D* **68** (2003) 104004 [hep-th/0211026].

[93] D. Benedetti, N. Delporte, S. Harribey and R. Sinha, *Sextic tensor field theories in rank* 3 *and* 5, *JHEP* **06** (2020) 065 [1912.06641].

[94] M. Salmhofer, *Renormalization*, Springer Science & Business Media, New York (1999).

[95] N. Halmagyi and S. Mondal, *Tensor Models for Black Hole Probes*, *JHEP* **07** (2018) 095 [1711.04385].

[96] F. Ferrari, *The large D limit of planar diagrams*, *Ann. Inst. Henri Poincaré Comb. Phys. Interact.* **6** (2019) 427 [1701.01171].

[97] T. Azeyanagi, F. Ferrari and F.I. Schaposnik Massolo, *Phase diagram of planar matrix quantum mechanics, tensor, and Sachdev-Ye-Kitaev models*, *Phys. Rev. Lett.* **120** (2018) 061602 [1707.03431].

[98] T. Azeyanagi, F. Ferrari, P. Gregori, L. Leduc and G. Valette, *More on the new large D limit of matrix models*, *Annals Phys.* **393** (2018) 308 [1710.07263].

[99] F. Ferrari and F.I. Schaposnik Massolo, *Phases Of Melonic Quantum Mechanics*, *Phys. Rev. D* **100** (2019) 026007 [1903.06633].

[100] D. Benedetti, S. Carrozza, R. Toriumi and G. Valette, *Multiple scaling limits of $\mathrm{U}(N)^2 \times \mathrm{O}(D)$ multi-matrix models*, *Ann. Inst. H. Poincare D Comb. Phys. Interact.* **9** (2022) 367 [2003.02100].

[101] S. Carrozza, F. Ferrari, A. Tanasa and G. Valette, *On the large D expansion of Hermitian multi-matrix models*, *J. Math. Phys.* **61** (2020) 073501 [2003.04152].

[102] V. Bonzom, V. Nador and A. Tanasa, *Double scaling limit of multi-matrix models at large D*, 2209.02026.

[103] R. Emparan, R. Suzuki and K. Tanabe, *The large D limit of General Relativity*, *JHEP* **06** (2013) 009 [1302.6382].

[104] A. Tanasa, *The multi-orientable random tensor model, a review*, *SIGMA* **12** (2016) 056 [1512.02087].

[105] R. Gurau and G. Schaeffer, *Regular colored graphs of positive degree*, *Ann. Inst. Henri Poincaré Comb. Phys. Interact.* **3** (2016) 257 [1307.5279].

[106] E. Fusy and A. Tanasa, *Asymptotic expansion of the multi-orientable random tensor model*, *The electronic journal of combinatorics* **22** (2015) 1 [1408.5725].

[107] J. Ambjørn, B. Durhuus and T. Jonsson, *Quantum Geometry: A Statistical Field Theory Approach*, Cambridge Monographs on Mathematical Physics, Cambridge Univ. Press, Cambridge, UK (12, 2005), 10.1017/CBO9780511524417.

[108] F. David, *Planar diagrams, two-dimensional lattice gravity and surface models*, *Nucl. Phys.* **B257** (1985) 45.

[109] B. Duplantier and S. Sheffield, *Liouville quantum gravity and kpz*, *Invent. math.* **185** (2011) 333?393 [0808.1560].

[110] B. Duplantier, J. Miller and S. Sheffield, *Liouville quantum gravity as a mating of trees*, 1409.7055.

[111] F. David, A. Kupiainen, R. Rhodes and V. Vargas, *Liouville Quantum Gravity on the Riemann sphere*, *Commun. Math. Phys.* **342** (2016) 869 [1410.7318].

[112] E. Brezin, C. Itzykson, G. Parisi and J.B. Zuber, *Planar diagrams*, *Commun. Math. Phys.* **59** (1978) 35.

[113] E. Gardner, *SPIN GLASSES WITH P SPIN INTERACTIONS*, *Nucl. Phys. B* **257** (1985) 747.

[114] L.F. Cugliandolo, D.R. Grempel and C.A. da Silva Santos, *Imaginary-time replica formalism study of a quantum spherical p-spin-glass model*, *Phys. Rev. B* **64** (2001) 014403 [cond-mat/0012222].

[115] S. Dartois, H. Erbin and S. Mondal, *Conformality of* $1/N$ *corrections in Sachdev-Ye-Kitaev-like models*, *Phys. Rev. D* **100** (2019) 125005 [1706.00412].

[116] D. Benedetti and R. Gurau, *2PI effective action for the SYK model and tensor field theories*, *JHEP* **05** (2018) 156 [1802.05500].

[117] J. Berges, *Introduction to nonequilibrium quantum field theory*, *AIP Conf. Proc.* **739** (2005) 3 [hep-ph/0409233].

[118] J.P. Blaizot, E. Iancu and A. Rebhan, *Approximately selfconsistent resummations for the thermodynamics of the quark gluon plasma. 1. Entropy and density*, *Phys. Rev.* **D63** (2001) 065003 [hep-ph/0005003].

[119] J. Berges, S. Borsanyi, U. Reinosa and J. Serreau, *Renormalized thermodynamics from the 2PI effective action*, *Phys. Rev.* **D71** (2005) 105004 [hep-ph/0409123].

[120] J. Berges, S. Borsanyi, U. Reinosa and J. Serreau, *Nonperturbative renormalization for 2PI effective action techniques*, *Annals Phys.* **320** (2005) 344 [hep-ph/0503240].

[121] U. Reinosa and J. Serreau, *2PI functional techniques for gauge theories: QED*, *Annals Phys.* **325** (2010) 969 [0906.2881].

[122] J. Berges, *Controlled nonperturbative dynamics of quantum fields out-of-equilibrium*, *Nucl. Phys.* **A699** (2002) 847 [hep-ph/0105311].

[123] G. Aarts, D. Ahrensmeier, R. Baier, J. Berges and J. Serreau, *Far from equilibrium dynamics with broken symmetries from the 2PI - 1/N expansion*, *Phys. Rev.* **D66** (2002) 045008 [hep-ph/0201308].

[124] A. Jevicki, K. Suzuki and J. Yoon, *Bi-Local Holography in the SYK Model*, *JHEP* **07** (2016) 007 [1603.06246].

[125] A. Jevicki and K. Suzuki, *Bi-Local Holography in the SYK Model: Perturbations*, *JHEP* **11** (2016) 046 [1608.07567].

[126] A. Kitaev and S.J. Suh, *The soft mode in the Sachdev-Ye-Kitaev model and its gravity dual*, *JHEP* **05** (2018) 183 [1711.08467].

[127] N.D. Mermin and H. Wagner, *Absence of ferromagnetism or antiferromagnetism in one-dimensional or two-dimensional isotropic Heisenberg models*, *Phys. Rev. Lett.* **17** (1966) 1133.

[128] S.R. Coleman, *There are no Goldstone bosons in two-dimensions*, *Commun. Math. Phys.* **31** (1973) 259.

[129] E. Witten, *Chiral symmetry, the 1/N expansion, and the SU(N) Thirring model*, *Nucl. Phys. B* **145** (1978) 110.

[130] J. Magnen and V. Rivasseau, *Constructive phi**4 field theory without tears*, *Annales Henri Poincare* **9** (2008) 403 [0706.2457].

[131] P. Di Vecchia, M. Kato and N. Ohta, *Double scaling limit in O(N) vector models*, *Nucl. Phys. B* **357** (1991) 495.

[132] R. Gurau, *Quenched equals annealed at leading order in the colored SYK model*, *Europhys. Lett.* **119** (2017) 30003 [1702.04228].

[133] D.J. Gross and V. Rosenhaus, *A Generalization of Sachdev-Ye-Kitaev*, *JHEP* **02** (2017) 093 [1610.01569].

[134] D. Benedetti and I. Costa, *$SO(3)$-invariant phase of the $O(N)^3$ tensor model*, *Phys. Rev. D* **101** (2020) 086021 [1912.07311].

[135] M. Kwasnicki, *Ten equivalent definitions of the fractional Laplace operator*, *Fractional Calculus and Applied Analysis* **20** (2017) 51 [1507.07356].

[136] P. Stinga and J. Torrea, *Extension problem and harnack's inequality for some fractional operators*, *Communications in Partial Differential Equations* **35** (2009) 2092 [0910.2569].

[137] D. Karateev, P. Kravchuk and D. Simmons-Duffin, *Harmonic Analysis and Mean Field Theory*, *JHEP* **10** (2019) 217 [1809.05111].

[138] D. Mukamel, *Notes on the statistical mechanics of systems with long-range interactions*, 0905.1457.

[139] A. Campa, T. Dauxois and S. Ruffo, *Statistical mechanics and dynamics of solvable models with long-range interactions*, *Physics Reports* **480** (2009) 57 [0907.0323].

[140] F.J. Dyson, *Existence of a phase transition in a one-dimensional Ising ferromagnet*, *Commun. Math. Phys.* **12** (1969) 91.

[141] M.E. Fisher, S.-k. Ma and B. Nickel, *Critical exponents for long-range interactions*, *Phys.Rev.Lett.* **29** (1972) 917.

[142] J. Sak, *Recursion relations and fixed points for ferromagnets with long-range interactions*, *Phys. Rev. B* **8** (1973) 281.

[143] J. Honkonen, *Critical behaviour of the long-range $(\phi^2)^2$ model in the short-range limit*, *J.Phys.A* **23** (1990) 825.

[144] T. Blanchard, M. Picco and M. Rajabpour, *Influence of long-range interactions on the critical behavior of the Ising model*, *EPL* **101** (2013) 56003 [1211.6758].

[145] M.C. Angelini, G. Parisi and F. Ricci-Tersenghi, *Relations between short-range and long-range ising models*, *Phys. Rev. E* **89** (2014) 062120 [1401.6805].

[146] E. Brezin, G. Parisi and F. Ricci-Tersenghi, *The crossover region between long-range and short-range interactions for the critical exponents*, *J. Stat. Phys.* **157** (2014) 855 [1407.3358].

[147] N. Defenu, A. Trombettoni and A. Codello, *Fixed-point structure and effective fractional dimensionality for $O(N)$ models with long-range interactions*, *Phys. Rev. E* **92** (2015) 052113 [1409.8322].

[148] C. Behan, L. Rastelli, S. Rychkov and B. Zan, *Long-range critical exponents near the short-range crossover*, *Phys. Rev. Lett.* **118** (2017) 241601 [1703.03430].

[149] C. Behan, L. Rastelli, S. Rychkov and B. Zan, *A scaling theory for the long-range to short-range crossover and an infrared duality*, *J.Phys.A* **50** (2017) 354002 [1703.05325].

[150] K. Gawedzki and A. Kupiainen, *Renormalizing the nonrenormalizable*, *Phys. Rev. Lett.* **55** (1985) 363.

[151] M. Aizenman and R. Fernandez, *Critical exponents for long-range interactions*, *Lett. Math. Phys.* **16** (1988) 39.

[152] D.C. Brydges, P.K. Mitter and B. Scoppola, *Critical (Phi**4)(3, epsilon)*, *Commun. Math. Phys.* **240** (2003) 281 [hep-th/0206040].

[153] A. Abdesselam, *A complete renormalization group trajectory between two fixed points*, *Commun.Math.Phys.* **276** (2007) 727 [math-ph/0610018].

[154] G. Slade, *Critical exponents for long-range $O(n)$ models below the upper critical dimension*, *Communications in Mathematical Physics* **358** (2017) 343?436 [1611.06169].

[155] M. Lohmann, G. Slade and B.C. Wallace, *Critical two-point function for long-range o(n) models below the upper critical dimension*, *Journal of Statistical Physics* **169** (2017) 1132 [1705.08540].

[156] A. Giuliani, V. Mastropietro and S. Rychkov, *Gentle introduction to rigorous Renormalization Group: a worked fermionic example*, *JHEP* **01** (2021) 026 [2008.04361].

[157] M.F. Paulos, S. Rychkov, B.C. van Rees and B. Zan, *Conformal invariance in the long-range Ising model*, *Nucl.Phys.B* **902** (2016) 246 [1509.00008].

[158] C. Behan, *Bootstrapping the long-range Ising model in three dimensions*, *J. Phys. A* **52** (2019) 075401 [1810.07199].

[159] N. Chai, M. Goykhman and R. Sinha, *Long-range vector models at large N*, *JHEP* **09** (2021) 194 [2107.08052].

[160] N. Chai, S. Chakraborty, M. Goykhman and R. Sinha, *Long-range fermions and critical dualities*, *JHEP* **01** (2022) 172 [2110.00020].

[161] N. Chai, A. Dymarsky, M. Goykhman, R. Sinha and M. Smolkin, *A model of persistent breaking of continuous symmetry*, *SciPost Phys.* **12** (2022) 181 [2111.02474].

[162] S. Giombi, E. Helfenberger and H. Khanchandani, *Long Range, Large Charge, Large N*, 2205.00500.

[163] D. Benedetti, R. Gurau, S. Harribey and K. Suzuki, *Long-range multi-scalar models at three loops*, *J. Phys. A* **53** (2020) 445008 [2007.04603].

[164] O. Schnetz, *Numbers and functions in quantum field theory*, *Phys. Rev. D* **97** (2018) 085018 [1606.08598].

[165] D.J. Gross and V. Rosenhaus, *A line of CFTs: from generalized free fields to SYK*, *JHEP* **07** (2017) 086 [1706.07015].

[166] D. Benedetti, *Instability of complex CFTs with operators in the principal series*, *JHEP* **05** (2021) 004 [2103.01813].

[167] D. Benedetti, R. Gurau and K. Suzuki, *Conformal symmetry and composite operators in the $O(N)^3$ tensor field theory*, *JHEP* **06** (2020) 113 [2002.07652].

[168] I. Jack and H. Osborn, *Analogs for the c theorem for four-dimensional renormalizable field theories*, *Nucl. Phys. B* **343** (1990) 647.

[169] D. Benedetti, R. Gurau, S. Harribey and K. Suzuki, *Hints of unitarity at large N in the $O(N)^3$ tensor field theory*, *JHEP* **02** (2020) 072 [1909.07767].

[170] M.E. Fisher, *Yang-Lee edge singularity and phi**3 field theory*, *Phys. Rev. Lett.* **40** (1978) 1610.

[171] J.L. Cardy, *Conformal invariance and the Yang-Lee edge singularity in two-dimensions*, *Phys. Rev. Lett.* **54** (1985) 1354.

[172] O. de Alcantara Bonfim, J. Kirkham and A. McKane, *Critical exponents to order ϵ^3 for ϕ^3 models of critical phenomena in $6-\epsilon$ dimensions*, *J. Phys. A* **13** (1980) L247.

[173] J. Kirkham and D. Wallace, *Comments on the Field Theoretic Formulation of the Yang-lee Edge Singularity*, *J. Phys. A* **12** (1979) L47.

[174] A. Houghton, J. Reeve and D. Wallace, *High Order Behavior in ϕ^3 Field Theories and the Percolation Problem*, *Phys. Rev. B* **17** (1978) 2956.

[175] C. Fortuin and P. Kasteleyn, *On the Random cluster model. 1. Introduction and relation to other models*, *Physica* **57** (1972) 536.

[176] D. Benedetti, R. Gurau and S. Harribey, *Trifundamental quartic model*, *Phys. Rev. D* **103** (2021) 046018 [2011.11276].

[177] L.S. Brown, *Dimensional Regularization of Composite Operators in Scalar Field Theory*, *Annals Phys.* **126** (1980) 135.

[178] L. Caffarelli and L. Silvestre, *An extension problem related to the fractional laplacian*, *Communications in Partial Differential Equations* **32** (2007) 1245 [math/0608640].

[179] V. Dobrev, G. Mack, I. Todorov, V. Petkova and S. Petrova, *On the Clebsch-Gordan Expansion for the Lorentz Group in n Dimensions*, *Rept. Math. Phys.* **9** (1976) 219.

[180] V. Dobrev, V. Petkova, S. Petrova and I. Todorov, *Dynamical Derivation of Vacuum Operator Product Expansion in Euclidean Conformal Quantum Field Theory*, *Phys. Rev. D* **13** (1976) 887.

[181] V. Dobrev, G. Mack, V. Petkova, S. Petrova and I. Todorov, *Harmonic Analysis on the n-Dimensional Lorentz Group and Its Application to Conformal Quantum Field Theory*, vol. 63, Springer, Berlin, Heidelberg (1977), 10.1007/BFb0009678.

[182] S. Caron-Huot, *Analyticity in Spin in Conformal Theories*, *JHEP* **09** (2017) 078 [1703.00278].

[183] D. Simmons-Duffin, D. Stanford and E. Witten, *A spacetime derivation of the Lorentzian OPE inversion formula*, *JHEP* **07** (2018) 085 [1711.03816].

[184] J. Liu, E. Perlmutter, V. Rosenhaus and D. Simmons-Duffin, *d-dimensional SYK, AdS Loops, and* $6j$ *Symbols*, *JHEP* **03** (2019) 052 [1808.00612].

[185] G. Mack, *D-independent representation of Conformal Field Theories in D dimensions via transformation to auxiliary Dual Resonance Models. Scalar amplitudes*, 0907.2407.

[186] M.S. Costa, V. Goncalves and J. Penedones, *Conformal Regge theory*, *JHEP* **12** (2012) 091 [1209.4355].

[187] A. Gadde, *In search of conformal theories*, 1702.07362.

[188] M. Hogervorst and B.C. van Rees, *Crossing symmetry in alpha space*, *JHEP* **11** (2017) 193 [1702.08471].

[189] C. Sleight and M. Taronna, *Anomalous Dimensions from Crossing Kernels*, *JHEP* **11** (2018) 089 [1807.05941].

[190] C. Sleight and M. Taronna, *Spinning Mellin Bootstrap: Conformal Partial Waves, Crossing Kernels and Applications*, *Fortsch. Phys.* **66** (2018) 1800038 [1804.09334].

[191] R. de Mello Koch, A. Jevicki, K. Suzuki and J. Yoon, *AdS Maps and Diagrams of Bi-local Holography*, *JHEP* **03** (2019) 133 [1810.02332].

[192] O. Aharony, S.M. Chester and E.Y. Urbach, *A Derivation of AdS/CFT for Vector Models*, *JHEP* **03** (2021) 208 [2011.06328].

[193] S. Ferrara, A. Grillo, G. Parisi and R. Gatto, *The shadow operator formalism for conformal algebra. Vacuum expectation values and operator products*, *Lett. Nuovo Cim.* **4S2** (1972) 115.

[194] F.A. Dolan and H. Osborn, *Conformal partial waves and the operator product expansion*, *Nucl. Phys. B* **678** (2004) 491 [hep-th/0309180].

[195] F.A. Dolan and H. Osborn, *Conformal Partial Waves: Further Mathematical Results*, 1108.6194.

[196] D. Simmons-Duffin, *Projectors, Shadows, and Conformal Blocks*, *JHEP* **04** (2014) 146 [1204.3894].

[197] D. Benedetti, R. Gurau, S. Harribey and D. Lettera, *The F-theorem in the melonic limit*, *JHEP* **02** (2022) 147 [2111.11792].

[198] D. Benedetti and N. Delporte, *Remarks on a melonic field theory with cubic interaction*, *JHEP* **04** (2021) 197 [2012.12238].

[199] R. Gurau, *Notes on tensor models and tensor field theories*, 1907.03531.

[200] D. Grabner, N. Gromov, V. Kazakov and G. Korchemsky, *Strongly γ-deformed $\mathcal{N} = 4$ supersymmetric yang-mills theory as an integrable conformal field theory*, *Phys.Rev.Lett.* **120** (2018) 111601 [1711.04786].

[201] V. Kazakov and E. Olivucci, *Biscalar integrable conformal field theories in any dimension*, *Phys.Rev.Lett.* **121** (2018) 131601 [1801.09844].

[202] S.S. Gubser and I.R. Klebanov, *A Universal result on central charges in the presence of double trace deformations*, *Nucl. Phys. B* **656** (2003) 23 [hep-th/0212138].

[203] Z. Komargodski and A. Zhiboedov, *Convexity and Liberation at Large Spin*, *JHEP* **11** (2013) 140 [1212.4103].

[204] D.L. Jafferis, *The Exact Superconformal R-Symmetry Extremizes Z*, *JHEP* **05** (2012) 159 [1012.3210].

[205] D.L. Jafferis, I.R. Klebanov, S.S. Pufu and B.R. Safdi, *Towards the F-Theorem: N=2 Field Theories on the Three-Sphere*, *JHEP* **06** (2011) 102 [1103.1181].

[206] I.R. Klebanov, S.S. Pufu and B.R. Safdi, *F-Theorem without Supersymmetry*, *JHEP* **10** (2011) 038 [1105.4598].

[207] S.S. Pufu, *The F-Theorem and F-Maximization*, *J. Phys. A* **50** (2017) 443008 [1608.02960].

[208] H. Casini and M. Huerta, *On the RG running of the entanglement entropy of a circle*, *Phys. Rev. D* **85** (2012) 125016 [1202.5650].

[209] H. Casini, M. Huerta and R.C. Myers, *Towards a derivation of holographic entanglement entropy*, *JHEP* **05** (2011) 036 [1102.0440].

[210] A.B. Zamolodchikov, *Irreversibility of the Flux of the Renormalization Group in a 2D Field Theory*, *JETP Lett.* **43** (1986) 730.

[211] Z. Komargodski and A. Schwimmer, *On Renormalization Group Flows in Four Dimensions*, *JHEP* **12** (2011) 099 [1107.3987].

[212] Z. Komargodski, *The Constraints of Conformal Symmetry on RG Flows*, *JHEP* **07** (2012) 069 [1112.4538].

[213] D.E. Diaz and H. Dorn, *Partition functions and double-trace deformations in AdS/CFT*, *JHEP* **05** (2007) 046 [hep-th/0702163].

[214] A.F. Faedo, C. Hoyos, D. Mateos and J.G. Subils, *Holographic Complex Conformal Field Theories*, *Phys. Rev. Lett.* **124** (2020) 161601 [1909.04008].

[215] A. Dymarsky, I. Klebanov and R. Roiban, *Perturbative search for fixed lines in large N gauge theories*, *JHEP* **08** (2005) 011 [hep-th/0505099].

[216] A. Dymarsky, I.R. Klebanov and R. Roiban, *Perturbative gauge theory and closed string tachyons*, *JHEP* **11** (2005) 038 [hep-th/0509132].

[217] E. Pomoni and L. Rastelli, *Large N Field Theory and AdS Tachyons*, *JHEP* **04** (2009) 020 [0805.2261].

[218] D.B. Kaplan, J.-W. Lee, D.T. Son and M.A. Stephanov, *Conformality Lost*, *Phys. Rev. D* **80** (2009) 125005 [0905.4752].

[219] F. Benini, C. Iossa and M. Serone, *Conformality Loss, Walking, and 4D Complex Conformal Field Theories at Weak Coupling*, *Phys. Rev. Lett.* **124** (2020) 051602 [1908.04325].

[220] N. Gromov, V. Kazakov and G. Korchemsky, *Exact Correlation Functions in Conformal Fishnet Theory*, *JHEP* **08** (2019) 123 [1808.02688].

[221] V. Kazakov, E. Olivucci and M. Preti, *Generalized fishnets and exact four-point correlators in chiral CFT_4*, *JHEP* **06** (2019) 078 [1901.00011].

[222] A. Pittelli and M. Preti, *Integrable fishnet from γ-deformed $\mathcal{N} = 2$ quivers*, *Phys. Lett. B* **798** (2019) 134971 [1906.03680].

[223] S.S. Gubser, I.R. Klebanov and A.M. Polyakov, *Gauge theory correlators from noncritical string theory*, *Phys. Lett. B* **428** (1998) 105 [hep-th/9802109].

[224] E. Witten, *Anti-de Sitter space and holography*, *Adv. Theor. Math. Phys.* **2** (1998) 253 [hep-th/9802150].

[225] P. Breitenlohner and D.Z. Freedman, *Positive Energy in anti-De Sitter Backgrounds and Gauged Extended Supergravity*, *Phys. Lett. B* **115** (1982) 197.

[226] P. Breitenlohner and D.Z. Freedman, *Stability in gauged extended supergravity*, *Annals Phys.* **144** (1982) 249.

[227] W.A. Bardeen, M. Moshe and M. Bander, *Spontaneous Breaking of Scale Invariance and the Ultraviolet Fixed Point in O(N) Symmetric ($\bar{\phi}_3^6$ in Three-Dimensions) Theory*, *Phys. Rev. Lett.* **52** (1984) 1188.

[228] D.J. Amit and E. Rabinovici, *Breaking of Scale Invariance in ϕ^6 Theory: Tricriticality and Critical End Points*, *Nucl. Phys. B* **257** (1985) 371.

[229] H. Omid, G.W. Semenoff and L.C.R. Wijewardhana, *Light dilaton in the large N tricritical $O(N)$ model*, *Phys. Rev. D* **94** (2016) 125017 [1605.00750].

[230] D.F. Litim, E. Marchais and P. Mati, *Fixed points and the spontaneous breaking of scale invariance*, *Phys. Rev. D* **95** (2017) 125006 [1702.05749].

[231] C. Fleming, B. Delamotte and S. Yabunaka, *Finite N origin of the Bardeen-Moshe-Bander phenomenon and its extension at $N = \infty$ by singular fixed points*, *Phys. Rev. D* **102** (2020) 065008 [2001.07682].

[232] S. Harribey, *Sextic tensor model in rank 3 at next-to-leading order*, *JHEP* **10** (2022) 037 [2109.08034].

[233] D.J. Amit and D.V.I. Roginsky, *Exactly soluble limit of ϕ^3 field theory with internal Potts symmetry*, *J. Phys.* **A12** (1979) 689.

[234] O. Gurdogan and V. Kazakov, *New integrable 4d quantum field theories from strongly deformed planar $\mathcal{N} = 4$ supersymmetric Yang-Mills theory*, *Phys.Rev.Lett.* **117** (2016) 201602 [1512.06704].

[235] M.A. Vasiliev, *From Coxeter Higher-Spin Theories to Strings and Tensor Models*, *JHEP* **08** (2018) 051 [1804.06520].

[236] R. de Mello Koch, A. Jevicki, K. Jin and J.P. Rodrigues, *AdS_4/CFT_3 Construction from Collective Fields*, *Phys. Rev. D* **83** (2011) 025006 [1008.0633].

[237] M. Borinsky, G.V. Dunne and M. Meynig, *Semiclassical Trans-Series from the Perturbative Hopf-Algebraic Dyson-Schwinger Equations: ϕ^3 QFT in 6 Dimensions*, *SIGMA* **17** (2021) 087 [2104.00593].

[238] L.F. Cugliandolo, *Dynamics of glassy systems*, cond-mat/0210312.

[239] A. Crisanti and H.-J. Sommers, *The sphericalp-spin interaction spin glass model: the statics*, *Zeitschrift für Physik B Condensed Matter* **87** (1992) 341.

[240] L.F. Cugliandolo, J. Kurchan, G. Parisi and F. Ritort, *Matrix models as solvable glass models*, *Phys. Rev. Lett.* **74** (1995) 1012 [cond-mat/9407086].

[241] F.K. Popov and Y. Wang, *Non-perturbative defects in tensor models from melonic trees*, *JHEP* **11** (2022) 057 [2206.14206].